SOLVING GEOMETRIC PUZZLES WITH DIVIDE AND CONCUR

A Dissertation

Presented to the Faculty of the Graduate School

of Cornell University

in Partial Fulfillment of the Requirements for the Degree of

Doctor of Philosophy

by

Yoav Kallus

August 2011

SOLVING GEOMETRIC PUZZLES WITH DIVIDE AND CONCUR

Yoav Kallus, Ph.D.

Cornell University 2011

In this dissertation we discuss a variety of geometric constraint satisfaction problems. The greatest part of the discussion is devoted to infinite packing problems, where the packing arrangement of an infinite number of congruent copies of an object with the greatest density is sought. We develop a general method, based on the *Divide and Concur* scheme, for discovering dense periodic packings of any convex object. We use this method to improve on the previous greatest known packing density of regular tetrahedra. We then generalize the discussion of regular tetrahedra to a one-parameter family of shapes interpolating between the regular tetrahedron and the sphere. We investigate how the likely optimal packing changes as the shape is changed and what continuous and abrupt transitions arise. We also use the method to reproduce the densest known lattice sphere packings and the best known lattice kissing arrangements in up to 14 and 11 dimensions respectively – the first such numerical evidence for their optimality in some of these dimensions. We then shift our discussion to the inverse problem of inferring the structure of biomolecules from a set of structural restraints derived from nuclear magnetic resonance experiments. We describe a constraint-based approach which avoids the minimization of a cost/energy function and use it to reconstruct the structure of a beta-amyloid fibril formed by a 40-amino-acid peptide associated with Alzheimer's disease based on restraints published in the literature. Finally, we study a simple model of rippling in a two-dimensional atomic sheet due to bond length heterogeneity. We describe a form of dislocations which is not present in a homogeneous crystal and use a relationship between the dislocation density and the Gaussian curvature to characterize

the relaxed conformation of the sheet. We find a relationship between this conformation and a surface in an abstract space associated with the combinatorial aspect of the bond length heterogeneity.

BIOGRAPHICAL SKETCH

Yoav Kallus was born in Haifa, Israel in 1986. A classic faculty brat, thanks to his professorial mother, he began sitting in on math courses at the Israeli Institute of Technology in Haifa (Technion) at age 15. The next year, moving with his family to Berkeley, California for his mother's sabbatical year, he stopped attending high school and began taking classes at the University of California full time. He continued in Berkeley for another year after his mother went back to teach in Haifa, but transferred to Rice University the following year, where in 2006 he earned a BSc in physics. Yoav then went on to seek a PhD in physics from Cornell University, where he worked under the advising of Veit Elser from 2007. He earned an MSc in 2010 and a PhD in 2011. Yoav expects to be a post-doctoral fellow with the Princeton Center for Theoretical Sciences from 2011 to 2014.

To my parents.

ACKNOWLEDGEMENTS

I first thank my adviser, Veit Elser, who has guided and supervised all the work presented. He has been remarkably devoted and enthusiastic in filling his advisory role, and virtuosic in his artfully minimalist application of motivational stimuli. While this dissertation marks the end of our formal attachment as student and adviser, I will surely keep seeking out his advice for years to come.

I shared this incredible adviser with an equally incredible group of lab mates. Simon Gravel, Duane Loh, Kartik Ayyer, Diarmuid Cahalane, and Zhen Wah Tan have all made working in the Elser group an incredible academic experience. I have my lab mates to thank for contributions to many of the ideas presented in this dissertation. Beside my lab mates and my adviser, others have been useful sources of insight and background to the material discussed in this dissertation, and I acknowledge useful conversations with Henry Cohn, Bob Connelly, Michael Engel, Sharon Glotzer, Chris Henley, Erich Mueller, Ricky Pollack, Sal Torquato, James Sethna, and Rob Thorne. The last two deserve special mention for serving on my special committee with Veit Elser and facilitating my degree candidacy and dissertation defense examinations. I should not forget to cite my brother Nathan Kallus in this context for the useful conversations I have had with him. There are other colleagues at Cornell whom I must thank for constantly sharing their ideas with me and critically hearing out my own: Srivatsan Chakram, Joe Chen, Bryan Daniels, Phil Kidd, Johannes Lischner, Ben Machta, Stefan Natu, Tim Novikoff, Stefanos Papanikolaou, Frank Petruzielo, Sumiran Pujari, Tristan Rocheleau, Mark Transtrum, and Arend van der Zande. I also thank the administrative and technical staffs of the Department of Physics, the Cornell Center for Materials Research, the Laboratory of Atomic and Solid State Physics, and the Graduate School.

To my parents, my sister, and my brother, I owe thanks for providing a moving home to escape to from Ithaca.

Finally, my time as a graduate student would not have been as enjoyable without the great people of Ithaca and Cornell: my house mates over the years, my office mates, my friends, and, of course, my wonderful girlfriend Alisa.

TABLE OF CONTENTS

Biographical Sketch . . . iii
Dedication . . . iv
Acknowledgements . . . v
Table of Contents . . . vii
List of Tables . . . ix
List of Figures . . . x

1 Introduction **1**
1.1 Geometric Puzzles . . . 1
1.1.1 Packing problems . . . 2
1.1.2 Distance Geometry . . . 4
1.2 The difference map . . . 6
1.3 Random walk reconstruction . . . 7
1.3.1 Background . . . 7
1.3.2 Divide and Concur . . . 8
1.3.3 Results . . . 10
1.4 Conclusion . . . 13

2 Dense periodic packings of tetrahedra with small repeating units **14**
2.1 Abstract . . . 14
2.2 Introduction . . . 14
2.3 One-parameter family of dimer-double-lattice packings . . . 15
2.4 Simple double-lattice packing . . . 21
2.5 Discussion . . . 22

3 A method for dense packing discovery **24**
3.1 Abstract . . . 24
3.2 Introduction . . . 25
3.3 Motivation . . . 30
3.3.1 The $D - C$ scheme . . . 30
3.3.2 The difference map . . . 35
3.4 Constraints . . . 37
3.4.1 Periodic sphere packing and kissing . . . 37
3.4.2 Convex polytope packing . . . 41
3.5 Implementation . . . 44
3.5.1 “Divide” projections . . . 44
3.5.2 “Concur” projections . . . 49
3.5.3 Formal configuration space maintenance . . . 53
3.6 Results . . . 56
3.6.1 Sphere packing . . . 56
3.6.2 Kissing number . . . 57
3.6.3 Polytope packing . . . 58
3.7 Conclusion . . . 61

4 Dense packing crystal structures of physical tetrahedra **64**
4.1 Abstract . . . 64
4.2 Introduction . . . 64
4.3 Methods . . . 66
4.4 Results . . . 69
4.5 Discussion . . . 72

5 Constraint-based method for structure determination **75**
5.1 Abstract . . . 75
5.2 Introduction . . . 75
5.3 Constraint-based approach . . . 78
5.3.1 Data restraints . . . 78
5.3.2 Local physical restraints . . . 79
5.3.3 Non-local physical restraints . . . 81
5.3.4 Divide and Concur . . . 82
5.4 Implementation . . . 85
5.4.1 The *divide* constraint . . . 85
5.4.2 Distance bound restraints . . . 86
5.4.3 Rigid unit restraints . . . 86
5.4.4 Torsion angle restraints . . . 87
5.4.5 The *concur* constraint . . . 88
5.4.6 Non-local energy bound . . . 88
5.5 Results . . . 90
5.6 Discussion . . . 93

6 Conformations of a graphene-like sheet with heterogeneity in bond lengths **97**
6.1 Abstract . . . 97
6.2 Bond length heterogeneity in an atomic sheet . . . 97
6.3 Fractional dislocations in a six-fold two-dimensional crystal . . . 98
6.4 Random tilings, projection, and the phason dimension . . . 100
6.5 A relationship between two apparently disparate surfaces . . . 102

Bibliography **107**

LIST OF TABLES

2.1 The construction of the dimer-double-lattice family of packings. . . . 16
2.2 The construction of the simple-double-lattice packing in a general triclinic coordinate basis. 21
2.3 Some studied transitive and non-transitive packings of regular tetrahedra 22

3.1 A summary of the $D - C$ constraints for periodic sphere packing, the average kissing number problem, and polytope packing. 44
3.2 Results of PDC searches for dense lattice packing in dimensions $d = 2, \ldots 14$. 57
3.3 Results of PDC searches for lattice packing with high kissing number in dimensions $d = 2, \ldots 11$. 58
3.4 Coordinates of the densest pentatope packing discovered by the PDC search. 61

5.1 Root-mean-square errors in four models of the amyloid fibril produced by the constraint based method and four models produced by a traditional method 92
5.2 Root-mean-square deviations between different models of the amyloid fibril. 92

LIST OF FIGURES

1.1 Reconstructions of a random walk with $N = 16000$ steps based on $M = 1600$, $M = 2400$, $M = 5200$, and $M = 8000$ non-local distance constraints. 11
1.2 The mean RMSD in an ensemble of solutions to the random walk reconstruction problem in the underconstrained region, averaged over ten random realizations for each value of N and M 12

2.1 Small portions of one layer and three stacked layers in the dimer-double-lattice packing. 18
2.2 The contacts on the surface of a dimer in the dimer-double lattice packing shown on a net diagram. 20
2.3 Small portions of one layer and three stacked layers in the simple-double-lattice packing. 20

3.1 An illustration of the $D - C$ scheme in the case of packing three disks into a square box. 32
3.2 An illustration of the "divide" and "concur" projections in the two-dimensional periodic sphere packing problem with $p = 3$. 41
3.3 An illustration of the polytope exclusion and rigidity constraint projections for the case of regular pentagons. 45
3.4 The course of a sample run searching for dense periodic packings ($p = 4$) of unit edge-length regular tetrahedra. 59
3.5 Lower dimensional cuts through dense packings of tetrahedra and pentatopes. 60

4.1 Tetrahedral puffs of varying asphericity. 66
4.2 A unit cell of each of the four structures described, (from left to right) the $\mathcal{S}_0$-, $\mathcal{D}_1$-, $\mathcal{S}_1$-, and $\mathcal{D}_0$-structures. 70
4.3 Highest densities ϕ achieved for packings of tetrahedral puffs of varying asphericity γ. 71

5.1 An aspargine residue partitioned into maximal rigid units. 81
5.2 The distribution of errors in the lowest error model of the amyloid fibril constructed in this work and a representative model constructed by a traditional method after a relaxation run. 93
5.3 Backbone traces of a model of the amyloid fibril constructed in this work and a representative model constructed by a traditional method after a relaxation run. 94

6.1 The five patterns of single and double bonds in a 6-cycle of the honeycomb lattice that are allowed in a Kekulé structure. 99
6.2 Correspondence of a Kekulé structure to a tiling by decorated rhombi. . 101
6.3 Correspondence of a Kekulé structure to the projection of a three dimensional surface. 101

6.4 The five possible arrangements of rhombi around a vertex of the tiling. 103
6.5 The Gaussian curvature in the manifold traced out by the bond network in equilibrium can be shown, by direct enumeration of local arrangements, to be proportional to the Gaussian curvature of the surface whose projection gives the rhombus tiling corresponding to the Kekulé structure. 104
6.6 Two ordered Kekulé structures which demonstrate the relationship between positive or negative Gaussian curvature in the surface whose projection is the corresponding tiling and in the manifold traced out by the bond network in equilibrium. 105

CHAPTER 1

INTRODUCTION

1.1 Geometric Puzzles

The problems we address in this dissertation, covering work done in the Laboratory of Atomic and Solid State Physics between 2007 and 2011, are problems of geometric constraint satisfaction. Though in each of the following chapters we present a relatively isolated discussion of a specific problem and the results we find in our investigation of it, the central theme connecting all the chapters is that they deal with geometric problems of constraint satisfaction. Additionally, in all but the last chapter we use the *Divide and Concur* scheme as a numerical method of discovering solutions. In this introduction we will discuss these two shared aspects, reviewing first some of the many contexts in which geometric constraint satisfaction problems arise and then some of the many considerations which arise when attempting to solve such problems using the Divide and Concur scheme.

Many geometric constraint satisfaction problems take the form of puzzles: the problem consists of individual pieces which need to be arranged in space according to some rules. Putting all the pieces together in such a way that is consistent with all the rules yields a solution. In a physical setting, such problems usually arise in one of two ways: as a direct problem or as an inverse problem. If we have a model of how the microscopic elements in a system interact, and wish to know what collective structure is consistent with such interactions, we arrive at a direct type of constraint satisfaction problem where the structure is the physical result of the constraints. If we wish to study a structure, which cannot be observed directly, by utilizing a number of indirect observations, we arrive at an inverse type of constraint satisfaction problem, where the constraints are the

physical result of the structure.

Formally, we can describe constraint satisfaction problems using a factor graph. The factor graph is a bipartite graph, with one set of nodes A identified with the elements of the puzzle, another set of nodes B associated with constraints, and edges E connecting constraints to the elements they constrain. A configuration is a possible way of laying out the elements, namely an assignment to each element a point in layout space: $y : A \to \Omega$. A configuration satisfies constraint $b \in B$ if its restriction to A_b, the set of elements it is connected to, satisfies some condition $f_b(y|_{A_b}) = 0$. The constraint satisfaction problem is then to find an assignment which simultaneously satisfies all the constraints B. Though each constraint individually might be simple to satisfy, they are hard to satisfy simultaneously because multiple constraints involve the same variable (i.e. they are dependent). Below are some examples of geometric constraint satisfaction problems.

1.1.1 Packing problems

Packing problems might be the simplest and most versatile family of geometric puzzles. In a finite packing problem, we are given a number of solids and we must lay them out in some box so that there are no overlaps between elements. For example, we might be asked to pack N unit disks into a square box of side a. A common problem of interest is to find the largest density possible for some particular type of packing. In the previous example, that would mean finding for a given N the smallest side length a for which a packing is possible [65]. We can also consider the problem of packing an infinite number of unit spheres with the greatest density possible [34]. If we wish to avoid a box with boundaries, but still to consider finite packings, we can consider packings on a compact manifold. For example, the problem of packing spherical caps on an n-sphere

is known as the problem of spherical codes [16].

Spheres have only translational degrees of freedom, so the layout space becomes more complicated when we consider non-spherical objects. For example, in Chapter 2, we consider the problem of packing an infinite number of regular tetrahedra and discover a packing with greater density than any packing previously known. In Chapter 4, we generalize our discussion to a one-parameter family of shapes interpolating between the regular tetrahedron and the sphere. We investigate how the likely optimal packing changes as the shape is changed and what continuous and abrupt transitions arise.

Soft objects may be used instead of hard objects. Soft objects are ones that are allowed to either overlap with each other or deform at some energetic cost. In soft packing problems, we might ask how a finite number of these soft objects may be packed into a given box (or an infinite number at some given density) with the smallest energy (resp. energy density) possible.

Another interesting variation on the infinite packing problem is to limit the type of arrangements allowed. For example, we can ask for the greatest density possible if we restrict ourselves to lattice packings of some object, where the packing is generated from a single object by the action of a group of translations (i.e. a Bravais lattice). In many cases the answer is the same as for the unrestricted problem: for example, for all convex, centrally-symmetric, two-dimensional objects, and for spheres in up to three dimension and probably also other low dimensions [4, 34, 16]. One of the problems considered in Chapter 3 is the problem of lattice sphere packings in up to 14 dimensions. We successfully reproduce in that chapter the densest lattice packings known in each dimension, a result which has not been achieved previously by an unbiased numerical search.

It is worth noting that although packing is very well-suited to this constraint-based formulation, some equally basic and versatile families of problems are not. Notably, the covering problem and the quantizer problem [16] do not have natural formulations in terms of constraint satisfaction problems. It is possible, if unnatural and cumbersome, to formulate these problems as soft packing problems with a series of two-body interactions, three-body interactions, four-body interactions, and so on [67].

1.1.2 Distance Geometry

Another wide family of geometric puzzles are distance geometry problems. In distance geometry problems we attempt to determined a structure, represented by a number of points, based on some knowledge about the distances between the points. For example, we might be given a list of data of the form "the distance between point i and point j is d", and asked to determine a structure that is consistent with this data. Unless we are given the absolute positions of some of the points, we can only determine the structure up to rotations, reflections, and translations. Of course, depending on whether the list of distances is consistent and underconstrained, consistent and overconstrained, or inconsistent, the problem might have, respectively, many, one, or no solutions. In Section 1.3, we study the ensemble of solutions in the underconstrained regime of the problem of random walk reconstruction, where we attempt to reconstruct a random walk based on a partial list of distances.

In some problems, we are not given the distances exactly. This can happen due to noise in the measurement of the distance (in an inverse problem), or because the distance is flexible (in a direct problem). In either case, what we have is a soft distance geometry problem, where we must minimize a cost function that is written in terms of the dis-

tances. The inverse version of the soft distance geometry problem occurs for example in network localization [5], where nodes in a network measure their spatial distances to neighboring nodes (with some noise), and we try to reconstruct the spatial location of the nodes based on the measurements. The direct version occurs when we have a network of atoms connected by bonds of various types, and we wish to determine the equilibrium conformation of the network. In Chapter 6 we consider a theoretical version of such a network, inspired by graphene. We consider a network of atoms connected with bonds as in the honeycomb lattice, except that instead of all bonds being identical, our network has two types of bonds (say, single and double bonds) with different relaxed lengths. We discover an interesting relationship between the relaxed conformation such a sheet takes when allowed to relax in three-dimensional space and an abstract surface associated with the combinatorics of possible assignments of single and double bonds.

Some geometrical puzzles combine many types of constraints. For example, the biomolecular structure determination problem, considered in Chapter 5, combines aspects of soft distance geometry, hard distance geometry, and soft packing. More importantly, it combines aspects of direct and inverse problems: some of the constraints on the structure come from the underlying physical and chemical interactions, while others are derived from nuclear magnetic resonance spectroscopy. In Chapter 5, we develop a framework for biomolecular structure determination using the *Divide and Concur* scheme and use it to reconstruct the structure of a beta-amyloid fibril formed by a peptide associated with Alzheimer's disease [58]. The rigid unit constraint, to be introduced in Chapter 5, is simply a more efficient way of combining many distance constraints.

1.2 The difference map

Some constraint satisfaction problems possess a special structure where the set of constraints B can be partitioned into two sets B_1 and B_2 such that each set is easy to satisfy on its own and in fact allows the projection to the set of satisfying configurations to be computed efficiently. The projection map P_1 (resp. P_2) is a map in the space of configurations, taking any configuration y to the nearest configuration (according to some appropriate metric) that satisfies all the constraints in B_1 (resp. B_2). This map is a projection, in the geometric sense, to the set $\{y|y \text{ satisfies } B_1\}$, or briefly a projection to B_1. In these cases, the difference map becomes a useful tool for discovering solutions. Specifically, if B_1 consists of independent constraints (involving distinct sets of variables), which are easy to satisfy (in the sense of allowing an efficient projection), then B_1 would also be easy to satisfy.

Assuming the configuration space is an affine space, we can construct the difference map as an iterated map in configuration space out of projections and affine combinations:

$$y_{n+1} = DM(y_n) = y_n + \beta(P_1(f_2(y_n)) - P_2(f_1(y_n))) \tag{1.1}$$

$$f_i(y_n) = (1 + \gamma_i)P_i(y_n) - \gamma_i y_n, \tag{1.2}$$

where $\gamma_1 = -1/\beta$ and $\gamma_2 = 1/\beta$. The benefits of using the difference map as a search dynamic in configuration space are manifold, but are not the focus of the discussion here. More details about the workings of the difference map can be found elsewhere [29, 30, 23, 20]. It suffices to mention that the map is computationally simple, that all its fixed points correspond to solutions, fixed points are attractive, and the dynamics of the iteration are such that fixed points are usually rapidly discovered.

In problems where the assumptions above do not hold, we can use the Divide and Concur scheme to convert the problem into one on which the difference map can nev-

ertheless be used. It is possible to give a general recipe for how to apply the scheme, which is universally well defined. However, such a recipe does not capture the flexibility of the scheme and subtleties of how it is used in practice. Therefore, we prefer to give an example of its application, noting where variations might occur.

1.3 Random walk reconstruction

1.3.1 Background

The problem we consider is an instance of the (hard) distance geometry problem. We define a random realization of this problem by generating a three-dimensional random walk $\mathbf{y}_1, \mathbf{y}_2, \ldots \mathbf{y}_N \in \mathbb{R}^3$, where $\|\mathbf{y}_i - \mathbf{y}_{i+1}\| = 1$. Then, we randomly sample M distances from the set of non-fixed distances. The distances we will use to reconstruct the random walk are the $N - 1$ step lengths and the M sampled distances. We use a random walk instead of independently distributed points so that the graph of distances is guaranteed to be connected. More importantly, this is a nice toy model for the biomolecular structure determination problem discussed in Chapter 5, where the chemical bonding along the chain gives local constraints and nuclear Overhauser effect spectroscopy gives non-local constraints.

A typical consideration in constraint satisfaction inverse problems is the transition, as more constraints are introduced, between an underconstrained problem with multiple solutions and an overconstrained problem with a unique solution (the designed solution). Much work has been done to study this transition in discrete problems such as 3SAT, where the transition between underconstraint and overconstraint in the thermodynamic limit occurs at a certain ratio of constraints to variables [55, 56]. At a lower ratio still, in

the underconstrained regime, typical solutions start to resemble to a greater and greater degree the design solution. Namely, the space of solutions acquires an extensive backbone – a finite fraction of the variables in the thermodynamic limit take a fixed value in all solutions [56, 76].

In continuous problems, a simple Maxwellian constraint counting usually predicts the transition between underconstraint to overconstraint [11, 42]. The growth of resemblance of a typical solution to the design solution in the underconstrained regime is our interest here. A measure of how well a reconstructed walk matches the original walk is the root-mean-square deviation (RMSD), which is the root-mean-square distance between the two point configurations after rotations and translations have been applied to one to minimize this distance. Here we attempt to quantify the RMSD between reconstructed solutions and the original walk as a function of N and M.

1.3.2 Divide and Concur

Since the set of $M' = M+N-1$ constraints in this problem cannot be partitioned into two sets which are each easy to satisfy individually, we use the Divide and Concur scheme to make the constraints independent from each other at the expense of introducing a new set of constraints, which will also be independent from each other. We do this by considering replica configurations instead of configurations. Recalling the factor graph, where A is the set of configuration elements (here points), B is the set of constraints (here prescribed distances), and E is the set of edges in the graph (here connecting a distance constraint to the two points defining the distance), configurations are maps $y : A \to \Omega$, where $\Omega = \mathbb{R}^3$ is our layout space in this problem. A replica configuration shall be a map $x : E \to \Omega$, where each edge is assigned a point in the layout space. Since many edges

are incident on each element in A, in a replica configuration each element is represented by multiple replicas that may all be laid out differently. A constraint $b \in B$ is said to be satisfied in a replica configuration if it is satisfied by the replicas on the edges E_b incident on it: $f_b\left(x|_{E_b}\right) = 0$. Thus, the constraints of set B are rendered independent.

We reinterpret the set A as another set of constraints. Namely, we interpret each node in A as an equality constraint between all the layout assignments on the edges incident on it. A replication map takes any configuration into a replica configuration by letting $R(y)(e) = y(a)$ if $e \in E_a$, the set of edges incident on a. Thus, any replica configuration satisfying the constraints A is in the range of R and can be mapped to a configuration $y = R^{-1}(x)$. If a replica configuration satisfies both A and B, it is the replication image of a configuration satisfying B, and is thus a solution.

In the present problem, since the layout space is affine, our replica configuration space is automatically also an affine space and we can use the projections to A and B in the difference map to find solutions. If the layout space is not affine, as when packing disks in a square or when packing spherical caps on the surface of a sphere, we must modify the constraints associated with set A. If the layout space is not already embedded in an affine space, we must embed it as $\Omega \subseteq \mathbb{R}^d$ and define replica configurations as maps $x : E \to \mathbb{R}^d$. Then, in addition to requiring a unique assignment to all edges incident on $a \in A$, we must also require that assignment to lie on Ω. This modification does not usually make the projection much harder to compute.

In some cases, the replication map used above to construct replica configurations results in an unnecessarily high-dimensional configuration space. The important properties of R are that it renders all the constraints B independent, and that we can project with ease to its range. The particular form of R given above is a simple one, that works in general, but there is no particular reason to be restricted to it in any particular prob-

lem. In general, it is often useful and more economical to construct our replication map so that no extraneous replica variables are created. We wish to create enough replica variables so that each constraint is independent, but no more. Therefore, it is usually desirable that for each constraint, the replica configuration space includes as few variables as possible, while keeping projections to the constraint and inversion of the replication computationally simple. In Chapters 3 and 4, where we consider periodic packings, we avoid creating extraneous replicas of the unit vectors defining the periodicity by adding them directly into the relevant replicas.

1.3.3 Results

For each value of the parameters N and M we construct 10 random realizations of the random walk reconstruction problem. We then use 100 runs of the difference map from random initial conditions to obtain an ensemble of solutions. We consider configurations where the root-mean-square deviation from the prescribed distances does not exceed 10^{-14} to be solutions. Figure 1.1 presents sample reconstructions of a random walk based on different numbers of constraints.

In Figure 1.2 we give the expected value (averaged over random realizations) of the mean (averaged over the ensemble) RMSD. We observe that the data collapses nicely when the axes are rescaled by appropriate powers of the length of the walk. That the RMSD should scale as $N^{1/2}$ is an intuitive result, at least for $M = 0$. A less intuitive result is that the relevant number of distance constraints also scales as $M \sim N^{\beta}$ with $\beta \approx 0.5$.

A simple way to interpret these results are in terms of the following scaling argument for a lower bound on the RMSD when $M \ll N$: imagine that the positions of all points

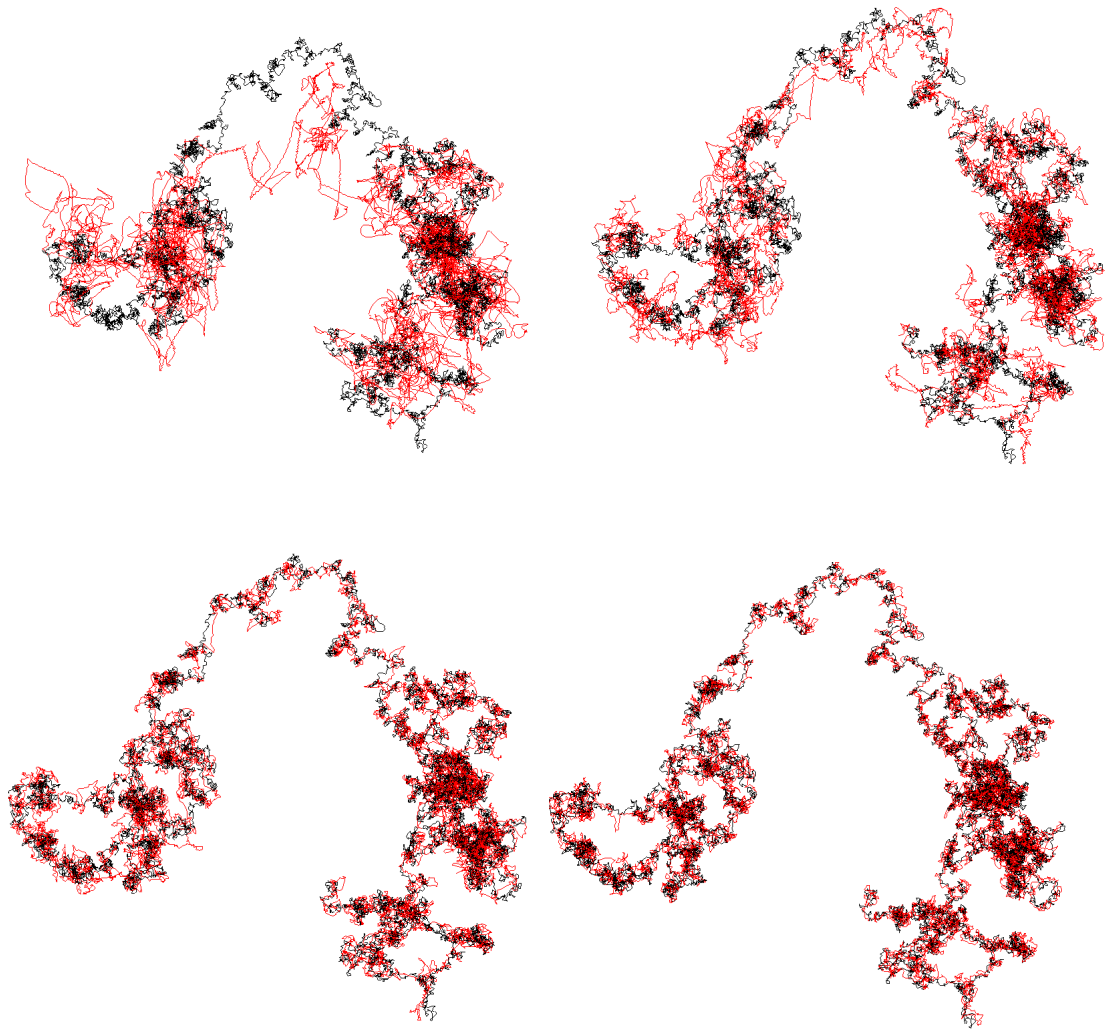

Figure 1.1: Reconstructions of a random walk with $N = 16000$ steps based on $M = 1600$ (top left), $M = 2400$ (top right), $M = 5200$ (bottom left), and $M = 8000$ (bottom right) non-local distance constraints. The original walk is shown in black, and the reconstruction is shown in red.

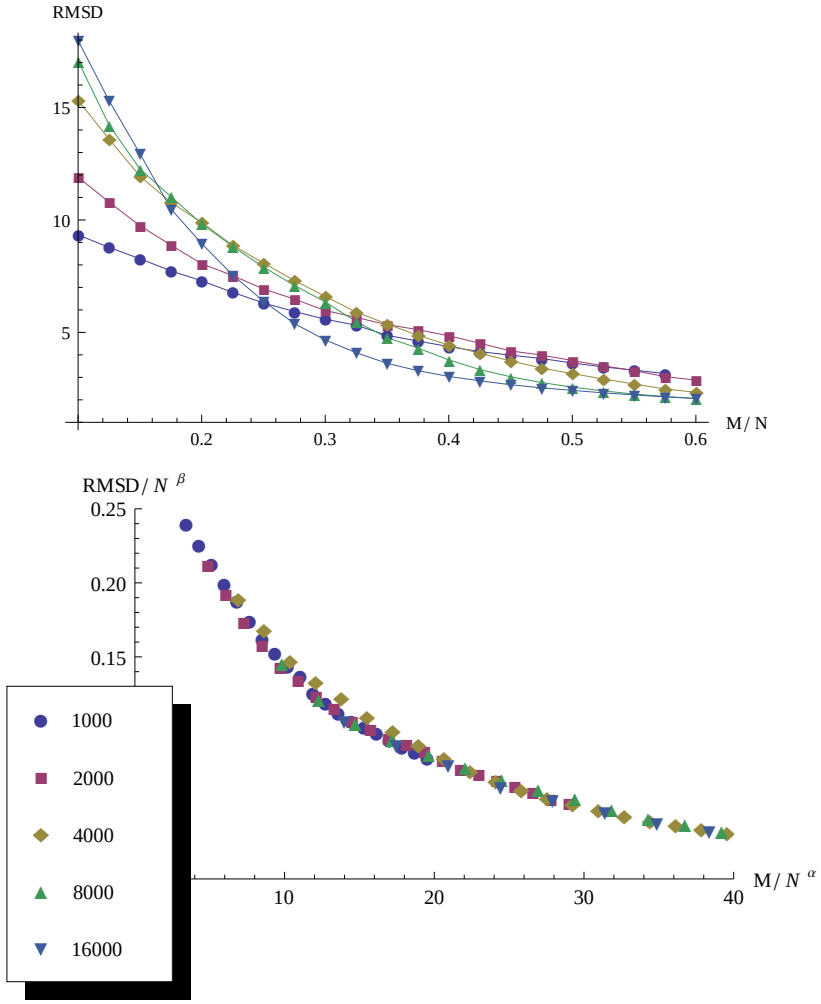

Figure 1.2: The mean RMSD in an ensemble of solutions to the random walk reconstruction problem in the underconstrained region, averaged over ten random realizations for each value of N and M (top). We scale the axes so as to collapse the data on a single curve (bottom). We use $\alpha = 0.51$ and $\beta = 0.53$, although a large range of exponents gives an equally visually pleasing collapse.

participating in a distance constraint were correctly identified – we can hope for no more information than this from the constraints – then the $M + 1$ segments between constrained points, each of approximately N/M steps, would be free chains fixed only at their end points. If the solutions were sampled uniformly from all configurations where the constrained points were at their original positions, then the RMSD would go as $(N/M)^{1/2}$ due to the typical extent of a random walk with fixed ends. This would mean that RMSD$/N^{1/2}$ would vary with M, not $M/N^{1/2}$ as we find. The fact that we find the latter suggests that the solutions are not sampled uniformly and that the free segments more resemble extended chains than a random walk. If we assume extended chains, with a typical extent linear with the number of steps – our lower bound gives that the RMSD should go as N/M, and therefore RMSD$/N^{1/2}$ goes as function of $M/N^{1/2}$ as observed. The non-uniform sampling of the solution space is a property of the particular algorithm used. In fact, this behavior should be expected because the algorithm would quit upon reaching the solution space, yielding a structure on its boundary and not in its interior.

1.4 Conclusion

From the discussion above, we see that applying the Divide and Concur scheme is not achieved simply by following a recipe. Apart from the considerations described above – the embedding of the layout space in an affine space and the choice of an appropriate replication map – there are others – such as optimization of the β parameter and dynamic assignment of metric weights – which are discussed elsewhere [29, 30, 20]. In the subsequent chapters we apply the Divide and Concur scheme to the study of a variety of problems of physical and mathematical interest as discussed earlier in the introduction.

CHAPTER 2

DENSE PERIODIC PACKINGS OF TETRAHEDRA WITH SMALL REPEATING UNITS

The contents of this chapter have been published in *Discrete and Computational Geometry* with coauthors Veit Elser and Simon Gravel [46].

2.1 Abstract

We present a one-parameter family of periodic packings of regular tetrahedra, with the packing fraction $100/117 \approx 0.8547$, that are simple in the sense that they are transitive and their repeating units involve only four tetrahedra. The construction of the packings was inspired from results of a numerical search that yielded a similar packing. We present an analytic construction of the packings and a description of their properties. We also present a transitive packing with a repeating unit of two etrahedra and a packing fraction $\frac{139+40\sqrt{10}}{369} \approx 0.7194$.

2.2 Introduction

The optimization problem of packing regular tetrahedra densely in space has seen invigorated interest over the last few years [17, 12, 69, 68, 33]. This interest has helped drive up the packing fraction of the densest-known such packings from 0.7174 in 2006 [17] to 0.8503 [33] most recently (see Table 2.3). These improved packing fractions have been obtained from more and more complex packings, with larger and larger repeating units. This trend has led some to conjecture that the densest packing of tetrahedra might have inherent disorder [68]. The more restrictive problem of packing tetrahedra transitively

— that is, so that all tetrahedra in the packing are equivalent (a more rigorous definition is given below) — has been less extensively studied and the densest previously-reported transitive packing of regular tetrahedra fills only $2/3$ of space [17]. Here we present a one-parameter family of transitive but dense packings of tetrahedra with the packing fraction $100/117 \approx 0.8547$.

The discovery of this family of dense packings was inspired by the results of a numerical search, which yielded a dense packing with similar structural properties to the packing we present. The numerical method used was adapted from the *divide and concur* approach to constraint satisfaction problems [30]. The *divide and concur* formalism enables us to set up an efficient search through the parameter space consisting of the positions and orientations of tetrahedra inside the repeating unit and the translation vectors governing its lattice repetition, subject to the constraint that no two tetrahedra overlap. The dynamics involved in the *divide and concur* search are highly non-physical, which might explain why our method was able to discover this dense packing, while earlier methods involving more physical dynamics were not [69, 68, 33]. In this note we present only the analytically constructed packing without a full explication of the numerical method, which will be forthcoming.

2.3 One-parameter family of dimer-double-lattice packings

The first set of packings we report on are naturally described as double lattices of bipyramidal dimers. A double lattice is the union of two Bravais lattices related to each other by an inversion operation about some point. In [49], Kuperberg and Kuperberg used the idea of a double lattice in the Euclidean plane to show that any planar convex body can be packed in an arrangement with a packing fraction no smaller than $\sqrt{3}/2$. We

fundamental tetrahedron	$T_0 = \text{conv}\{\mathbf{r}_i \mid i = 1, 2, 3, 4\}$ $\mathbf{r}_1 = \frac{27}{28}\mathbf{a} - \frac{7}{30}\mathbf{b} + \frac{10}{39}\mathbf{c}$ $\mathbf{r}_2 = \frac{1}{4}\mathbf{a} - \frac{9}{10}\mathbf{b}$ $\mathbf{r}_3 = \frac{1}{14}\mathbf{a} + \frac{1}{10}\mathbf{b} + \frac{5}{13}\mathbf{c}$ $\mathbf{r}_4 = \frac{3}{7}\mathbf{a} + \frac{1}{10}\mathbf{b} - \frac{5}{13}\mathbf{c}$
other tetrahedra in the unit cell	$T_1 = R_2(T_0) = \text{conv}\{\frac{2}{3}(\mathbf{r}_2 + \mathbf{r}_3 + \mathbf{r}_4) - \mathbf{r}_1, \mathbf{r}_2, \mathbf{r}_3, \mathbf{r}_4\}$ $T_2 = I(T_0) = -T_0$ $T_3 = I(T_1) = -T_1$
space group generators	translations by $\mathbf{a}$, $\mathbf{b}$, $\mathbf{d}_x = \frac{1}{2}\mathbf{b} + \frac{1}{2}\mathbf{c} + x\mathbf{a}$ I = inversion about 0 R_2 = two-fold rotation about $\{\frac{1}{4}\mathbf{a} + t\mathbf{b} \mid t \in \mathbb{R}\}$
packing fraction	$100/117$
coordinate basis for which tetrahedra are regular with unit edge length	$\mathbf{a} = (2\sqrt{7}/5, 0, 0)$ $\mathbf{b} = (0, \sqrt{3}/2, 0)$ $\mathbf{c} = (0, 0, 13\sqrt{3/14}/5)$

Table 2.1: The construction of the dimer-double-lattice family of packings in terms of the parameter $29/56 \leq x \leq 9/14$ in a general monoclinic coordinate basis ($\mathbf{a} \cdot \mathbf{b} = \mathbf{b} \cdot \mathbf{c} = 0$). The packing is generated starting from the fundamental tetrahedron by the action of the space group. A packing of regular tetrahedra is obtained when the general monoclinic coordinate basis reduces to the specified orthogonal coordinate basis.

naturally extend the idea of the double lattice to the three-dimensional Euclidean space. The repeating unit of one constituent lattice is a bipyramidal dimer: two regular tetrahedra sharing a common face. Two of these dimers with mutually-inverted orientation — a Kuper-pair — form the repeating unit of the double lattice, which thus has four tetrahedra of distinct orientations. We state the existence of the packings as Theorem 1.

Theorem 1. *There exists a one-parameter family of packings of regular tetrahedra, each having packing fraction* $110/117$. *These packings are periodic, with each unit cell of the lattice containing two bipyramidal dimers. The group of isometries leaving each packing invariant is a crystallographic space group of type* $C2/c$ *(following the classification and notation of [54]) and acts transitively on the individual tetrahedra of the packing.*

Proof. We construct each packing by acting on a single regular tetrahedron with a group of isometries. For a coordinate basis we use three pair-wise orthogonal vectors **a**, **b**, and **c**, of norms $|\mathbf{a}| = 2\sqrt{7}/5$, $|\mathbf{b}| = \sqrt{3}/2$, and $|\mathbf{c}| = 13\sqrt{3/14}/5$. The initial tetrahedron $T_0 = \mathrm{conv}\{\mathbf{r}_i \mid i = 1, 2, 3, 4\}$ is the convex hull of four vertices whose coordinates are given in Table 2.1; it is a regular tetrahedron of unit edge length. The group of isometries is the group of crystallographic type $C2/c$ generated by the translations **a**, **b**, and $\mathbf{d}_x = \frac{1}{2}\mathbf{b} + \frac{1}{2}\mathbf{c} + x\mathbf{a}$ ($29/56 \le x \le 9/14$), by the inversion about the point 0, and by the rotation by 180 degrees about the axis $\{\frac{1}{4}\mathbf{a} + t\mathbf{b} \mid t \in \mathbb{R}\}$ [54]. This space group has a point group of order 4 and its translations generate a centered monoclinic point lattice. The construction is summarized in Table 2.1.

By construction, each tetrahedron in the packing is the image of T_0 under an isometry in the group. We have immediately then that all tetrahedra are congruent with T_0, that the packing is invariant under the action of the group, and that the group acts transitively on individual tetrahedra. As the tetrahedra divide into four orbits of the lattice translations, the packing fraction is given by

$$\phi = \frac{4\,\mathrm{vol}(T_0)}{|\det([\mathbf{a}, \mathbf{b}, \mathbf{d}_x])|} = \frac{4(\sqrt{2}/12)}{|\mathbf{a}||\mathbf{b}||\mathbf{c}|/2} = \frac{100}{117}$$

All that is left then to prove the theorem is to verify that the arrangement of tetrahedra thus constructed is indeed a packing. As the packing is transitive (in the sense that its symmetry group acts transitively on the constituent tetrahedra), it is enough to check that one tetrahedron, T_0, does not overlap any other tetrahedron. By means of a closest-lattice-point algorithm such as the one in [1], we generate a list of all tetrahedra whose centroid is, for any $29/56 \le x \le 9/14$, at a distance less than $\sqrt{3/2}$ from the centroid of T_0. There are 46 such tetrahedra. All other tetrahedra have circumspheres which do not intersect the circumsphere of T_0, and therefore they do not intersect T_0. For each tetrahedron in the list we can establish the existence of a separating plane separating it

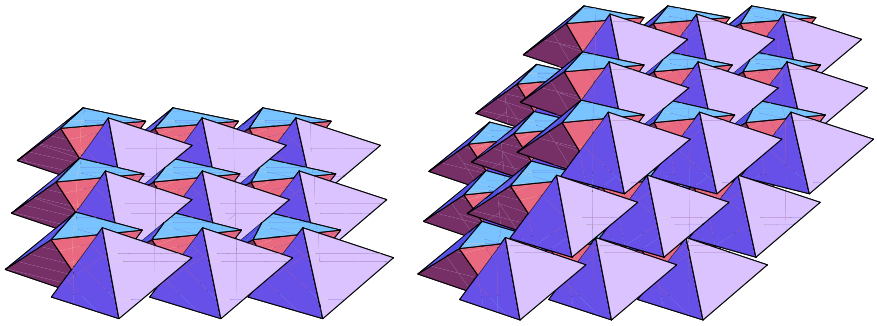

Figure 2.1: Small portions of one layer and three stacked layers in the dimer-double-lattice packing given by $x = 4/7$.

from T_0. Two tetrahedra have no overlap if and only if they are separated by a plane, and moreover, such a plane always exists which passes through three of the eight vertices of the two tetrahedra. By exhaustively verifying that one of the finitely many planes that pass through three of the vertices separates the two tetrahedra, we establish that each tetrahedron in the list can be separated from T_0. □

Note that the above construction, which uses a specific orthogonal coordinate basis $\{\mathbf{a}, \mathbf{b}, \mathbf{c}\}$, is a special case of a general family of packings of non-regular tetrahedra that can be obtained using the same construction, but with a general monoclinic coordinate basis ($\mathbf{a} \cdot \mathbf{b} = \mathbf{b} \cdot \mathbf{c} = 0$). Each of these more general packings is an image of a packing in the original family under an affine map from a three-parameter family (not counting pure dilation). As the lack of overlap between tetrahedra and the packing fraction are both affine-invariant, these are also transitive packings of the same packing fraction.

By the construction of the double lattice, there is an inversion center that sends one lattice of dimers into the other. Note that a lattice translation composed with an inversion about a point corresponds to an inversion about a point related to the original inversion center by half the lattice vector. It follows then that in any primitive unit cell

of the lattice, there are eight such inversion centers. These eight inversion centers form the vertices of a parallelepiped one-eighth the volume of the primitive unit cell of the lattice. This parallelepiped is the equivalent of the "extensive parallelogram" described in [49] whose vertices are the inversion points that generate the double lattice. As in [49], the parallelepiped is inscribed in the body being packed — the bipyramidal dimer in our case.

An interesting feature of the packing is the presence of the free parameter x. The effect of a change in x is to slide fixed layers of the packing relative one another along the **a**-direction. These layers are the layer generated by the translations **a** and **b** from the four tetrahedra of the primitive unit cell and the layers parallel to it. The construction yields a valid packing when the small protrusions in one layer are staggered to fit into small gaps in the neighboring layer, which is the case for all $29/56 \leq x \leq 9/14 \pmod 1$. Within this range, each layer can slide against the neighboring layer without changing the spacing between the two or creating collisions. It is possible then to obtain equally dense, non-transitive packings by staggering consecutive layers arbitrarily within the allowed range.

We describe next the contacts formed by each dimer in the packing, and they are illustrated in Figures 2.1 and 2.2. Each of the eight vertices of the inscribed parallelepiped corresponds to the center of a face-face contact between bipyramids of opposite orientations, accounting for all contacts between oppositely-oriented bipyramids. Four of these contacts are within one layer and four of them are with the layers above and below. The contacts formed between like-oriented bipyramids vary with the parameter x: for all values of x there are two edge-edge contacts, a vertex-edge contact and an edge-vertex contact (all of these contacts occur on two-fold axes and are within one layer); for $x = 29/56$ there are four additional edge-edge contacts with dimers in neighboring

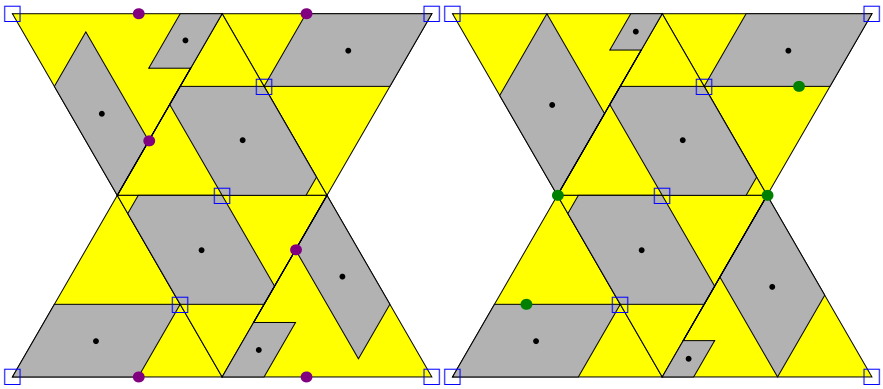

Figure 2.2: The contacts on the surface of a dimer in the dimer-double lattice packing shown on a net diagram for $x = 29/56$ (left) and $x = 9/14$ (right): the face-face contacts (gray), whose centers (black dots) lie on inversion centers, four of which are fixed and four of which move as a function of x; the four point contacts made regardless of the value of x (blue squares), all lying on two-fold axes; the four point contacts formed only for $x = 29/56$ (purple dots); and the four point contacts formed only for $x = 9/14$ (green dots).

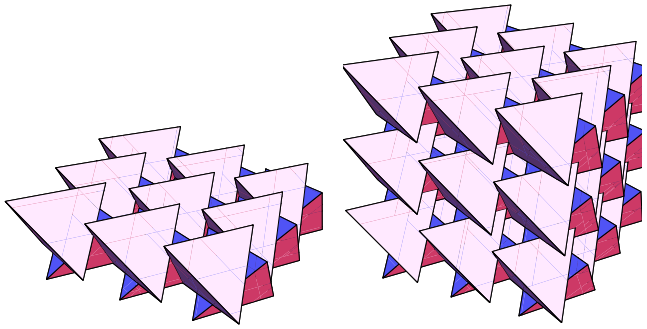

Figure 2.3: Small portions of one layer and three stacked layers in the simple-double-lattice packing.

layers (which turn into overlaps for $x < 29/56$); and for $x = 9/14$ there are instead two vertex-face contacts and two face-vertex contacts with dimers in neighboring layers (which again turn into overlaps for $x > 9/14$). Thus, each dimer makes respectively twelve, sixteen, or sixteen contacts in the three cases, and correspondingly, each tetrahedron makes eight, ten, or eleven contacts.

fundamental tetrahedron	$T_0 = \text{conv}\{\mathbf{r}_i \mid i = 1, 2, 3, 4\}$ $\mathbf{r}_1 = [(433 - 86\sqrt{10})\mathbf{a} + (611 - 133\sqrt{10})\mathbf{b} +$ $(188 - 22\sqrt{10})\mathbf{c}]/246$ $\mathbf{r}_2 = [(111 - 30\sqrt{10})\mathbf{a} + (93 - 75\sqrt{10})\mathbf{b} +$ $(-66 - 42\sqrt{10})\mathbf{c}]/246$ $\mathbf{r}_3 = [(-85 - 28\sqrt{10})\mathbf{a} + (13 - 29\sqrt{10})\mathbf{b} +$ $(4 + 10\sqrt{10})\mathbf{c}]/246$ $\mathbf{r}_4 = [(179 - 106\sqrt{10})\mathbf{a} + (427 - 101\sqrt{10})\mathbf{b} +$ $(-20 - 50\sqrt{10})\mathbf{c}]/246$
other tetrahedron in the unit cell	$T_1 = I(T_0) = -T_0$
space group generators	translations by $\mathbf{a}$, $\mathbf{b}$, $\mathbf{c}$ I = inversion about 0
packing fraction	$(139 + 40\sqrt{10})/369$
coordinate basis for which tetrahedra are regular with unit edge	$\mathbf{a} = (1, -(13 - 4\sqrt{10})/3, 0)$ $\mathbf{b} = (-(4 - \sqrt{10})/3, 3 - \sqrt{10}, -1)$ $\mathbf{c} = (3 - \sqrt{10}, 1, (4 - \sqrt{10})/3)$

Table 2.2: The construction of the simple-double-lattice packing in a general triclinic coordinate basis.

2.4 Simple double-lattice packing

Our numerical search also yielded a packing with two tetrahedra per repeating unit, which we could identify as a simple double lattice (that is a double lattice of tetrahedra, not of dimers) with packing fraction $\frac{139+40\sqrt{10}}{369} \approx 0.7194$. We present therefore a second theorem.

Theorem 2. *There exists a packing of regular tetrahedra having packing fraction* $\frac{139+40\sqrt{10}}{369}$. *This packing is periodic, with each unit cell of the lattice containing two tetrahedra. The group of isometries leaving the packing invariant is a crystallographic space group of type* $P\bar{1}$ *and acts transitively on the individual tetrahedra of the packing.*

The proof of this theorem proceeds equivalently to the proof of Theorem 1. The vertices of the initial tetrahedron T_0 are given in Table 2.2 in terms of a triclinic coordi-

Name	ϕ	N	$\bar{Z}$	Transitive
Optimal lattice[41]	$18/49 \approx 0.3673$	1	14	Yes
Warp and weft[17]	$2/3 \approx 0.6666$	2	10	Yes
Welsh[17]	$17/24 \approx 0.7083$	34	25.9	No
Simple double lattice	$\frac{139+40\sqrt{10}}{369} \approx 0.7194$	2	19	Yes
Wagon wheels[12]	0.7786	18	7.1	No
Compressed wagon wheels[69]	0.7820	72	7.6	No
Disordered wagon wheels[68]	0.8226	314	7.4	No
Quasicrystal approximant[33]	0.8503	656		No
Dimer double lattice	$100/117 \approx 0.8547$	4	8 to 11	Yes

Table 2.3: Some studied transitive and non-transitive packings of regular tetrahedra with packing fraction ϕ, number of tetrahedra in the repeating unit N, and average number of contacts per tetrahedron $\bar{Z}$ where available.

nate basis which is also given in Table 2.2. The group of isometries we use to construct the packing is generated by translation by the three vectors **a**, **b**, and **c** and by inversion about the origin. This is a space group of crystallographic type $P\bar{1}$, with a point group of order 2 and a triclinic lattice [54]. Figure 2.3 shows a portion of the packing.

The simple-double-lattice packing again has eight inversion centers per primitive cell at the vertices of a parallelepiped. However, in this case only five of the vertices are on the surface of the tetrahedron. Each tetrahedron in the packing is in contact with nineteen others.

2.5 Discussion

In Table 2.3, we compare the packings presented here to other studied packings of regular tetrahedra. Both packings are denser than the densest previously-reported transitive packing, a double lattice presented by Conway and Torquato (which we call the ”warp-and-weft” packing due to the interweaving arrangement of its tetrahedra) [17], and the dimer double lattice is denser than any previously-reported packing.

The results presented go against the recent trend of ever-growing repeating units in densest-known packings and demonstrate that a large repeating unit is not a necessary property of a dense packing of regular tetrahedra. It is curious that previous simulations, utilizing a more physical search dynamic [69, 68, 33], yielded dense packings that were either disordered, had quasicrytalline order, or had crystalline order characterized by a very large repeating unit, and were not able to find the denser class of structures presented here, (reminiscent perhaps of Kurt Vonnegut's ice-nine, a fictional phase of water that is more stable, but kinetically unreachable).

Our results yield the surprising situation wherein the densest-known packing of icosahedra is now sparser than the corresponding packing of tetrahedra, a solid which just four years ago was a prime candidate for a counterexample of a conjecture by Ulam that the sphere is the sparsest-packing convex solid [17]. As the packing can be generally extended to any tetrahedron in a three-parameter family generated by deformations of the monoclinic coordinate basis, if any tetrahedron provides a counterexample of Ulam's conjecture, it is not a tetrahedron of that family.

The regular tetrahedron is no longer outcast, as it long was, from the respectable family of convex polyhedra whose largest-achieved packing density is realized by a transitive arrangement. While there are some convex solids whose maximum packing density clearly cannot be achieved by a transitive arrangement (the convex Schmitt-Conway-Danzer polyhedron can tile space, but only in aperiodic and non-transitive ways [18]), the majority of regular and semi-regular polyhedra have been to-date packed most densely in transitive packings [69]. Whether this situation is accidental, the result of bias favoring the discovery of transitive packings, or a more fundamental property governing the packing of a certain class of solids is still an open question.

CHAPTER 3

A METHOD FOR DENSE PACKING DISCOVERY

The contents of this chapter have been published in *Physical Review E* with coauthors Veit Elser and Simon Gravel [47].

3.1 Abstract

The problem of packing a system of particles as densely as possible is foundational in the field of discrete geometry and is a powerful model in the material and biological sciences. As packing problems retreat from the reach of solution by analytic constructions, the importance of an efficient numerical method for conducting *de novo* (from-scratch) searches for dense packings becomes crucial. In this paper, we use the *divide and concur* framework to develop a general search method for the solution of periodic constraint problems, and we apply it to the discovery of dense periodic packings. An important feature of the method is the integration of the unit cell parameters with the other packing variables in the definition of the configuration space. The method we present led to previously reported improvements in the densest-known tetrahedron packing. Here, we use the method to reproduce the densest known lattice sphere packings and the best known lattice kissing arrangements in up to 14 and 11 dimensions respectively (the first such numerical evidence for their optimality in some of these dimensions). For non-spherical particles, we report a new dense packing of regular four-dimensional simplices with density $\phi = 128/219 \approx 0.5845$ and with a similar structure to the densest known tetrahedron packing.

3.2 Introduction

The dense packing behavior of a general solid body (particle) in a Euclidean space is a problem of interest in mathematics, physics, and many other fields. A packing is a collection of particles in the Euclidean space $\mathbb{R}^d$, wherein no two particles overlap (i.e., the intersection of any two particles has an empty interior) and the packing fraction or density ϕ is then the volume fraction of space covered by the particles. Of particular interest are packings of a given particle (wherein all particles are congruent), and the problem of interest is to determine the maximum possible density $\phi_{\max}$ among all packings of a given particle. A packing that realizes this maximum can be thought of as the equilibrium state of the system of classical hard particles in the limit of infinite pressure or zero temperature.

The general problem of packing congruent particles was posed as a part of the eighteenth of David Hilbert's famous *Mathematische Probleme*:

> How can one arrange most densely in space an infinite number of equal solids of a given form, e.g., spheres with given radii or regular tetrahedra with given edges (or in prescribed position), that is, how can one so fit them together that the ratio of the filled to the unfilled space may be as large as possible? [38]

This part of the problem has been taken over the years as the resolution of the Kepler conjecture about the densest packing of spheres in three dimensions [60], and has therefore been considered resolved since the latter was proved by Hales [34]. However, Hilbert's statement of the problem does not single out the sphere, and actually mentions the regular tetrahedron as another particle of interest. Recent work diverging from the focus on spherical particles has spotlighted ellipsoids [19], regular and semi-regular

polyhedra [69, 68] (and the regular tetrahedron in particular [12, 33, 46, 70, 13]), and superballs [44]. Few bounds are known for the maximum packing fraction of general convex particles. Kuperberg and Kuperberg have shown that for any convex particle in two dimensions, $\phi_{\max} \geq \sqrt{3}/2 \approx 0.86602$ [49]. Torquato *et al.* used the known maximal packing density of spheres to derive an upper bound on the packing density of any solid, but this bound is trivial (i.e., $\phi_{\max} \leq \phi^U$, where $\phi^U > 1$) for many solids [69]. Ulam has conjectured that in three dimensions, the sphere achieves the lowest maximum packing fraction, $\phi_{\max} = \pi/\sqrt{18} \approx 0.74048$, among all convex particles [27].

In the quest for dense packings of various particles, analytic and numerical investigations have both played important roles. The former have been very successful in the study of the dense packing of spheres, where analytic constructions based on groups, codes, and laminated lattices have produced the densest-known sphere packings and lattice sphere packings in many dimensions [16]. However, the analytic approach to the construction of dense packings relies on the imagination of the constructor, and for a variety of other problems the densest packings have evaded the creativity of analytic investigators and were only uncovered in computational investigations. While complete (i.e., exhaustive) algorithms exist for some problems (such as the algorithm in Ref. [62], which gave new best known results for the lattice covering and covering-packing problems in some dimensions), they do not exist or have runtimes that are too long for other problems. In those cases, incomplete search algorithms become necessary.

One example of a dense packing that has only been uncovered by a *de novo* numerical search is the currently densest-known packing of tetrahedra, whose structure was first hinted at by a numerical search using the method described in this paper [46]. The structure was later optimized by Torquato and Jiao [70] and by Chen *et al.* [13]. Results of subsequent Monte Carlo simulations have reproduced this structure and suggest it is the

densest packing of regular tetrahedra at least with a small number ($\leq$ 16) of tetrahedra in the unit cell [70, 13]. Another *de novo* search with Monte Carlo dynamics has uncovered a packing based on a quasicrystal approximant reminiscent of the Frank-Kasper σ-phase with a slightly lower density [33]. As these two structures were overlooked by previous analytical investigations [12, 17], it is quite likely that without the results of *de novo* searches, they would have remained unimagined and undiscovered.

In the best case, such searches would produce the optimal packing possible subject to the built-in restrictions (such as number of particles in the unit cell or unit cell shape). However, in problems exhibiting a large degree of frustration, the presence of many local optima that are separated from each other by high barriers complicates the task of finding the optimal packing. The tendency of simulations to get stuck in the local optima of such a rugged optimization landscape, especially when these local optima proliferate as more particles are simulated, has been held responsible for suboptimal results in searches [69, 68]. One technique which has been observed to relieve dynamical stagnation in Monte Carlo simulations at high pressures has been to allow slightly unphysical moves, such as allowing particles to temporarily overlap [33].

We propose a novel search method as an alternative to Monte Carlo simulations, with a number of features that directly address these observations. The method is based on the dynamics of the difference map, a constraint-satisfaction iterative search algorithm, and on the *divide and concur* constraint framework (we abbreviate this combination $D-C$, where the minus sign stands for the difference map) [23, 30, 29]. It adapts the $D-C$ approach to the case of periodic problems and we shall call it *periodic divide and concur* (PDC). The difference map is designed to avoid being trapped in local optima and has been demonstrated in multiple applications to find solutions of highly non-convex problems, including finite packing problems with large numbers of particles, from ran-

dom starting configurations [23, 30, 29]. The search proceeds through a non-physical configuration space, cutting through the conventional physical optimization landscape. Still, it is to be expected that the exponential growth in the number of local optima in the configuration space, which the search will still have to traverse, will nevertheless lead to suboptimal results when many independent particles are included in the search. Therefore, as discussed below, it is crucial for the unit cell variables to be aggressively optimized so that the number of particles to be simulated can be reduced. The incorporation of the unit cell variables directly into the basic dynamics of the search achieves this goal.

Numerical searches are restricted to finite-dimensional configuration spaces, and therefore have been largely limited to investigating periodic packings, packings which are preserved under translations by a lattice Λ. In a general periodic packing, the particles are partitioned into p orbits of the lattice Λ, and when $p = 1$ the packing is called a lattice packing. In physics, any periodic arrangement is usually referred to as a lattice and the special case of $p = 1$ is known as a Bravais lattice. In general, the maximum density need not be realizable by a periodic packing, but arbitrarily close densities are realizable with periodic packings of arbitrarily large p. Similarly, arbitrarily accurate approximations of any packing can be obtained using a sufficiently large cubic or orthorhombic unit cell. However, due to the rapid increase in computational complexity and the proliferation of local optima as the number of independent particles rises, it is often preferable to include fewer particles but allow for a variable unit cell shape. We focus then on searching for packings with a small number of particles in the unit cell.

To our knowledge, variable unit cells have only been introduced recently to searches for dense packings, for instance with the adaptive shrinking cell scheme in Refs. [19, 68] and with the use of Parrinello-Rahman dynamics in the space of lattices in Ref. [14].

The increased particle population associated with restricting unit cell variability can sometimes be tolerated in two and three dimensions, but in high dimensions the number of particles that must be simulated grows exponentially due to the curse of dimensionality and this approach becomes impractical. The constraint-satisfaction formulation of the periodic packing problem used in PDC features a variable unit cell and naturally treats the positions of particles in the unit cell and the unit cell parameters on the same footing. This new approach allows us to successfully look for dense sphere packings in dimensions as high as 14, further than probed by any previously reported unbiased numerical exploration of periodic packings.

Besides the density of a packing, another attribute of interest is the coordination number, that is, the number of nearest neighbors of particles in the packing. In the case of spherical particles, this amounts to the number of spheres in contact with a given sphere, known as the kissing number [16]. Searching for high-coordination number arrangements around a single sphere has been accomplished previously with the $D-C$ method [30]. Here we apply PDC to search for space-filling periodic arrangements of high coordination number, and particularly lattice arrangements.

An efficient *de novo* numerical search method can provide critical utility in the field of packing. In addition to the ability of a *de novo* search to provide confidence in a putative, but not proven, optimal result, a *de novo* search has often been responsible for surprising new results: two recent examples in which unexpected (as it turns out, quasiperiodic) packings were found as the results of *de novo* searches are in the problem of tetrahedron packing [33] and in the ten-dimensional kissing number problem [21]. It is with these motivations that we introduce the PDC method in this paper. In Section 3.3 we introduce the $D-C$ scheme by presenting a simple example which serves to motivate the constructions in the subsequent sections. In Section 3.4 we formulate the problems

tackled in this paper — sphere packing, the lattice kissing number, and polytope packing — in terms of constraint satisfaction. In Section 3.5 we describe in detail aspects of our implementation of the PDC search, including efficient computation of projections to the constraints of Section 3.4. In Section 3.6 we present some results of PDC for the problems discussed, including a newly discovered packing of regular four-dimensional simplices. In Section 3.7 we present concluding remarks.

3.3 Motivation

3.3.1 The $D - C$ scheme

The key step in applying the $D-C$ approach to packing problems is to recast the problem as a problem of constraint satisfaction. Particularly, we must express it as the problem of finding a configuration in a Euclidean configuration space (Ω), which satisfies two constraints. We identify a constraint C with the subset $C \subseteq \Omega$ of configurations satisfying the constraint. A projection of a configuration x to a constraint C is the operation of finding a configuration $x' \in C$ that minimizes the distance $||x - x'||$. Each of the two constraints ($C, D \subseteq \Omega$), must be simple enough that the operation of projecting an arbitrary configuration to it can be computed efficiently. The iterative map used in exploring the configuration space takes advantage of the formulation of the problem in terms of two simple constraints, as outlined in section 3.3.2. In this section we present the application of the $D - C$ scheme to finite sphere packing problems, which has been developed and implemented in Ref. [30], as an introduction to the main ideas of the scheme.

The defining constraint of packing problems is the constraint that no particles in the packing overlap, which we call the *exclusion constraint*. As a simple illustration of this

constraint, consider the exclusion of a pair of unit-radius disks in $\mathbb{R}^2$. In this case, the configuration space Ψ is parameterized by the positions of the centers of the two disks:

$$\Psi = \{(\mathbf{x}_1, \mathbf{x}_2) \colon \mathbf{x}_1, \mathbf{x}_2 \in \mathbb{R}^2\}. \tag{3.1}$$

The exclusion constraint is then

$$K_{\text{excl}} = \{(\mathbf{x}_1, \mathbf{x}_2) \in \Psi \colon \|\mathbf{x}_1 - \mathbf{x}_2\| \geq 2\} \subseteq \Psi. \tag{3.2}$$

This constraint adheres to the simplicity criterion of having an efficient method to compute a projection to it. Specifically, the projection is given by

$$\pi_{K_{\text{excl}}}[(\mathbf{x}_1, \mathbf{x}_2)] = \begin{cases} (\mathbf{x}_1', \mathbf{x}_2') & \text{if } \|\mathbf{x}_1 - \mathbf{x}_2\| < 2 \\ (\mathbf{x}_1, \mathbf{x}_2) & \text{otherwise,} \end{cases} \tag{3.3}$$

where,

$$\mathbf{x}_1' = \mathbf{x}_1 + \frac{2 - \|\mathbf{x}_1 - \mathbf{x}_2\|}{2\|\mathbf{x}_1 - \mathbf{x}_2\|}(\mathbf{x}_1 - \mathbf{x}_2) \tag{3.4}$$

$$\mathbf{x}_2' = \mathbf{x}_2 - \frac{2 - \|\mathbf{x}_1 - \mathbf{x}_2\|}{2\|\mathbf{x}_1 - \mathbf{x}_2\|}(\mathbf{x}_1 - \mathbf{x}_2) \tag{3.5}$$

as illustrated in Figure 3.1.

A more complicated case arises when three or more disks are considered. In this case, the exclusion constraint,

$$K_{\text{excl}} = \{(\mathbf{x}_1, \ldots \mathbf{x}_n) \in \Psi \colon \\ \|\mathbf{x}_i - \mathbf{x}_j\| \geq 2 \text{ for all } 1 \leq i < j \leq n\},$$

is not a simple constraint according to the criterion above. Alternatively, we could replace K_{excl} by many pairwise exclusion constraints

$$K_{\text{excl}}^{i,j} = \{(\mathbf{x}_1, \ldots \mathbf{x}_n) \in \Psi \colon \|\mathbf{x}_i - \mathbf{x}_j\| \geq 2\}. \tag{3.6}$$

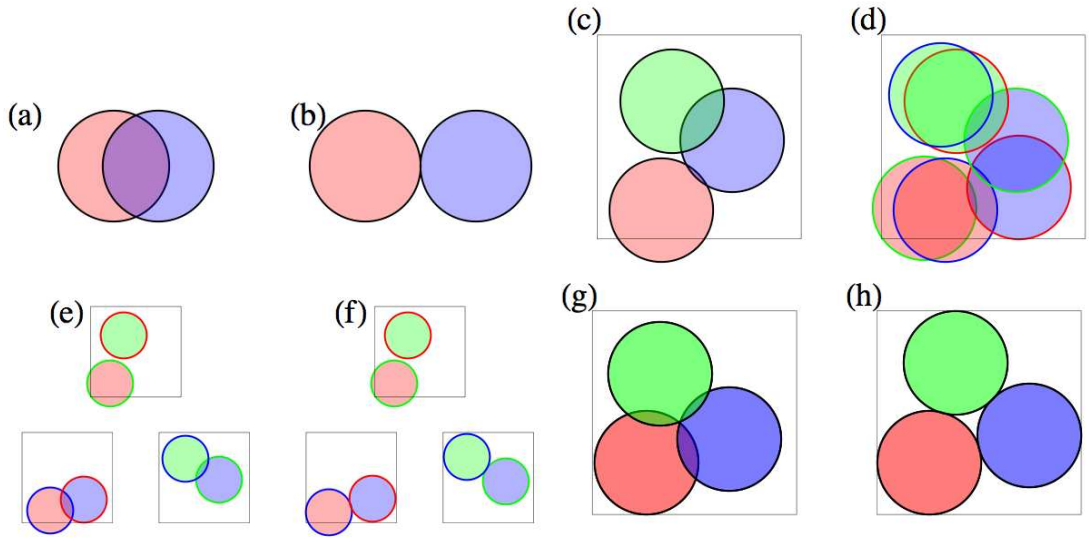

Figure 3.1: An illustration of the $D-C$ scheme in the case of packing three disks into a square box. In the case of two overlapping disks (a), the exclusion constraint is simple in the sense that a projection to the constraint can be performed efficiently. The projection is given by (3.3) and yields the configuration (b). In the case of three disks (c), there is no similarly efficient projection method to the constraint that no overlaps occur. In the $D-C$ scheme, each disk is represented by two replicas (d), which together make three independent replica pairs (e). The exclusion constraint, now also called the "divide" constraint, is modified so that only replica pairs are prohibited from overlapping, and any other overlaps are allowed. Thus, the projection to the exclusion constraint can be performed independently on each replica pair as in the case of two disks (f). A second constraint, the "concur" constraint, requires all replicas representing a single disk to coincide and requires the disk to lie within the confinement box. The result of projecting the configuration (d) to this constraint is the configuration (g). In order to search for a configuration satisfying both constraints, we do not alternately project from one constraint to the other, but instead use the difference map (3.12) to evolve the configuration. The result of a successful search is a configuration (h) satisfying both constraints, which by construction corresponds to a solution of the problem.

The pairwise constraints are all individually simple. However, as noted above, we are limited to problems described by only two simple constraints.

Divide and concur provides a general procedure for reducing the number of simple constraints to two, at the expense of enlarging the configuration space. This reduction is achieved by parameterizing the configuration space with more variables than are necessary to fully specify a configuration. In the example at hand, the new configuration space is

$$\Omega = \{(\mathbf{x}_{1,2}, \ldots \mathbf{x}_{n,n-1}) \colon \mathbf{x}_{i,j} \in \mathbb{R}^2 \text{ for all } i \neq j\}, \tag{3.7}$$

where we call all the variables $\mathbf{x}_{i,j}$ for a particular index i the *replicas* of the original variable $\mathbf{x}_i$. Every configuration $(\mathbf{x}_1, \ldots \mathbf{x}_n) \in \Psi$ can be identified with a configuration $(\mathbf{x}_{1,2}, \ldots \mathbf{x}_{n,n-1}) \in \Omega$, wherein $\mathbf{x}_{i,j} = \mathbf{x}_i$ for all i, j, through a simple linear map A. Enough redundant variables have been introduced to the configuration space so that each pairwise exclusion constraint can now be written in terms of a private set of variables, disjoint from the private variables of other constraints:

$$D^{i,j} = \{(\mathbf{x}_{1,2}, \ldots \mathbf{x}_{n,n-1}) \in \Omega \colon \|\mathbf{x}_{i,j} - \mathbf{x}_{j,i}\| \geq 2\}. \tag{3.8}$$

The intersection, $D \subseteq \Omega$, of all of the pairwise exclusion constraints, which we will call the "divide" constraint, is now also simple, since the projection can be performed independently on each set of private variables (Figure 3.1).

The map $A : \Psi \to \Omega$ from the original configuration space (the *physical configuration space*) to the new one (the *formal configuration space*) is not surjective, and so a general point in the formal configuration space does not correspond to a valid physical configuration. The "concur" constraint $C = A(\Psi)$ is given by the range of A, the subset of Ω that does correspond to valid configurations. That is, the constraint requires redundant specifications of an original variable to concur in regard to its value. Since A is linear, C is also a simple constraint.

Another constraint that must usually be addressed in packing problems with a finite number of particles is the confinement constraint. In most cases the particles, or their centers, are confined to lie in some subset M of space, where M can be either some region of finite volume, or a compact manifold (as in the case of spherical codes). As a subset of the original configuration space, the confinement constraint is written as

$$K_{\text{conf}} = \{(\mathbf{x}_1, \ldots \mathbf{x}_n) \in \Psi \colon \mathbf{x}_i \in M \text{ for all } i\} \subseteq \Psi. \tag{3.9}$$

We can incorporate this constraint into the "concur" constraint, C, by modifying it to be the image $A(K_{\text{conf}})$ instead of the entire range of A. In our example, this would give the constraint

$$C = \{(\mathbf{x}_{1,2}, \ldots \mathbf{x}_{n,n-1}) \in \Omega \colon \mathbf{x}_{i,j} = \mathbf{x}_i \in M \text{ for all } i, j\}. \tag{3.10}$$

Since A is linear, the projection to $C = A(K_{\text{conf}})$ can be decomposed into a projection to $A(\Psi)$ followed by a projection to $A(K_{\text{conf}})$. The first step is performed by taking the average position of all the replicas of each disk. The second step is performed by projecting this average position to M (see Figure 3.1). In general, this two-step projection method is valid for handling the constraints in the physical configuration space that are simple at the outset and do not require the introduction of new variables.

The result of the above construction is that a configuration in Ω satisfies the "divide" and "concur" constraints simultaneously if and only if it corresponds to a configuration in Ψ which satisfies all the exclusion constraints and the confinement constraint; that is, it corresponds to a solution of the packing problem under consideration.

In the following sections we modify the above simple construction so as to generalize the method in two major ways. The first generalization is to packings of infinite regions, instead of only finite ones. Specifically, we allow for periodic packings with an arbitrary unit cell. This is achieved by generalizing the idea of replicas of particles to include also their periodic images. When the unit cell vectors are included in the original

set of parameters, the map from the original parameter space to the space of replica configurations is still linear, though a little more elaborate. Additionally, the confinement constraint of finite packings is replaced in the case of periodic packings by a constraint on the unit cell volume, ensuring a specified density.

The second generalization is to packings of non-spherical particles, specifically convex polytopes. This is achieved by representing each particle not only by the position of its centroid, but by the positions of all its vertices. A new constraint, the rigidity constraint, is added to ensure that the particle is not deformed in the solution. Despite the mathematical complications that arise from these two generalizations, the conceptual framework is identical to the above example, and the constructions in the following sections will draw attention to the analogy with the construction presented above.

3.3.2 The difference map

Given a problem formulated as the task of finding a configuration $\mathbf{x} \in C \cap D$, simultaneously satisfying the constraints $C, D \subseteq \Omega$, we wish to use the availability of efficient methods for computing the projections π_C and π_D to the constraints in order to set up an iterated map to search through the configuration space for a solution. Naive schemes, such as the alternating projections map $\mathbf{x} \mapsto \pi_D(\pi_C(\mathbf{x}))$, suffer from the problem of stagnation at near solutions (local minima of the distance between the two constraints). The difference map, a slightly more sophisticated scheme, is designed to provide efficient search dynamics while avoiding the traps of local minima [23].

The difference map (DM) can be written in terms of the projections π_C and π_D and one parameter β:

$$\mathrm{DM} : \Omega \to \Omega \tag{3.11}$$

$$\mathbf{x} \mapsto \mathbf{x} + \beta \left[\pi_D \left(f_C(\mathbf{x}) \right) - \pi_C \left(f_D(\mathbf{x}) \right) \right], \tag{3.12}$$

where

$$f_D(\mathbf{x}) = \left(1 - \frac{1}{\beta} \right) \pi_D(\mathbf{x}) + \frac{1}{\beta} \mathbf{x},$$
$$f_C(\mathbf{x}) = \left(1 + \frac{1}{\beta} \right) \pi_C(\mathbf{x}) - \frac{1}{\beta} \mathbf{x}.$$

In this paper we use only $\beta = 1$. A difference map search proceeds by starting from a random initial configuration $\mathbf{x}_0$ and iteratively applying the difference map: $\mathbf{x}_i = \mathrm{DM}(\mathbf{x}_{i-1})$ [23]. When the map reaches a fixed point $\mathbf{x}_{fp}$, a solution is obtained by

$$\mathbf{x}_{sol} = \pi_C \left(f_D(\mathbf{x}_{fp}) \right) = \pi_D \left(f_C(\mathbf{x}_{fp}) \right). \tag{3.13}$$

Notice that the ability to obtain a solution from any fixed point of the map, due to the cancelation of the two bracketed terms in (3.12), relies on the definition of the problem in terms of only two simple constraints. For a given iterate $\mathbf{x}_i$, the terms $\pi_C \left(f_D(\mathbf{x}_i) \right)$ and $\pi_D \left(f_C(\mathbf{x}_i) \right)$ provide two estimates of the solution, each satisfying one of the two constraints. We call these respectively the *C*- and *D*-estimates of the solution at the *i*th iteration. The distance between the two estimates is the error ϵ and the search terminates when the error converges to zero.

To summarize, a simple difference map solver for continuous constraints would consist of the following simple steps:

1. Initialize the iterate $\mathbf{x}$ to a random configuration.
2. Compute the two estimates of the solution $\mathbf{x}_C \leftarrow \pi_C \left(f_D(\mathbf{x}) \right)$ and $\mathbf{x}_D \leftarrow \pi_D \left(f_C(\mathbf{x}) \right)$.
3. Compute the error $\epsilon \leftarrow \|\mathbf{x}_C - \mathbf{x}_D\|$. If it is below a predefined convergence threshold, the search terminates, and the solution is given by $\mathbf{x}_C \approx \mathbf{x}_D$.
4. Advance the iterate $\mathbf{x} \leftarrow \mathbf{x} + \beta(\mathbf{x}_D - \mathbf{x}_C)$. Start the next iteration at Step 2.

3.4 Constraints

3.4.1 Periodic sphere packing and kissing

A periodic packing of equal-sized spheres (radius r) in d dimensions can be generated by the action of a lattice Λ on a set of p primitive spheres. Let P be the set of centers of the primitive spheres. We define a *generating matrix* of the packing as a $(d + p) \times d$ matrix M whose first d rows are a set of generators of Λ and whose remaining p rows are the vectors in the set P. Combining these quite different sets of configuration variables into a single matrix serves to remind us that at the highest level of our search algorithm both sets are treated in a uniform manner by the projection operators. The detailed constraints, of course, distinguish among the two parts of M, which we denote M_0 (lattice generators) and M_1 (primitive sphere centers). The set of all the centers of spheres in the packing is then the Minkowski sum

$$\begin{aligned} \Lambda + P &= \{\mathbf{b}_0\mathrm{M}_0 + \mathbf{y} \colon \mathbf{b}_0 \in \mathbb{Z}^d,\ \mathbf{y} \in P\} \\ &= \{\mathbf{b}\mathrm{M} \colon \mathbf{b} \in \mathbb{Z}^d \oplus E_p\}, \end{aligned} \tag{3.14}$$

where E_p is the set of all cyclic permutations of the p-element vector $(1, 0, 0, \ldots, 0)$. The space $\mathbb{R}^{(d+p)\times d}$ of generating matrices takes the role of the physical configuration space Ψ.

A matrix M generates a valid packing if the centers of any two sphere of the packing, $\mathbf{b}_1\mathrm{M}$ and $\mathbf{b}_2\mathrm{M}$, are separated at least by a distance of $2r$ when $\mathbf{b}_1 \neq \mathbf{b}_2$. Each choice of $\mathbf{b}_1$ and $\mathbf{b}_2$ generates a constraint on the matrix M

$$\|\mathbf{b}_1\mathrm{M} - \mathbf{b}_2\mathrm{M}\| \geq 2r, \tag{3.15}$$

which we call an *exclusion constraint*. Note that there are infinitely many independent exclusion constraints (constraints with $\mathbf{b}_1 - \mathbf{b}_2 = \mathbf{b}'_1 - \mathbf{b}'_2$ are not independent).

However, for any non-degenerate matrix M only finitely many independent exclusion constraints are violated or are even remotely close to being violated. In practice, only those constraints need be tested in our computations. We call those constraints the *relevant* exclusion constraints (let there be n of them), and we define a $2n \times (d + p)$ matrix A whose rows $\mathbf{a}_{2i-1}$ and $\mathbf{a}_{2i}$ are the vectors $\mathbf{b}_1$ and $\mathbf{b}_2$ related to the ith relevant exclusion constraint. We discuss below how the relevant constraints are identified.

The linear map $A : \mathrm{M} \mapsto \mathrm{X} = \mathrm{AM}$ is a map from the physical configuration space Ψ to a larger-dimensional space, $\Omega = \mathbb{R}^{2n \times d}$, which we use as the formal configuration space. As before, since the map A is not surjective, only a subset (a linear subspace, in fact) of formal configurations have a corresponding generating matrix in the physical configuration space. The choice of constraints below will guarantee that solutions belong to this subset. The size of the configuration space grows as the number of relevant independent exclusion constraints, which is the number of independent near neighbor pairs for which overlap needs to be actively avoided. Notice that each relevant exclusion constraint can now be written in terms of a private set of variables. Specifically, each row of the matrix X corresponds to the position of one particle, and the ith relevant exclusion constraint is given by

$$D_i = \{\mathrm{X} \in \Omega \colon \|\mathbf{x}_{2i-1} - \mathbf{x}_{2i}\| \geq 2r\}. \tag{3.16}$$

The intersection of all the relevant exclusion constraints forms our "divide" constraint,

$$D = \{\mathrm{X} \in \Omega \colon \|\mathbf{x}_{2i-1} - \mathbf{x}_{2i}\| \geq 2r \text{ for } i = 1, \ldots n\}. \tag{3.17}$$

Each set of private variables associated with one exclusion constraint is composed of the coordinates of replicas of two particles, and we call these two replicas a *replica pair*.

As mentioned in Section 3.3.1, the confinement constraint of finite packing problems is replaced in the case of periodic packings with a constraint on the density of the

packing. The density of a packing generated by a matrix M is given by the density of the unit cell, whose volume is $|\det \mathrm{M}_0|$ and which contains p particles of volume V_1:

$$\phi = \frac{pV_1}{|\det \mathrm{M}_0|}. \tag{3.18}$$

Therefore, if we wish to find a packing of density $\phi \geq \phi_{\text{target}}$, the *density constraint* on the generating matrix will be

$$K_{\text{density}} = \{\mathrm{M} \in \Psi : |\det \mathrm{M}_0| \leq V_{\text{target}}\}, \tag{3.19}$$

where $V_{\text{target}} = pV_1/\phi_{\text{target}}$.

As in the example of Section 3.3.1, since the map A is not surjective, a general element $\mathrm{X} \in \Omega$ of the formal configuration space does not correspond to a well-defined physical configuration. We therefore impose a constraint that requires X to lie in the range of A. In the context of the PDC construction we call this the *lattice constraint* because it requires different periodic images of a primitive particle to lie on the points of a lattice, and requires that lattice to be the same for all primitive particles (up to translation). Again, as in Section 3.3.1, we combine the lattice constraint with the density constraint to form the "concur" constraint:

$$\begin{aligned} C =& A(K_{\text{density}}) \\ =& \{\mathrm{X} = \mathrm{AM} \in \Omega : |\det M_0| \leq V_{\text{target}}\}. \end{aligned} \tag{3.20}$$

With these definitions of the constraint sets, $\mathrm{X} = \mathrm{AM} \in C \cap D$ if and only if M generates a periodic packing of density $\phi \geq \phi_{\text{target}}$. The action of the projections π_D and π_C to the two constraints is illustrated in Figure 3.2 and Sections 3.5.1 and 3.5.2 discuss how the projections are computed efficiently.

The basic operations of the search — projections — depend directly on the metric defined on the formal configuration space. Therefore, the choice of metric affects both

the complexity of implementing the projection and the search dynamics. The simplest choice for the metric is the distance induced from the Frobenius (Euclidean) norm

$$\|\mathrm{X}_1 - \mathrm{X}_2\|_F^2 = \mathrm{trace}\left((\mathrm{X}_1 - \mathrm{X}_2)(\mathrm{X}_1 - \mathrm{X}_2)^T\right). \tag{3.21}$$

This choice of metric amounts to giving all replicas of a particle equal weight in influencing its consensus position in the "concur" projection. We can use a slightly different Euclidean metric, given by

$$\|\mathrm{X}_1 - \mathrm{X}_2\|_\mathrm{W}^2 = \mathrm{trace}\left(\mathrm{W}(\mathrm{X}_1 - \mathrm{X}_2)(\mathrm{X}_1 - \mathrm{X}_2)^T\right), \tag{3.22}$$

where W is a diagonal matrix whose diagonal elements w_i are the metric weights of different replicas. Performance is greatly enhanced by adjusting the metric weights throughout the search to afford greater weight to replica pairs that continually violate their constraints and smaller weight to replica pairs that are in low risk of violating their constraints [30]. Note that removing a constraint from the list of relevant constraints (i.e., removing the corresponding pair of rows from A and X) is equivalent to setting the metric weight of its replicas to zero. Therefore, in the course of the search we not only adjust the weights w_i of replica pairs, but also add and remove replica pairs. The details of how these changes are applied systematically are given in Section 3.5.3.

This constraint formulation of the periodic sphere packing problem (finding a periodic packing with density ϕ_{target}) can be straightforwardly modified to describe instead the periodic kissing number problem (finding a periodic packing with average coordination number τ_{target}). First, the "divide" constraint is modified so that each replica pair must still be separated by a distance of at least $2r$, but at least $p\tau_{\mathrm{target}}$ replica pairs must be separated by a distance of exactly $2r$. Second, the condition on the volume of the unit cell is dropped from the "concur" constraint. Projections to these modified constraints are also given in Section 3.5.

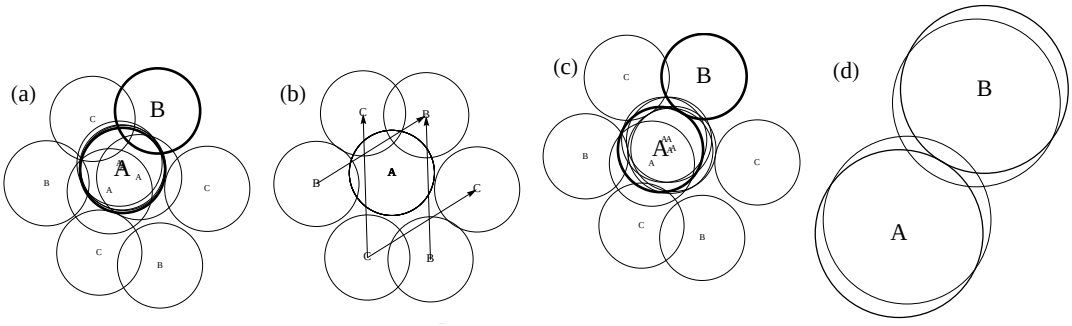

Figure 3.2: An illustration of the "divide" and "concur" projections in the two-dimensional periodic sphere packing problem with $p = 3$. (a) A hypothetical configuration of six replica pairs involving the primitive disk A. Disks with the same letter marking their centers are replicas of the same primitive disk (as for disk *A*) or of its lattice translates (as for disks *B* and *C*). One replica pair, violating its exclusion constraint, is emphasized. (b) The output of the "concur" projection: the closest configuration to (a) such that all replicas of a particular primitive disk lie on top of each other, or a lattice translation apart (arrows), and such that those lattice translations define a lattice with a sufficiently small unit cell volume. This projection is a modification of the "concur" projection depicted in Figure 3.1d,g. (c) The output of the "divide" projection: the closest configuration to (a) such that no replica pair violates its exclusion constraint. This is identical to the "divide" projection depicted in 3.1d-f. Detail: (d) the emphasized replica pair before the "divide" projection (thin-outline disks) and after (thick-outline disks) isolated for clarity.

3.4.2 Convex polytope packing

The symmetry of the spherical particle allows its configuration to be described solely by the position of its center. In the case of a general convex particle, the variables of the configuration space need to include information also about the orientation of the particle. One possible description of the particle assigns variables separately to the position of its centroid and to the description of the rotation about the centroid (e.g., a rotation matrix or a quaternion). In this paper, however, we find it more convenient to describe convex polytopes by reference to the positions of their vertices. Therefore,

a polytope with v vertices is represented by a $v \times d$ vertex matrix and is given by the convex hull of these vertices. Although the configuration of a single particle is no longer represented by a single vector but by a matrix composed of v vectors, it is convenient to treat these matrices as vectors, which we typeset as bold-face upper-case Latin letters (e.g., $\mathbf{X}$ for the vertex matrix of the polytope $K = \operatorname{conv}\mathbf{X} = \operatorname{conv}\{\mathbf{x}_i : i = 1, \dots v\}$), and to construct matrices whose rows are such vectors. A translation by $\mathbf{t}$ of a polytope $\operatorname{conv}\mathbf{X}$ is given by $\operatorname{conv}(\mathbf{X} + \mathbf{c}^T\mathbf{t})$, where $\mathbf{c}^T$ is a column vector of unit elements and $\mathbf{c}^T\mathbf{t}$ is the translation matrix corresponding to the translation vector $\mathbf{t}$. Similarly, a rotation is given by $\operatorname{conv}(\mathbf{X}\mathrm{R})$, where R is a $d \times d$ orthogonal matrix.

A periodic packing is again generated by the action of a lattice Λ on a set of p primitive polytopes whose vertex matrices form the set P. The set of all vertex matrices of polytopes in the packing is the Minkowski sum

$$\begin{aligned} \mathbf{c}^T\Lambda + P &= \{\mathbf{b}_0\mathrm{M}_0 + \mathbf{Y} : \mathbf{b}_0 \in \mathbb{Z}^d,\ \mathbf{Y} \in P\} \\ &= \{\mathbf{b}\mathrm{M} : \mathbf{b} \in \mathbb{Z}^d \oplus E_p\}, \end{aligned} \tag{3.23}$$

where M is a generating matrix of the packing, whose first d rows (comprising M_0) are translation matrices generating Λ, and whose remaining p rows (comprising M_1) are the vertex matrices of the set P. The space of generating matrices $\Psi = \mathbb{R}^{(d+p)\times(v\times d)}$ is the physical configuration space.

Each exclusion constraint between two particles of the packing requires the convex hulls $\operatorname{conv}(\mathbf{b}_1\mathrm{M})$ and $\operatorname{conv}(\mathbf{b}_2\mathrm{M})$ not to overlap for any $\mathbf{b}_1 \neq \mathbf{b}_2$. To construct the formal configuration space we again form one replica pair for the particles involved in each relevant exclusion constraint, which gives $\Omega = \mathbb{R}^{2n\times(v\times d)}$. The map A from physical configurations to formal configurations is given by the matrix A whose rows $\mathbf{a}_{2i-1}$ and $\mathbf{a}_{2i}$ are the vectors $\mathbf{b}_1$ and $\mathbf{b}_2$ related to the ith relevant exclusion constraint. The "divide" constraint is given by the intersection of all the relevant exclusion constraints, each

expressed in terms of its private replica pair:

$$D = \{\mathrm{X} \in \Omega\colon\ \mathrm{int}(\mathrm{conv}\,\mathbf{X}_{2i-1} \cap \mathrm{conv}\,\mathbf{X}_{2i}) = \emptyset \quad \text{for } i = 1, 2, \ldots n\}. \tag{3.24}$$

In addition to the lattice constraint and the density constraints, which combine in Section 3.4.1 to form the "concur" constraint, in the case at hand we must include a third constraint, the *rigidity constraint*. The primitive particles of a packing generated by a general matrix M are only constrained in their number of vertices, not in the arrangement of those vertices. However, we are interested only in packing where all the particles are congruent with a given shape, and so we impose the constraint on M that the vertices of its primitive particles are obtained from the vertices of the given particle by a rigid motion:

$$K_{\mathrm{rigidity}} = \{\mathrm{M} \in \Psi\colon\ \mathbf{Y} = \mathbf{Y}^{(0)}\mathrm{R}_i + \mathbf{c}^T\mathbf{t}_i \quad \text{for all } p \text{ rows } \mathbf{Y} \text{ of } \mathrm{M}_1\}, \tag{3.25}$$

where $\mathbf{Y}^{(0)}$ is the vertex matrix of the given particle. The "concur" constraint $C = A(K_{\mathrm{density}} \cap K_{\mathrm{rigidity}})$ is given by combining the density and rigidity constraints on the generating matrix with the lattice constraint. The result of constructing the "divide" and "concur" constraints is that a formal configuration satisfies both of them if and only if it corresponds to a generating matrix in the physical configuration space which yields a packing of the given particle with the desired density. Table 3.1 summarizes the $D - C$ constraints for the three problems discussed and Section 3.5 describes in detail the projections to these constraints.

	"divide" constraint	"concur" constraint
sphere packing	$\|\mathbf{x}_{2i-1} - \mathbf{x}_{2i}\| \geq 2r$ for all n replica pairs	X = AM M $\in K_{\text{density}}$
kissing number	$\|\mathbf{x}_{2i-1} - \mathbf{x}_{2i}\| \geq 2r$ for all n replica pairs and $= 2r$ for $p\tau_{\text{target}}$ pairs	X = AM
polytope packing	convex hulls of $\mathbf{X}_{2i-1}$ and $\mathbf{X}_{2i+1}$ non-overlapping for all n replica pairs	X = AM M $\in K_{\text{density}}$ and M $\in K_{\text{rigidity}}$

Table 3.1: A summary of the $D - C$ constraints for periodic sphere packing, the average kissing number problem, and polytope packing. The "divide" constraint encompasses the relevant exclusion constraints, while the "concur" constraint encompasses, where applicable, the density, rigidity, and lattice constraints.

3.5 Implementation

3.5.1 "Divide" projections

Sphere packing and kissing

In order to implement an iterated difference map search, whose iterations are given by (3.12), we must implement efficient projections to the "divide" and "concur" constraints. These implementations are the subject of Sections 3.5.1 and 3.5.2. In the course of the search, considerations of efficiency require certain changes to the formal configuration space – specifically adding and removing replica pairs, changing metric weights, and lattice reduction. In section 3.5.3 we discuss when and how these changes are applied.

In the case of sphere packing, the "divide" constraint simply requires that the centers of the two spheres comprising each replica pair be a certain distance apart. This is obtained by applying equation (3.3) to each replica pair. Note that the "divide" projec-

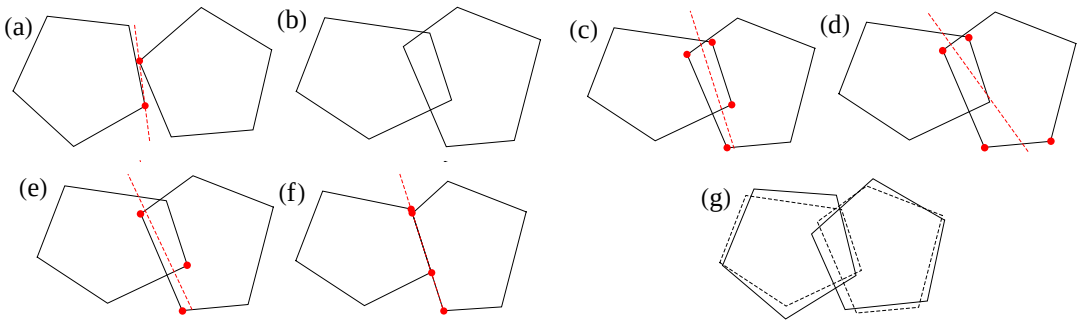

Figure 3.3: An illustration of the polytope exclusion and rigidity constraint projections for the case of regular pentagons. (a) The pentagons are non-overlapping, as demonstrated by the existence of a separating axis (dashed red line) that passes through one vertex of each pentagon (red dots). (b) A hypothetical situation of overlapping pentagons. No axis, and particularly no axis passing through one vertex of each pentagon, separates the two sets of vertices. (c) For the input pentagons in (b), the subset $S = T$ (red dots) that minimizes $\delta(S)^2$, the sum of squared-distances to the least-squares axis (dashed red line) while satisfying that the latter separates the remaining vertices. (d) Another choice of S that yields a valid separating axis, but a larger sum of squared-distances. (e) A choice of S that yields an axis that fails to separate the remaining vertices. (f) Using T found in (c), the output of the projection to the exclusion constraint is determined by moving the points of T onto their least-squares axis. (g) The output (solid line) of the rigidity projection for the input pentagons (dashed) in (b).

tion acts independently on each replica pair, and since the metric weight of all variables specifying one replica pair are equal, the metric weights have no influence on this projection. The action of this projection is illustrated in Figure 3.2. For the kissing number problem, the first case of (3.3) is also used if the replica pair is one of the $p\tau_{\text{target}}$ closest replica pairs.

Convex polytope packing

Although identifying and resolving overlaps between two spheres is straightforward, the same task is more challenging in the case of other convex objects, where more degrees of freedom come into play. The literature on the topic of detecting overlaps (collisions) between polyhedral solids is extensive (driven in part by applications in computer graphics), and many efficient techniques exist for checking whether two convex polyhedra, $\operatorname{conv} X_1$ and $\operatorname{conv} X_2$, overlap (see e.g., [72, 10]). In our case, as we are interested in computing the projection to the exclusion constraint, we also need to determine the distance-minimizing resolution of the overlap. That is, we must find the smallest displacement of the vertices such that the new polyhedra do not overlap. As far as we have been able to determine, there is not an established, efficient computational method developed for this specific problem. The method we provide here is efficient enough for the purpose of packing polyhedra with a small number of vertices, but the computation time required grows exponentially with the number of vertices. A more efficient resolution method for particles with more vertices and for smooth particles is currently in development.

The method relies on the separating plane theorem: the convex hulls of two sets of vertices in $\mathbb{R}^d$ do not overlap if and only if there is a $(d-1)$-dimensional plane that separates the two sets, so that each is contained in a different half-space. The theorem can be made even stronger by specifying that the separating plane can always be chosen to contain d vertices from the given sets, including at least one from each. Therefore, one can check whether two polytopes overlap by checking whether they are separated by any of the planes defined by any such subset of vertices (Figure 3.3a–b). If the polytopes are non-overlapping, the resolution leaves the vertices unchanged.

If the polytopes overlap, we must find the smallest displacement of their vertices

that resolves the overlap. In the resolved configuration there is a separating plane, $V_{sp} = \{\mathbf{r} \in \mathbb{R}^d \colon \hat{\mathbf{n}}_{sp} \cdot \mathbf{r} = h_{sp}\}$, that separates the two sets of vertices. As a consequence of distance minimization, the only vertices moved in the course of the resolution are the vertices which lie on V_{sp} in the resolved configuration. Let T and T' be the pre- and post-resolution positions, respectively, of those vertices that are displaced during the resolution. Therefore, T' is the set of points in V_{sp} closest to the points of T:

$$T' = \{\mathbf{r} + (h_{sp} - \mathbf{r} \cdot \hat{\mathbf{n}}_{sp})\hat{\mathbf{n}}_{sp} \colon \mathbf{r} \in T\} \subseteq V_{sp}. \tag{3.26}$$

The squared norm of the resolution displacement is

$$\sum_{\mathbf{r} \in T} (h_{sp} - \mathbf{r} \cdot \hat{\mathbf{n}}_{sp})^2. \tag{3.27}$$

For any set of points S there is at least one plane $V = \{\mathbf{r} \in \mathbb{R}^d \colon \hat{\mathbf{n}} \cdot \mathbf{r} = h\}$ that minimizes the sum of squared distances

$$\sum_{\mathbf{r} \in S} (\hat{\mathbf{n}} \cdot \mathbf{r} - h)^2. \tag{3.28}$$

We call such a plane a least-squares plane of S. The separating plane of the resolved configuration is always a least-squares plane of T. If this were not the case, a small tilting of the separating plane towards such a least-squares plane (with a corresponding movement of the points in T') would result in a resolution by a smaller displacement. In order to resolve an overlap between polytopes $\operatorname{conv} X_1$ and $\operatorname{conv} X_2$, we therefore have to solve a discrete problem: among all subsets S of $X_1 \cup X_2$ with a least-squares plane separating the remaining vertices $X_1 \setminus S$ from $X_2 \setminus S$, find the one with the minimal sum of squared distances (3.28). This is the set T (Figure 3.3c–f).

The least-squares plane V_{ls} of a set S is determined by minimizing the sum of squared distances (3.28). Note that for a fixed normal direction $\hat{\mathbf{n}}$, the value of h that minimizes the sum is $h = \hat{\mathbf{n}} \cdot \overline{\mathbf{r}}$, where $\overline{\mathbf{r}} = \sum_{\mathbf{r} \in S} \mathbf{r}/|S|$ is the centroid of S. Therefore, we

wish to minimize

$$\sum_{\mathbf{r}\in S}[\hat{\mathbf{n}}\cdot(\mathbf{r}-\overline{\mathbf{r}})]^2 = \hat{\mathbf{n}}\left[\sum_{\mathbf{r}\in S}(\mathbf{r}-\overline{\mathbf{r}})^T(\mathbf{r}-\overline{\mathbf{r}})\right]\hat{\mathbf{n}}^T, \tag{3.29}$$

the minimum of which is equal to the smallest eigenvalue of the symmetric matrix $\sum_{\mathbf{r}\in S}(\mathbf{r}-\overline{\mathbf{r}})^T(\mathbf{r}-\overline{\mathbf{r}})$. The minimum is realized when $\hat{\mathbf{n}}$ is the corresponding eigenvector. Degenerate cases with equal lowest eigenvalues occur, but they do not pose a problem: whenever an optimal separating plane occurs as a degenerate least-squares plane of some set S, its degeneracy implies that there is a least-squares plane of S which also includes an extra vertex; this plane will be equally optimal and will occur as a less degenerate least-squares plane of a superset $S' \supseteq S$. Therefore, the optimal least-squares plane always occurs as a non-degenerate least-squares plane of a set S.

To summarize, the overlap detection and resolution algorithm consists of three steps (illustrated in Figure 3.3a–f):

1. Consider all subsets $S \subseteq X_1 \cup X_2$ of size $|S| = d$ with at least one point from each polytope. Let $V = \{\mathbf{r} \in \mathbb{R}^d : \hat{\mathbf{n}}\cdot\mathbf{r} = h\}$ be a plane that includes S. For each S let

$$\Delta_+^2(S) = \sum_{\substack{\mathbf{x}\in X_1\\ \hat{\mathbf{n}}\cdot\mathbf{x}>h}}(\hat{\mathbf{n}}\cdot\mathbf{x}-h)^2 + \sum_{\substack{\mathbf{x}\in X_2\\ \hat{\mathbf{n}}\cdot\mathbf{x}\le h}}(\hat{\mathbf{n}}\cdot\mathbf{x}-h)^2, \tag{3.30}$$

$$\Delta_-^2(S) = \sum_{\substack{\mathbf{x}\in X_1\\ \hat{\mathbf{n}}\cdot\mathbf{x}\le h}}(\hat{\mathbf{n}}\cdot\mathbf{x}-h)^2 + \sum_{\substack{\mathbf{x}\in X_2\\ \hat{\mathbf{n}}\cdot\mathbf{x}>h}}(\hat{\mathbf{n}}\cdot\mathbf{x}-h)^2, \tag{3.31}$$

$$\Delta^2(S) = \min(\Delta_+^2(S), \Delta_-^2(S)), \tag{3.32}$$

   and let

$$\Delta^2 = \min_S \Delta^2(S). \tag{3.33}$$

   Δ^2 provides a measure for the interpenetration of the two polytopes. If $\Delta^2 = 0$, then a separating plane exists, the input polytopes do not overlap, and the algorithm ends here by returning the original vertex positions X_1 and X_2. If $\Delta^2 > 0$, the polytopes overlap and the algorithm continues to Step 2.

2. Consider all subsets $S \subseteq X_1 \cup X_2$ of size $|S| > d$ with at least one point from each polytope. Let $V = \{\mathbf{r} \in \mathbb{R}^d : \hat{\mathbf{n}} \cdot \mathbf{r} = h\}$ be a least-squares plane of S. If the plane separates the vertex sets with the points of S removed — $X_1 \setminus S$ and $X_2 \setminus S$ — let $\delta^2(S)$ be the sum of squared-distances from S to the plane. Otherwise, let $\delta^2(S) = \infty$. Among the subsets S considered, let T be the subset that minimizes $\delta^2(S)$ and $V_T = \{\mathbf{r} \in \mathbb{R}^d : \hat{\mathbf{n}}_T \cdot \mathbf{r} = h_T\}$ be its associated least-squares plane. As $\delta^2(S) < \infty$ if S contains all vertices, the minimum is always finite. Continue to Step 3.

3. The sets of vertices returned are given by X'_1 and X'_2, wherein $\mathbf{x}' \in X'_1 \cup X'_2$ is given by

$$\mathbf{x}' = \begin{cases} \mathbf{x} & \text{if } \mathbf{x} \notin T \\ \mathbf{x} + (h_T - \mathbf{x} \cdot \hat{\mathbf{n}}_T)\hat{\mathbf{n}}_T & \text{if } \mathbf{x} \in T, \end{cases} \tag{3.34}$$

   where $\mathbf{x} \in X_1 \cup X_2$ is the corresponding original vertex position.

The projection $\pi_D(\mathrm{X})$ to the "divide" constraint (3.24), of an input matrix X comprised of pairs of vertex matrices $\mathbf{X}_{2i-1}$ and $\mathbf{X}_{2i}$, is then achieved by applying the above algorithm independently to all $i = 1, \ldots n$ pairs.

3.5.2 "Concur" projections

Lattice constraint

All the "concur" constraint sets described in this paper are of the form

$$\mathrm{C} = A(K) = \{\mathrm{X} = \mathrm{AM} \in \Omega : \mathrm{M} \in K\} \tag{3.35}$$

where A is constant, and M is variable, but must satisfy a constraint $\mathrm{M} \in K$. The projection then is given by

$$\pi_C : \mathrm{X} \mapsto \mathrm{X}' = \mathrm{AM}, \tag{3.36}$$

where M realizes the minimum over K of the distance

$$\|X - X'\|^2 = \mathrm{trace}\left(\mathrm{W}(\mathrm{X} - \mathrm{AM})(\mathrm{X} - \mathrm{AM})^T\right). \tag{3.37}$$

Absent any constraints on M (as for example in the "concur" constraint for the kissing number problem, where $K = \Psi$), the solution would be given by

$$\overline{\mathrm{M}} = (\mathrm{A}^T\mathrm{WA})^{-1}\mathrm{A}^T\mathrm{WX}. \tag{3.38}$$

This can easily be seen by writing $\mathrm{M} = \overline{\mathrm{M}} + \delta\mathrm{M}$, which gives

$$\begin{aligned} \|X - X'\|^2 &= \mathrm{trace}\left(\mathrm{W}(\mathrm{X} - \mathrm{AM})(\mathrm{X} - \mathrm{AM})^T\right) \\ &= c + \mathrm{trace}(\mathrm{WA}\,\delta\mathrm{M}\,\delta\mathrm{M}^T\,\mathrm{A}^T) \\ &= c + \mathrm{trace}(\mathrm{W}'\delta\mathrm{M}\,\delta\mathrm{M}^T), \end{aligned} \tag{3.39}$$

where $\mathrm{W}' = \mathrm{A}^T\mathrm{WA}$ and the constant term c does not depend on δM. The second term is non-negative, and when M is unconstrained, (3.39) is minimized by letting $\mathrm{M} = \overline{\mathrm{M}}$. Additionally, we have just reduced the constrained case to the problem of finding $\mathrm{M} \in K$ that minimizes the cost function

$$f(\mathrm{M}) = \mathrm{trace}\left(\mathrm{W}'(\mathrm{M} - \overline{\mathrm{M}})(\mathrm{M} - \overline{\mathrm{M}})^T\right). \tag{3.40}$$

This projection strategy parallels the two-step strategy used in Section 3.3.1. First, the formal configuration X is projected to the range $A(\Psi)$ of the physical configuration space, giving $\mathrm{A}\overline{\mathrm{M}}$. Then, the projection of $\overline{\mathrm{M}}$ to the additional constraint K is performed in the physical configuration space using the metric induced on its image in the formal configuration space. Below, we solve the second step of this projection problem for various constraints K.

Density constraint

In the "concur" constraint for the sphere packing problem, the only constraint on the generating matrix is the density constraint. The set of generating matrices M satisfying the density constraint is

$$K_{\text{density}} = \{M : |\det \mathrm{M}_0| \leq V_{\text{target}}\}, \tag{3.41}$$

where M_0 is the generating matrix of the lattice and is given by the first d rows of M. If $|\det \overline{\mathrm{M}}_0| \leq V_{\text{target}}$, then the projection to the constraint (the choice of M that minimizes the cost function (3.40)) is trivially $\mathrm{M} = \overline{\mathrm{M}}$. Otherwise, since M_1 is unconstrained, we can minimize (3.40) with respect to M_1 for a given M_0. This yields $\mathrm{M}_1 = \overline{\mathrm{M}}_1 - \mathrm{W}'^{-1}_{11}\mathrm{W}'_{10}(\mathrm{M}_0 - \overline{\mathrm{M}}_0)$, where W'_{IJ} are the block-elements of W′ acting on M_I to the left and on M_J to the right. Thus, the cost function for M_0 is simply

$$f(M_0) = \operatorname{trace}\left(\mathrm{W}''(\mathrm{M}_0 - \overline{\mathrm{M}}_0)(\mathrm{M}_0 - \overline{\mathrm{M}}_0)^T\right), \tag{3.42}$$

where $\mathrm{W}'' = \mathrm{W}'_{00} - \mathrm{W}'_{01}\mathrm{W}'^{-1}_{11}\mathrm{W}'_{10}$.

The projection becomes easier to analyze in terms of the matrix $\mathrm{L} = (\mathrm{W}'')^{1/2}\mathrm{M}_0$. The cost function then takes the form of the simple Frobenius distance

$$f(\mathrm{L}) = \operatorname{trace}\left((\mathrm{L} - \overline{\mathrm{L}})(\mathrm{L} - \overline{\mathrm{L}})^T\right), \tag{3.43}$$

and the density constraint is still in the form

$$|\det \mathrm{L}| \leq V'_{\text{target}}, \tag{3.44}$$

where $V'_{\text{target}} = V_{\text{target}}/|\det W''|^{1/2}$. Since the absolute value of the determinant of L is given by the product of its singular values, the solution to this minimization problem is given by a matrix $\mathrm{L} = \mathrm{U}\Sigma\mathrm{V}$ with the same (right and left) singular vectors as the matrix

$\overline{\mathrm{L}} = \mathrm{U}\overline{\Sigma}\mathrm{V}$, but different singular values. The cost function expressed in terms of the singular values σ_i and $\overline{\sigma_i}$ of, respectively, L and $\overline{\mathrm{L}}$ takes the form

$$f(\Sigma) = \sum_{i=1}^{d} (\sigma_i - \overline{\sigma_i})^2. \tag{3.45}$$

We numerically minimize this quadratic function subject to the density constraint (3.44). Through back substitution we then have the matrix M that minimizes (3.37) and $\pi_C(X) = \mathrm{X}' = \mathrm{AM}$.

Rigidity constraint

In the "concur" constraint for the polytope packing problem, an additional constraint on the generating matrix M is that the primitive polytopes that make up M_1 are congruent with a given polytope. The generating matrix is then constrained to the set

$$K = K_{\text{density}} \cap K_{\text{rigidity}} \tag{3.46}$$

where

$$K_{\text{density}} = \{\mathrm{M} : |\det \mathrm{M}_0| \leq V_{\text{target}}\},$$

$$K_{\text{rigidity}} = \{\mathrm{M} : \mathbf{Y} = \mathbf{Y}^{(0)}\mathrm{R}_i + \mathbf{c}^T\mathbf{t}_i \quad \text{for all } p \text{ rows } \mathbf{Y} \text{ of } \mathrm{M}_1\}.$$

To calculate the projection $\pi_C(\mathrm{X})$, the cost function (3.40) must be minimized over K. However, since the off-diagonal block W'_{01} couples the lattice parameters M_0 to the primitive particle parameters M_1, this minimization is complicated. Instead of exact minimization, we employ a two-step heuristic method, which results in an approximate projection.

In the first step, we calculate the matrix $\mathrm{M}' \in K_{\text{density}}$ that minimizes the cost function, as in Section 3.5.2. Then, in the second step, we calculate the matrix $\mathrm{M} \in K$ by

applying to each row $\mathbf{Y}$ of M_1' the smallest change so that it becomes a vertex matrix of a polytope congruent with the reference polytope. The second step is achieved by finding the rigid motion applied to the reference polytope which brings its vertices as close as possible to the vertices of $\mathbf{Y}$ as measured by the sum of squared distances (Figure 3.3g). The problem of finding the rigid motion that brings one given list of points closest to another given list, sometimes known as the problem of absolute orientation, occurs frequently in a variety of fields (e.g., in calculating RMSD between two conformations of a biomolecule) and several efficient methods for its solution have been developed (see [39, 40]).

The output of the approximate projection is then given by $X' = \tilde{\pi}_C(X) = AM \approx \pi_C(X)$. As $X' \in C$, the approximate projection gives a configuration in the constraint set, but might not give the closest one to the input configuration. We justify the use of the approximate projection by noting that it is an exact projection if the off-diagonal block W_{01}' is zero. A non-zero off-diagonal block is the result of correlations in the relevant exclusion constraint vectors $\mathbf{b}$ between the coefficients of lattice translations and the coefficients of primitive particle vertex positions. We expect these coefficients to give uncorrelated contributions and to add up to small off-diagonal elements due to random cancellations. Indeed, we find that the off-diagonal block is small in comparison with the diagonal blocks, and we expect our heuristic to yield a good approximate projection.

3.5.3 Formal configuration space maintenance

In our discussion of the choice of metric in Section 3.4, we discussed the ideas of dynamically readjusting the metric (through the weights w_i of the various replicas) and of removing and adding replicas (removing replicas is formally equivalent to setting their

weight to zero). The latter is necessary for implementation reasons: there are infinitely many independent exclusion constraints (and therefore replicas), but we can only represent a finite number of replicas in our implementation. As the set of relevant constraints changes over the course of the search, we must remove and add replicas. Our criterion for which replicas to represent is based on the difference map's current "concur" estimate: we include a replica pair for each pair of particles whose centroids in the "concur" estimate are closer than some cut-off distance. Using the generating matrix obtained in the "concur" projection we can easily find all such pairs using the method of Agrell *et al.* [1]. The cut-off distance is chosen so that at least all replicas that might be in risk of overlap are represented.

The problem of implementation is not the only reason we wish to limit the number of replicas we represent. A proliferation of unnecessary replicas has the adverse effect of attenuating the information obtained from the "concur" projection by diluting the influence of more critical replicas. We observe that such replica proliferation could result not only in a slower search, but also in an increased tendency to become trapped in local optima. Limiting the number of replicas is one way to avoid this effect, but we find it useful to further amplify the information from critical constraints by giving them greater weights [30]. We perform the weight adjustments adiabatically, that is, slowly over the course of many iterations, by updating the weights of each replica pair according to the rule

$$w_i \to \frac{\tau w_i + w_i'(\mathrm{X}_c)}{\tau + 1}, \tag{3.47}$$

where $w_i'(\mathrm{X}_c)$ is a function that assigns replicas weights based on their configuration in the "concur" estimate, and τ is a relaxation time for the replica weights in units of iterations.

In the sphere packing problem (in d dimensions, with unit spheres), we choose the

weight function to be

$$w_i'(\mathrm{X}_c) = \begin{cases} e^{\alpha(4-\|\mathbf{x}_i\|^2)} & \text{if } \|\mathbf{x}_i\| \leq 2 \\ (\|\mathbf{x}_i\|^2 - 3)^{-2-d/2} & \text{if } \|\mathbf{x}_i\| > 2, \end{cases} \tag{3.48}$$

with $\alpha \approx 20$. The dimensional dependence is chosen so that under the assumption of uniform density, the total weight from replicas over a certain distance follows a dimension-independent power law. In the polytope packing problem, we similarly use

$$w_i'(\mathrm{X}_c) = \begin{cases} e^{\alpha\Delta_i^2} & \text{if the polytopes overlap} \\ (1 + r_i^2 - 4r_{in}^2)^{-2} & \text{if not,} \end{cases} \tag{3.49}$$

with $\alpha \approx 10$, where r_{in} is the inradius of the polytope, r_i is the centroid-centroid distance of the polytopes, and Δ_i^2 is the measure of the overlap between the polytopes defined in (3.33).

In addition to the maintenance of replicas, which is performed after every iteration of the difference map, we also periodically perform a lattice reduction using the LLL algorithm [50]. The lattice generated by M_0 is re-represented using the LLL-reduced generating matrix $\mathrm{M}_0' = \mathrm{G}_0\mathrm{M}_0$, where G_0 is a unimodular integer matrix. Additionally, all primitive particles whose centroids are outside of the unit cell given by $\{\sum_i \lambda_i \mathbf{a}_i : -1/2 \leq \lambda_i < 1/2\}$ are re-represented by their lattice-translate in that cell. In summary, the new packing generating matrix M' is given by

$$\mathrm{M}' = \mathrm{G}\mathrm{M} = \begin{pmatrix} \mathrm{G}_0 & 0 \\ \mathrm{G}_1 & 1 \end{pmatrix} \mathrm{M}, \tag{3.50}$$

where G_1 gives the lattice translations to be applied to the primitive particles. Since the actual positions of the particles, as represented in the matrix $\mathrm{X} = \mathrm{A}\mathrm{M}$, should be unchanged, the lattice reduction must also be applied to the nominally constant matrix A ($\mathrm{A} \to \mathrm{A}' = \mathrm{A}\mathrm{G}^{-1}$).

3.6 Results

3.6.1 Sphere packing

Using the PDC scheme described in the previous sections we perform a *de novo* search for the densest lattice ($p = 1$) sphere packings in dimensions 2—14. The PDC search, starting from random initial configurations, was able to reproduce the densest packing lattices known for all cases, and the results of the search are summarized in Table 3.2. For dimensions 2—8 the lattices are known to be optimal, and for dimensions 9—14 these results are, to our knowledge, the first numerical evidence from a *de novo* search that the known lattices are optimal.

Note that the number of replicas is determined by the number of near neighbors of each sphere, which rises rapidly with the number of dimensions. This rise causes an increased computational storage cost per physical degree of freedom in a PDC search, compared to a constant storage cost per physical degree of freedom in a method involving a local search in the physical configuration space. However, this rise need not affect the scaling of CPU costs, since both search methods need necessarily check a comparable number of particle pairs for possible overlaps.

In dimensions $d = 10, 11, 13$ there are known non-lattice packings with $p = 40, 72, 144$ respectively that are denser than the densest known lattices [16]. In up to 11 dimensions, we searched for non-lattice packings with as many as $p = 12$ primitive spheres, but the searches did not produce packings denser than the lattice packings. For a density target matching the lattice density, the searches reproduced the lattice packing, suggesting that the lattice packing in these dimensions is the optimal packing with a small number of spheres in the unit cell.

d	Λ_{densest}	$\phi^{(L)}_{\text{densest}}$	$\langle N_{\text{iter}} \rangle$	$\langle n \rangle$	t_{iter}	success rate
2	A_2	0.90690	42	11	$0.1ms$	100/100
3	D_3	0.74047	230	38	$0.2ms$	100/100
4	D_4	0.61685	191	127	$0.4ms$	100/100
5	D_5	0.46526	308	323	$1ms$	100/100
6	E_6	0.37295	173	977	$2ms$	100/100
7	E_7	0.29530	217	2740	$5ms$	96/100
8	E_8	0.25367	99	8528	$20ms$	96/100
9	Λ_9	0.14577	161	16314	$30ms$	85/100
10	Λ_{10}	0.092021	394	31433	$70ms$	47/100
11	K_{11}	0.060432	421	68722	$0.3s$	54/100
12	K_{12}	0.049454	397	204321	$0.9s$	55/100
13	K_{13}	0.029208	577	430796	$2s$	25/100
14	Λ_{14}	0.021624	1652	1007250	$6s$	4/10

Table 3.2: Results of PDC searches for dense lattice packing in dimensions $d = 2, \ldots 14$. For each dimension, 100 runs from random initial conditions were performed with the density target $\phi_{\text{target}} = \phi^{(L)}_{\text{densest}}$, the density of the densest known lattice Λ_{densest} [16]. The runs were limited to 5000 iterations, and the number of converged runs is quoted in the right-most column. For dimensions 10 and above, each run was first allowed to converge at a density target of $0.8\phi_{\text{densest}}$ and then continued with the final target. The mean number of difference map iterations in converged runs was $\langle N_{\text{iter}} \rangle$, and the mean number of relevant exclusion constraint used was $\langle n \rangle$. Each iteration took an average runtime of t_{iter} on a single 3 GHz CPU. In $d = 14$ only 10 runs were performed with three intermediate targets.

3.6.2 Kissing number

For the kissing number problem, PDC searches were able to reproduce the best known lattice kissing arrangements in dimensions 2—11. In dimensions 2—9, the result is known to be optimal, and for dimensions 10 and 11, we are not aware of previous numerical evidence for their optimality. Table 3.3 summarizes the performance of our method.

d	Λ_{highest}	$\tau^{(L)}_{\text{highest}}$	$\langle N_{\text{iter}} \rangle$	$\langle n \rangle$	success rate
2	A_2	6	27	12	100/100
3	D_3	12	54	40	100/100
4	D_4	24	132	118	98/100
5	D_5	40	163	331	94/100
6	E_6	72	225	928	64/100
7	E_7	126	597	2729	66/100
8	E_8	240	511	6988	55/100
9	Λ_9	272	350	15604	63/100
10	Λ_{10}	336	438	32203	28/100
11	Λ_{11}	438	549	73766	10/100

Table 3.3: Results of PDC searches for lattice packing with high kissing number in dimensions $d = 2, \ldots 11$. For each dimension, 100 runs from random initial conditions were performed with a target coordination $\tau_{\text{target}} = \tau^{(L)}_{\text{highest}}$, the highest coordination number known for a lattice of that dimension, Λ_{highest} [16]. The runs were limited to 5000 iterations, and the number of converged runs is quoted in the right-most column. The mean number of difference map iteration in converged runs was $\langle N_{\text{iter}} \rangle$, and the mean number of relevant exclusion constraints used was $\langle n \rangle$.

3.6.3 Polytope packing

By inspection of a packing of regular tetrahedra yielded by our numerical search during early phases of its development, we were able to construct a new transitive, periodic ($p = 4$) packing of tetrahedra with a higher density ($\phi \approx 0.8547$) than previously reported [46]. This packing takes the form of a double lattice of bipyramidal dimers (the union of two face-sharing tetrahedra). The packing has since been slightly improved to a closely related, but less symmetric packing with density $\phi \approx 0.8563$ [70, 13]. In its current form, our search method is able to reproduce this densest known packing reliably (fifteen out of a hundred runs converged within the iteration limit), and Figure 3.4 shows the results of a sample run converging to this packing.

For the problem of packing regular four-dimensional simplices (pentatopes) in four-

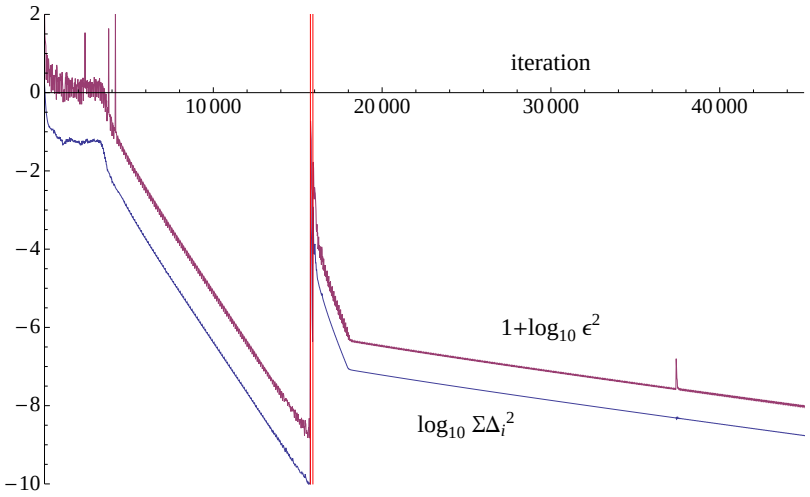

Figure 3.4: The course of a sample run searching for dense periodic packings ($p = 4$) of unit edge-length regular tetrahedra. The plot shows $\sum \Delta_i^2$, a measure of the total interpenetration between tetrahedra in the "concur" estimate (lower blue line, defined in (3.33)), and ϵ^2, the squared distance between the "divide" and "concur" estimates (upper purple line, shifted up for clarity), both on a logarithmic scale. The density target for the search is started at $\phi_{\text{target}} = 0.75$ and adjusted when the search is converged on a solution (vertical red lines) to $\phi_{\text{target}} = 0.82$ (at iteration 15751) and then to $\phi_{\text{target}} = 0.8563$ (at iteration 15898). Each iteration took 14 millisecond on average on a single 3 GHz CPU.

dimensional Euclidean space, we report a new packing discovered by our search method (Figure 3.5). This packing, with density $\phi = 128/219 \approx 0.5845$, is, to our knowledge, denser than any previously reported packing of regular pentatopes. Like the densest known tetrahedron packing, this packing also takes the form of a double lattice of dimers (a dimer here is the union of two cell-sharing pentatopes). This structure, composed of a repeating unit of two oppositely oriented dimers, repeatedly came up as the densest in *de novo* PDC searches with $p = 4$ and $p = 8$ pentatopes in the unit cell, whereas searches with intermediate values of p yielded sparser packings. We subsequently refined the packing with a restricted search where the dimer was taken as the basic particle.

Note that the density reported is slightly lower than that of the densest known pack-

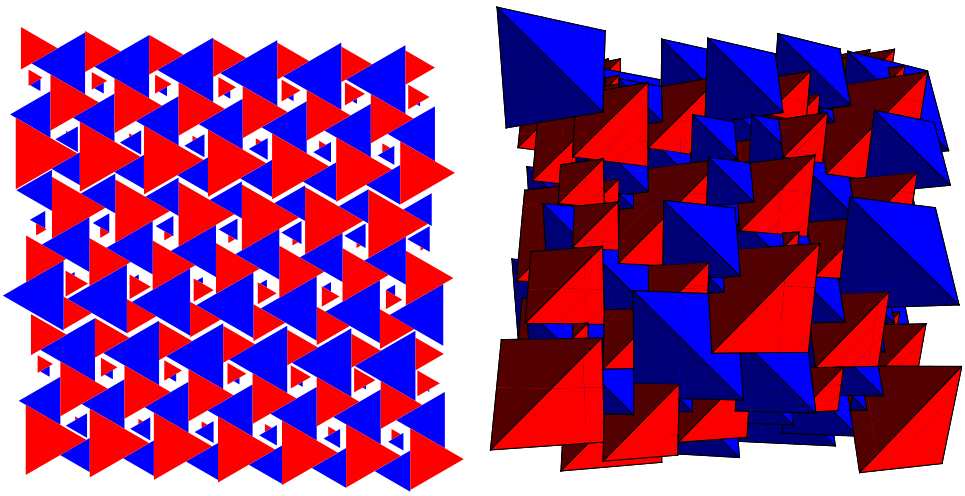

Figure 3.5: Lower dimensional cuts through dense packings of tetrahedra and pentatopes. The top figure shows a two-dimensional cut through the densest known packing of tetrahedra. The plane of the cut is parallel to the bases of the bipyramidal dimers. Triangular sections from dimers of one orientation (red triangles pointing right) and from dimers of inverted orientation (blue triangles pointing left) are visible. The bottom figure shows a three-dimensional cut through the densest known packing of pentatopes. The cut is taken parallel to the bases of the pentatope dimers, and tetrahedral sections from the two dimer orientations (tetrahedra with fore-facing edges oriented in perpendicular diagonal directions) are visible.

ing of four-dimensional spheres ($\phi = \pi^2/16 \approx 0.6169$). It remains to be determined whether this is the case because the optimal packing density of pentatopes is smaller than that of spheres or because the dimer double lattice is suboptimal. The vertex coordinates of the four primitive pentatopes and the generating matrix of the lattice are given in Table 3.4.

primitive pentatopes	$K_1 = \text{conv}\{\mathbf{r}_1, \mathbf{r}_2, \mathbf{r}_3, \mathbf{r}_4, \mathbf{r}_5\}$
	$K_2 = \text{conv}\{\mathbf{r}_2, \mathbf{r}_3, \mathbf{r}_4, \mathbf{r}_5\, \mathbf{r}_6\}$
	$K_3 = \mathbf{t} - K_1$
	$K_4 = \mathbf{t} - K_2$
where	$\mathbf{r}_1 = \sqrt{5}(1,1,1,1)$
	$\mathbf{r}_2 = (3,-1,-1,-1)$
	$\mathbf{r}_3 = (-1,3,-1,-1)$
	$\mathbf{r}_4 = (-1,-1,3,-1)$
	$\mathbf{r}_5 = (-1,-1,-1,3)$
	$\mathbf{r}_6 = -\sqrt{5}(1,1,1,1)$
	$\mathbf{t} = \frac{1}{4}(-7,1,3,3) - \frac{\sqrt{5}}{4}(1,1,1,1)$
lattice	$\Lambda = \mathbb{Z}^4 \mathrm{M}_0$
where	$\mathrm{M}_0 = \frac{1}{4}\begin{pmatrix} -6 & 10 & -6 & 2 \\ -8 & -4 & 4 & 8 \\ -7 & 5 & 9 & -7 \\ 1 & -7 & 9 & -3 \end{pmatrix} + \frac{\sqrt{5}}{4}\begin{pmatrix} 2 & 2 & 2 & 2 \\ 2 & 2 & 2 & 2 \\ 1 & 1 & 1 & 1 \\ 3 & 3 & 3 & 3 \end{pmatrix}$

Table 3.4: Coordinates of the densest pentatope packing discovered by the PDC search ($\phi = 4\,\text{vol}(K_1)/\det(\mathrm{M}_0) = 128/219 \approx 0.5845$).

3.7 Conclusion

In this article we report on the development of PDC, a novel, constraint-based method for discovering dense periodic packings through *de novo* numerical searches. We lay out the principles of the method and demonstrate its application for selected problems. In addition to the dense packing of regular tetrahedra reported in Ref. [46], we also discover a new dense packing of regular pentatopes using the PDC method. We also use the method to numerically recover the lattice sphere packings of highest known density and highest known kissing number in a range of dimensions, providing empirical evidence of their optimality.

In developing the PDC scheme, we adapt the $D - C$ framework to periodic systems.

PDC retains the mindset of the traditional $D - C$ approach of Ref. [30], but generalizes its formalism in a few ways. We introduce an expanded configuration space parameterized by linear combinations of the original parameters, such that these new parameters over-determine the configuration. Therefore, by contrast with the traditional construction, where new parameters are, specifically, redundant copies of original parameters and concurrence is described by the equality of all copies of a given original parameter, here we allow concurrence to be described by a general linear relation. With this generalization, we can treat the periodic images of a particle as "replicas" of the particle, even as they are related by a lattice vector instead of being identical. Thus, the variables describing the periodic repetition of the configuration, namely the lattice vectors, are not imposed as constants or adjusted in dedicated steps. Instead, due to the projection formulation of the dynamics, the unit cell variables that minimize the change to the configuration are determined at each iteration. These variables are treated on the same footing as particle positions and orientations and are optimized as aggressively.

Additionally, we develop a displacement-minimizing overlap resolution algorithm for the convex hulls of two sets of points in $\mathbb{R}^d$. We use this algorithm to implement the projection to the exclusion constraint in the case of polytopal particles.

Unlike Monte Carlo simulations, which explore the physical optimization landscape using stochastic moves, a PDC search uses a deterministic map in an expanded, non-physical configuration space. As such, it is useful when interest lies more in discovering optimal configurations and less in discovering the physical pathways to such configurations. This is also the viewpoint espoused by the so-called "geometric-structure" approach, which emphasizes characterizing structures, without inordinate regard to physically-inspired methods for obtaining them [71]. Moreover, introducing non-physical dynamics has been observed to be important in overcoming dynamical

stagnation [33]. The projection-based dynamics make PDC particularly well-suited in problems with hard constraints, such as hard particle packing, or with step potentials, which prohibit the use of gradient information.

While no direct comparison has been made between the performance of PDC and Monte Carlo searches in the case of periodic packing problems, difference map and $D - C$ methods in the case of other problems have been shown to perform better than or on a par with specialized and general-purpose methods [23, 30, 29, 22]. The generality of the PDC scheme and its demonstrated ability to discover dense packings in a variety of settings indicate its utility as a general method for conducting *de novo* numerical searches and as a possibly attractive alternative to conventional methods [1].

Y. K. acknowledges N. Duane Loh for valuable discussions. This work was supported by grant NSF-DMR-0426568.

[1] An implementation of our algorithm is available upon request from the corresponding author.

CHAPTER 4

DENSE PACKING CRYSTAL STRUCTURES OF PHYSICAL TETRAHEDRA

The contents of this chapter have been published in *Physical Review E* with coauthor Veit Elser [45].

4.1 Abstract

We present a method for discovering dense packings of general convex hard particles and apply it to study the dense packing behavior of a one-parameter family of particles with tetrahedral symmetry representing a deformation of the ideal mathematical tetrahedron into a less ideal, physical, tetrahedron and all the way to the sphere. Thus, we also connect the two well studied problems of sphere packing and tetrahedron packing on a single axis. Our numerical results uncover a rich optimal-packing behavior, compared to that of other continuous families of particles previously studied. We present four structures as candidates for the optimal packing at different values of asphericity, providing an atlas of crystal structures which might be observed in systems of nano-particles with tetrahedral symmetry.

4.2 Introduction

Impenetrable (hard) mathematical bodies (e.g. spheres, spheroids, superballs, and polyhedra) have received much attention as models for the equilibrium behavior of systems of nano-particles and for the wealth of equilibrium and non-equilibrium structures they exhibit [19, 44, 4, 28, 69, 68]. For the tetrahedron alone, quasicrystal structures, novel crystal structures, and glassy structures have been reported in numerical simulations

[69, 68, 46, 33, 13]. However, in all cases, the tetrahedral particles studied were mathematically ideal (polyhedral) tetrahedra. By contrast, in an experiment which found that regular tetrahedra have random packings that are denser than observed for any other body, the tetrahedral macro-particles (dice) used had rounded edges and vertices [43, 2]. Tetrahedral nano-particles used as colloids are not only imperfectly-shaped tetrahedra, but are also sometimes soft, in the sense that the interactions beyond hard-core repulsion are significant [31, 66, 59, 3]. In this paper, we attempt to characterize the packing behavior of physical, rather than mathematical, tetrahedra by studying a one-parameter family of particles with tetrahedral symmetry that interpolates between the mathematical tetrahedron on one end of the parameter's range and the sphere on the other end. We explore the effect of this parameter by constructing, using a *de novo* numerical search, candidate structures for the optimal packing of the different particles in the family.

A particle interpolating between the sphere and the regular tetrahedron can be achieved by a variety of constructions. The simplest construction, probably, is to place the centers of four unit spheres at the vertices of a regular tetrahedron with edges of length a and consider the volume at the intersection of all four spheres. We call the resulting figure a *tetrahedral puff* (Figure 4.1). For a special value of a, the tetrahedral puff is the Reuleaux tetrahedron (a three-dimensional version of the Reuleaux triangle, but not a solid of constant width) [53]. A more convenient parameter than this edge length is the asphericity γ, which is the ratio between the radii of the particle's circumscribing and inscribed spheres. The value $\gamma = 1$ obtained when the four spheres coincide corresponds to a sphere. The value $\gamma = 3$, which is the largest asphericity possible for a convex particle with tetrahedral symmetry and corresponds to a regular tetrahedron, is obtained in the limit that the four spheres intersect at a point. The Reuleaux tetrahedron is the puff with asphericity $\gamma = (3 + \sqrt{24})/5 \approx 1.58$.

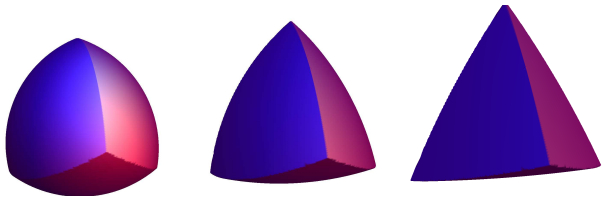

Figure 4.1: Tetrahedral puffs of varying asphericity. From left to right, the asphericities of the puffs shown are $\gamma = 4/3, 2, 8/3$.

4.3 Methods

To efficiently search for candidate optimal packing structures we run a numerical search for packings at increasing densities. To prevent overlaps between different particles in the structure we employ an overlap resolution step. In a packing of congruent particles, every particle can be obtained from a single primitive particle K by a rotation and a translation: $K_1 = \mathrm{R}_1 K + \mathbf{r}_1 = \{\mathrm{R}_1\mathbf{x} + \mathbf{r}_1 | \mathbf{x} \in K\}$, where R_1, a rotation matrix, and $\mathbf{r}_1$, a translation vector, parameterize the configuration of the particle K_1. We call an *exclusion projection* the operation of, for any two particles K_1 and K_2 that overlap, identifying the new set of configuration parameters $(\mathrm{R}_1', \mathrm{R}_2', \mathbf{r}_1', \mathbf{r}_2')$ that resolves the overlap while minimizing the distance in configuration-space from the original configuration, $(\mathrm{R}_1, \mathrm{R}_2, \mathbf{r}_1, \mathbf{r}_2)$. This is the projection in configuration-space to the set of non-overlapping configurations. Below we give the method of implementing this projection.

At high densities, however, we may have to resolve overlaps of a particle with multiple other particles, and the projection that applies to pairs cannot be used directly. Therefore, we introduce multiple independent copies (replicas) of the configuration parameters of each particle, so that after an exclusion projection, any pair of particles will have at least one overlap-free pair of replicas. Another projection ensures that in the final structure obtained from the search all replicas of a single particle agree on its configuration. The two projections are not applied alternately, but instead composed with

linear combinations to give the difference map iteration [23]. This scheme, called *divide and concur* ($D - C$), has previously allowed us to study dense packings of a variety of polyhedral and high-dimensional spherical particles, and is here generalized to any convex particle. Apart from the exclusion projection, described here, the rest of the application of the scheme to dense periodic packing discovery is described in Ref. [47].

Given a pair of particles (or replicas) in a configuration $(\mathrm{R}_1, \mathrm{R}_2, \mathbf{r}_1, \mathbf{r}_2)$ which overlaps, the exclusion projection resolves the overlap by identifying a new set of configuration parameters $(\mathrm{R}'_1, \mathrm{R}'_2, \mathbf{r}'_1, \mathbf{r}'_2)$ while minimizing the distance to the original configuration as defined by

$$d^2 = \sum_{i=1,2} \|\mathbf{r}_i - \mathbf{r}'_i\|^2 + \|\mathrm{R}_i - \mathrm{R}'_i\|^2, \tag{4.1}$$

where the matrix norm is the Frobenius norm. The projection algorithm for a general convex particle is most easily expressed in terms of the particle's support function $h(\mathbf{u}) = \max_{\mathbf{x}\in K} \mathbf{u}\cdot\mathbf{x}$. If the support function $h(\mathbf{u})$ of K is known, then the support function of K_i is $h_i(\mathbf{u}) = \max_{\mathbf{x}\in K} \mathbf{u}\cdot\mathrm{R}_i\mathbf{x} + \mathbf{u}\cdot\mathbf{r}_i = h(\mathrm{R}_i^T\mathbf{u}) + \mathbf{u}\cdot\mathbf{r}_i$ [61].

By the separating plane theorem, K_1 and K_2 do not overlap if and only if a vector $\mathbf{u}$ exists such that $\Delta h(\mathbf{u}) = h_1(\mathbf{u}) + h_2(-\mathbf{u}) \leq 0$ [61]. We can determine if such a vector exists by numerically minimizing $\Delta h(\mathbf{u})/\|\mathbf{u}\|$, which is bounded and attains a minimum over $\mathbf{u}$. If the minimum value of $\Delta h(\mathbf{u})/\|\mathbf{u}\|$ is positive, we must make the minimal change possible to the configuration parameters so that

$$h'_1(\mathbf{u}) + h'_2(-\mathbf{u}) = 0 \text{ for some } \mathbf{u}. \tag{4.2}$$

If we relax the condition that R'_i is a rotation matrix, then we can reduce this constrained optimization problem to a simple unconstrained optimization problem in three vector variables. Namely, these vectors are $\mathbf{u}$, $\mathbf{v}_1 = \mathrm{R}_1'^T\mathbf{u}$, and $\mathbf{v}_2 = \mathrm{R}_2'^T\mathbf{u}$. Given these

three vectors, the new configuration parameters which minimize (4.1) and satisfy (4.2) are given by

$$\mathbf{r}_1' = \mathbf{r}_1 - \frac{\mathbf{u}}{2||\mathbf{u}||^2}\Delta h \tag{4.3a}$$

$$\mathbf{r}_2' = \mathbf{r}_2 + \frac{\mathbf{u}}{2||\mathbf{u}||^2}\Delta h \tag{4.3b}$$

$$\mathrm{R}_i' = \mathrm{R}_i + \frac{\mathbf{u}}{||\mathbf{u}||^2}(\mathbf{v}_i^T - \mathbf{u}^T\mathrm{R}_i), \tag{4.3c}$$

where $\Delta h = h(\mathbf{v}_1) + h(-\mathbf{v}_2) + (\mathbf{r}_1 - \mathbf{r}_2)\cdot\mathbf{u}$ and the configuration distance is given by

$$d^2 = \frac{\Delta h^2/2 + ||\mathbf{u}\mathrm{R}_1 - \mathbf{v}_1||^2 + ||\mathbf{u}\mathrm{R}_2 - \mathbf{v}_2||^2}{||\mathbf{u}||^2}. \tag{4.4}$$

And so, we have reduced the problem, as promised, to an unconstrained minimization of (4.4) over three vector variables. Note that (4.4) is invariant under uniform positive rescaling of $\mathbf{u}$, $\mathbf{v}_1$, and $\mathbf{v}_2$, and the resulting vanishing gradient direction must be taken into account when performing the minimization.

The restriction on R_i to be a rotation matrix, i.e. the requirement on the rigidity of the particle, as in Ref. [47], is restored in the concurrence constraint of the $D-C$ scheme. The projection of a general matrix into the subset of orthogonal matrices is as simple as taking its singular value decomposition and setting all the singular values to unity [37].

As a method for exploring dense configurations of general hard particles, we believe our projection-based method to be more direct and efficient when compared to event-driven MD simulations and stochastic MC methods [44]. Partly, the $D-C$ scheme draws its power from temporarily allowing non-physical configurations, with overlaps, non-concurring replicas, and non-rigid particles, but then systematically acting to minimize these non-physicalities. In MC simulations, such temporary allowance has also been observed to be critical in efficiently exploring structures at high density [33].

4.4 Results

For a selection of puffs of different asphericities, we use the $D - C$ scheme to perform repeated *de novo* searches for periodic packings with $p = 1, 2, 3, 4, 6$, and 8 puffs per unit cell. The densest packing found for each value of γ is reported here as a candidate for the optimal packing structure. Every packing density that is reported here as putatively optimal for a puff of some asphericity has been reproduced by the numerical search at least 3 times from random initial conditions and if the structure has two puffs in the primitive unit cell, it has been reproduced in searches with both $p = 2$ and $p = 4$.

As suggested by the results of our numerical searches, four different packing structures are optimal at different asphericities, separated by one continuous structural transition and two abrupt ones. Of most interest are the structures of the optimal packing for puffs of small asphericity and large asphericity in the parameter ranges near the sphere and the tetrahedron respectively. The optimal packing structure for small asphericity, which we call the $\mathcal{S}_0$-structure (for *simple double lattice*), is a tetragonal double lattice – that is, the union of two lattices (with one particle per unit cell) that are related to each other by an inversion about a point (Figure 4.2) [49]. In the $\mathcal{S}_0$-structure, the puffs are arranged into square layers so that from each layer, the puffs stick out on one side in parallel ridges running in one direction and on the other side in parallel ridges running in a perpendicular direction. By stacking each consecutive layer with a 90° rotation, the ridges of one layer align with the ridges of the layer above it. In the limit $\gamma \to 1$, each layer approaches a square packing of spheres, and the $\mathcal{S}_0$-structure approaches the face-centered cubic sphere packing structure.

For large asphericities, the optimal packing structure, which we call the $\mathcal{D}_0$-structure, is a *dimer double lattice* (i.e. each of the two inversion-related lattices is a

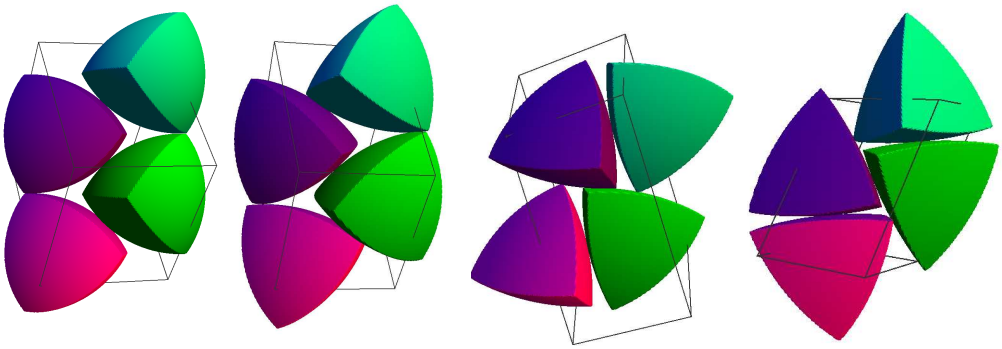

Figure 4.2: A unit cell of each of the four structures described, (from left to right) the $\mathcal{S}_0$-, $\mathcal{D}_1$-, $\mathcal{S}_1$-, and $\mathcal{D}_0$-structures. For the $\mathcal{S}_0$- and $\mathcal{S}_1$-structure, a unit cell consisting of two primitive unit cells is shown. In all cases, the purple (top-left) and pink (bottom-left) puffs are related by inversion to the green (bottom-right) and teal (top-right) puffs respectively. The $\mathcal{S}_0$-structure is a body-centered tetragonal crystal where the body-centered puff is inverted in orientation from the corner puffs. The $\mathcal{D}_1$-structure occurs when next-nearest square layers of the $\mathcal{S}_0$-structure come into contact, and its symmetry is broken by a re-orientation of different puffs of the same layer in different directions. By contrast, the $\mathcal{S}_1$-structure arises by an abrupt transition at both ends of the parameter interval on which it is optimal. In the $\mathcal{D}_0$-structure the mirror planes of the green and teal puffs, which form a dimer, are not aligned, so that both can be in contact with the purple puff. In the limit $\gamma \to 3$, the green and teal puffs become aligned and form a bipyramidal dimer. The structure becomes the dimer double lattice structure reported in Refs. [46, 13] as the densest known packing of regular tetrahedra.

lattice of dimers). The unit cell contains four puffs, two of which, which are in contact and form a shape similar to a triangular bipyramid, are related by inversion to the other two (Figure 4.2). We call each of the two inversion related pairs a dimer, in analogy with the dimer double lattice of Refs. [46, 13], which is the limit of the $\mathcal{D}_0$-structure as $\gamma \to 3$, and is the densest known packing of regular tetrahedra. In this limit, each dimer exactly forms a triangular bipyramid. Note that away from $\gamma = 3$, the mirror planes of the two puffs constituting the dimer are not aligned with each other, making the dimer look twisted. This allows both puffs to form a contact with a nearby puff (see Figure

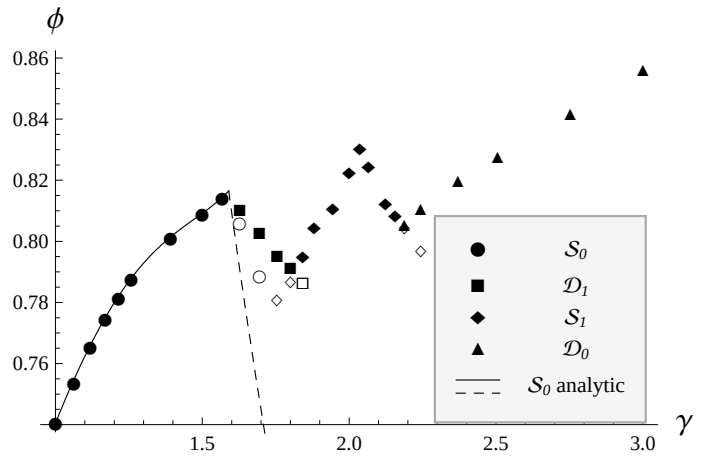

Figure 4.3: Highest densities ϕ (filled markers) achieved for packings of tetrahedral puffs of varying asphericity γ. Densities are obtained and reproduced to an accuracy of 0.0005, much smaller than the marker size. The empty markers represent the density attained by a structure at an asphericity where it is suboptimal, as determined either by runs where the search got trapped away from the optimal structure or by runs where the number of particles per unit cell was incompatible with the optimal structure. The two abrupt structural transitions can be easily seen here where the density line for the $\mathcal{S}_1$-structure crosses the lines for the other structures at critical asphericities at which the $\mathcal{S}_1$-structure coexists with them. On the other hand, the continuous structural transition between the $\mathcal{S}_0$- and $\mathcal{D}_1$-structures is associated with a broken symmetry instead: the line corresponds to an analytic construction of the $\mathcal{S}_0$-structure, imposing its tetragonal symmetry. At $\gamma \approx 1.63$, next-nearest layers come into contact with each other, leading to a sharp decline in density (dashed line). If we allow the tetragonal symmetry to be broken, but still allow only two particle orientations, the $D-C$ search produces slightly higher packing densities (empty disks). The $\mathcal{D}_1$-structure obtains higher densities by continuously breaking that symmetry as well.

4.2), which in the limit of the bipyramidal dimer is facilitated simply by a contact along a common edge or vertex.

The $\mathcal{S}_0$-structure appears to be the optimal packing structure from $\gamma = 1$ to $\gamma \approx 1.63$. On the other end of the asphericity scale, the $\mathcal{D}_0$-structure appears to be optimal from $\gamma \approx 2.19$ to $\gamma = 3$. However, in the intermediate range it appears that both of these

structures are suboptimal and different structures take over. For $\gamma \lesssim 1.63$, the density of the $\mathcal{S}_0$-structure increases monotonically with asphericity. However, for the puff with $\gamma \approx 1.63$, contacts between next-nearest layers of the $\mathcal{S}_0$-structure appear, and start to constrain the layer spacing. Assuming no change to the orientations of the puffs and to the construction of the layers, this constraint leads to a sharp drop in the density of the $\mathcal{S}_0$-structure. However, the structure found by the numerical searches shows a re-orientation of the puffs so that each layer is now composed of puffs of two different orientations (Figure 4.2). This structure, dubbed the $\mathcal{D}_1$-structure, still leads to a decline in the packing density, but a less dramatic one. Therefore, we have a local maximum in the packing density at the transition from the $\mathcal{S}_0$-structure to the $\mathcal{D}_1$-structure. This transition seems to arise by a continuous deformation of the $\mathcal{S}_0$-structure and is not abrupt. The re-orientation of the puffs suggests the beginning of a tendency towards the dimerization seen in the $\mathcal{D}_0$-structure. However, an intermediate structure is encountered between the $\mathcal{D}_1$-structure and the $\mathcal{D}_0$-structure, producing another local maximum in the optimal density. This structure, to be called the $\mathcal{S}_1$-structure, is a simple (non-dimer) double lattice without the tetragonal symmetries of the $\mathcal{S}_0$-structure (Figure 4.2), and is reminiscent of the simple double lattice structure reported in Ref. [46]. This structure appears to be separated from the others by an abrupt transition. Figure 4.3 plots out the densities of the different structures as obtained by the numerical search.

4.5 Discussion

The proper context for the results obtained here for tetrahedral puffs is in comparison to two other one-parameter families of particles that include the sphere as a special case and whose dense packing structures have been investigated vigorously, namely spheroids [19] and superballs [44]. The putative optimal packing of spheroids and su-

perballs becomes monotonically denser the less sphere-like they become. By contrast, the optimal packing density of puffs does not exhibit such monotonicity, although it is always higher than that of the sphere (consistently with a conjecture by Ulam that the sphere is the worst-packing three-dimensional convex solid [27]). Unlike superballs, but like spheroids, the optimal packing of puffs is in all cases (besides the sphere) not a lattice packing, and the crystal unit cell includes at least two particles of different orientations. However, like superballs, and unlike spheroids, the optimal packing structure of puffs goes through an abrupt transition, where two dissimilar structures obtain an equal, optimal density.

A major difference of tetrahedral puffs in comparison to spheroids and superballs is the lack of inversion symmetry. However, not only do the putative optimal packings of puffs in all cases have such a symmetry (Figure 4.2), it is in some cases the only symmetry of the packing besides its lattice translations. Presumably, inversion symmetry plays an important role in forming close-packed structures of particles with tetrahedral symmetry and maybe even of other particles, a result already observed in the plane by Kuperberg and Kuperberg [49].

The tetrahedral puffs exhibit a much richer optimal packing behavior than either spheroids or superballs, and this richness is likely to be mirrored in the behavior of tetrahedral nano-particles. The variety of qualitatively different dense packing structures observed for mathematical tetrahedra is compounded when a physical shape parameter is added. A possible way to experimentally access the parameter investigated here, which describes a swollen tetrahedron, is by using colloidal particles that swell as a function of their temperature [75]. Thus, a variety of structures and structural transitions could be explored. We have attempted here to provide an atlas of the possible crystal structures which might be observed in systems of particles with tetrahedral symmetry. Our

candidates for optimal tetrahedral puff packings provide a starting point for the study of the phase behavior of systems of particles with tetrahedral symmetry, both hard and soft, away from the limit of the mathematical tetrahedron. The method presented here, applicable to any hard convex particle, could also be useful in characterizing possible structures of many other particulate systems.

We thank Simon Gravel for noting the relation of the tetrahedral puff to the Reuleaux tetrahedron and for other helpful suggestions. This work was supported by NSF grant DMR-0426568.

CHAPTER 5

CONSTRAINT-BASED METHOD FOR STRUCTURE DETERMINATION

The contents of this chapter are co-authored with Veit Elser. We acknowledge Robert Tycko for assistance in acquiring and using his published data and results. We acknowledge support from the National Science Foundation under grant number DMR-0426568.

5.1 Abstract

The inverse problem of inferring the structure of biomolecules from a set of structural restraints is the important last step in the process of nuclear magnetic resonance structure determination. Traditional methods minimize a cost/energy function, consisting of physical potentials and restraint potentials, to obtain structural models. By contrast, we present a constraint-based approach where structural models are obtained by treating experimental and physical restraints as hard constraints and using the iterated difference map to obtain configurations that satisfy all the constraints. We apply our approach to determination of the structure of a beta-amyloid fibril formed by a 40-amino-acid peptide associated with Alzheimer's disease based on restraints published in the literature.

5.2 Introduction

Since the first publication of a biomolecular structure solved by nuclear magnetic resonance (NMR) spectroscopy in 1985 [74], the use of NMR techniques for determining the structure of biomolecules has become a leading complementary method to crystallography. Solution and solid state NMR techniques can provide many restraints on the structure of a molecule, including estimates of interatomic distances – based on nuclear

Overhauser effect (NOE) measurements, spin label measurements, or various solid state NMR techniques – estimates of torsional angles – based on chemical shift or J-coupling measurements – location of hydrogen bonds – based on rates of proton exchange – and bond orientation – based on residual dipolar coupling [32, 73, 58].

After acquiring the data and analyzing it to derive restraints on the underlying structure comes the task of using the restraints to construct a three-dimensional model of the structure. Such a molecular model is customarily constructed by minimizing a cost/energy function, which usually combines the potential energy function of a molecular dynamics (MD) force field with additional cost terms corresponding to the various experimental restraints.

Though this general approach has served for many years as a workhorse for structure determinations, there are many things about it that are unsatisfactory. The approach of minimizing a cost function is familiar to us from the problem of fitting a theoretical curve to experimental data. There, the cost function arises as a means of maximizing a statistical likelihood: we know that the theoretical curve cannot fit all data points without error, and the cost function is a way of correctly balancing out the different errors. In structure determination, however, our mindset should be different. To have confidence in a reconstructed model we wish to use a large number of conservative restraints so that all the restraints can be satisfied with good accuracy by a correct model, and the simultaneous satisfaction of all the restraints can lend credibility to the model. In contrast with the curve fitting case, we do expect all errors to be small.

To the cost function associated with the errors in satisfying the experimentally derived restraints, an energy function, associated with a physical force field, is usually added. What we understand from this mystifying mix of the two different types of forces is that the physical realizability of the structure is itself a restraint on it and must

be balanced out against the experimental restraints. Again, this need for balancing out errors belongs to the wrong mindset. That the structure is physically realizable, should always be the case, not merely in a likelihood maximizing way. Moreover, the fact that two structures have different energies, within this reasonable range, should not automatically make one be considered a better solution, since the MD force field energy is an approximation of the real free energy of the structure. This is especially true when the solvent is treated implicitly. Below a certain energy resolution, such force-field energy is unreliable as a discriminator, and over-reliance on it may bias the determined structure.

We present in this work an alternative approach to the problem of structure determination from NMR restraints, which is based directly on the nature of the data as restraints and does not attempt to convert it into an energy minimization problem. Our approach is based on the Difference Map (DM), an iterated dynamical system in the space of configurations. The DM has been used successfully before on a variety of problems that suggests its usefulness in the present case. For example, the protein folding problem has been compared to finding the ground state of spin glasses [9], a task at which a DM approach has been shown to do reasonably well [23]. More relevantly, Elser and Rankenburg have applied the DM to a toy model of the problem of finding ground state conformations of heteropolymers given their monomer sequence [24]. Their difference map implementation was able to discover lower energy conformations than other approaches could. In the toy model they study, the monomers are modeled as soft spheres. In real proteins, of course, amino acids come in a variety of shapes with internal degrees of freedom, and these shapes have to be packed into the core of the folded structure. It is promising then that the DM has also been successfully used for discovering dense packings of a variety of shapes [47, 45]. Finally, the DM has generally been found useful in inverse problems where a hidden configuration is used to generate data, which is then utilized to try to reconstruct the hidden configuration. Such problems include SAT,

where an unknown truth value assignment to a set of variables is reconstructed based on a list of clauses which the assignment satisfies, and phase retrieval, where a two dimensional image is reconstructed based on the magnitudes of its Fourier transform [30, 20].

5.3 Constraint-based approach

The difference map deals, on the lowest level, with constraints. Therefore we seek a formulation of the problem of structure determination from NMR restraints in terms of constraints. Particularly, we wish our formulation to be in terms of two simple constraints, that are each easily satisfied, but are in competition with each other, so that finding a configuration satisfying both (i.e. a solution) is hard. We achieve this with the Divide and Concur approach [30].

5.3.1 Data restraints

As discussed above, there are two sets of restraints which must be utilized to determine the structure. The first is the set of restraints which we extract from NMR data (data restraints), and the second is the set of restraints coming from physical realizability (physical restraints). Within the set of physical restraints, there are again two, fundamentally different, sets of restraints: local and non-local. We refer here to locality along the protein backbone, not to locality in space.

The data restraints are at the center of our structure determination problem. Whereas traditional methods formulate the information extracted from the NMR experiments as soft restraints – that is, potentials to be added on to the cost/energy function to be mini-

mized – we treat them as hard restraints – each to be satisfied individually in a solution. For example, an estimate on the distance between two atoms from a NOE measurement will be treated as a bound (single- or double-sided) on the distance, instead of as a force between the atoms.

5.3.2 Local physical restraints

The local physical restraints deal with the primary structure of the molecule, namely the geometry of covalent bonds. Covalent bonding generates a network of bonds, bond angles, and torsion angles. Bond lengths and bond angles are not given much freedom by quantum chemistry and stay, to a few per cent, at a fixed value, determined by the type of bonds and functional groups involved [25]. Therefore, the conformational freedom of the molecule comes principally from the possibility of torsional rotations about bonds, although the torsional angle about some bonds (like the peptide bond) is also fixed.

Most MD packages enforce this fixed covalent geometry by means of a potential energy where each bond length, bond angle, and dihedral angle is subject to a separate potential of the form $V(x) = k_x(x - x_0)^2$, where x_0 represents the equilibrium value of the variable [52]. Of course, the quantum chemistry leading to these equilibrium values is not as simple as the form of these potentials might suggest. For example, different bonds and angles should not vary independently, and should have some degree of correlation. While these potentials are therefore inadequate for appropriately capturing deviations from equilibrium values, they are quite adequate if all we want is to constrain the bond lengths and angles to the appropriate covalent geometry. In fact, for this purpose it is enough to have only a single potential for each maximal rigid unit.

A set of atoms is called a rigid unit if the distance between any pair of atoms in it

is fixed. The entire molecule can be partitioned into rigid units that are *maximal*, that is, not proper subsets of rigid units. In such a partitioning, two rigid units may overlap, but may have up to only two (assuming non-collinearity) atoms in common. The form of the potential associated with each rigid unit can be written as the root-mean-square deviation (RMSD) when its atoms are superimposed with the equilibrium configuration of the rigid unit:

$$V(\mathbf{r}_1, \mathbf{r}_2, \ldots) = \min_T \sum_{i=1}^{N} \|\mathbf{r}_i - T(\mathbf{y}_i)\|^2, \tag{5.1}$$

where $\mathbf{r}_1, \mathbf{r}_2, \ldots$ are the coordinates of the atoms comprising the rigid unit, T is any rigid transformation (i.e. a composition of rotations and translations), and $\mathbf{y}_1, \mathbf{y}_2, \ldots$ are the atomic coordinates of a reference rigid unit in equilibrium. We immediately see the advantage of this formulation when inspecting a simple amino acid such as aspargine. While three rigid unit restraints are enough to properly enforce the covalent geometry within the amino acid (see Figure 5.1), it would be necessary to use 11 bond length restraints and 18 angle restraints.

More important however than the form we choose for the restraints that enforce covalent geometry, is the way we choose to treat them within our constraint-based approach. Namely, because the deviations from rigidity are quite small compared to other variables in the problem (such as the softness of non-local potentials and uncertainty in distance bounds), we treat the local physical restraints as hard restraints, instead of soft ones. Practically, this means that instead of adding the local potentials to the combined cost/energy function to be minimized, we require that each potential individually vanishes. Thus, we treat the local physical restraints in the same way we treat the data restraints.

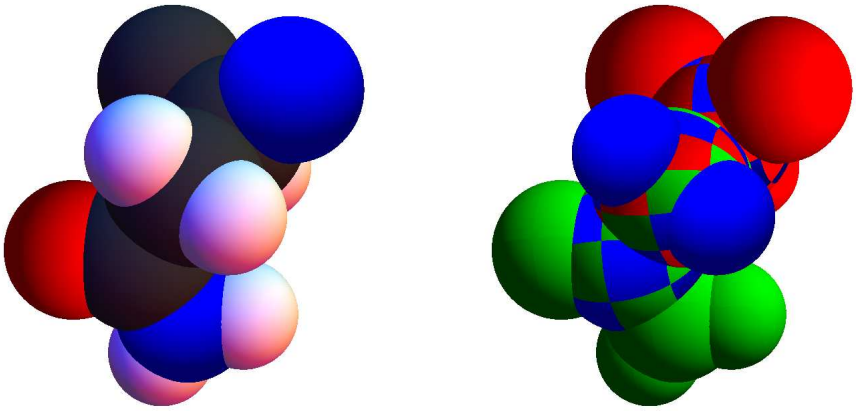

Figure 5.1: An aspargine residue partitioned into maximal rigid units (right). A view from the same angle and with traditional chemical element colors is given (left) for reference. The red, blue, and green rigid units are centered around the C_α, C_β and C_γ atoms respectively. We do not include the H_N and O' atoms, as they do not belong to a maximal rigid unit which is contained inside the residue. Each of these atoms belongs to a planar rigid unit which spans the peptide bond.

5.3.3 Non-local physical restraints

After we remove the local interaction potentials and the data restraint potentials, having turned them into hard restraints, the only components left in the cost/energy function are the non-local interactions. There are many non-local interaction which contribute to stabilizing protein folds and make the structure physically realizable. A balance between attractive interactions such as hydrophobic clustering, salt bridge formation, and hydrogen bonding, and repulsive interactions, such as exclusion of van der Waals spheres, stabilize the structure. However, when reconstructing structures based on NMR data, it is possible and customary to rely only on the experimental restraints and the repulsive interactions, ignoring the attractive ones [58]. As a model for the energy due to non-local interaction, we may use a standard MD force-field with all local energy terms

turned off.

While this energy function is no longer a mystifying mix of real and imaginary forces, we would still like to avoid a direct minimization of it. Instead we would formulate the requirement of physical realizability as an upper bound on this energy. We are inclined to do so because we do not want to bias the reconstructed structure based on a wrong, oversimplified model of the underlying forces. While imposing an upper bound on the energy of the structure is necessary for getting reasonable structures, we do not want to pretend to know more about the forces acting to stabilize it than we actually do. This is especially important because the model for the non-local interaction is very often chosen for computational efficiency as much as for accurately reproducing physical forces.

5.3.4 Divide and Concur

To summarize, in our formulation of the structure determination problem all we require of a solution is to satisfy three sets of restraints:

1. the experimentally derived restraints (data restraints),
2. the rigid unit restraints (local physical restraints), and
3. a bound on non-local interaction energy (non-local physical restraints).

Whereas the conventional approach to finding a configuration that satisfies a list of restraints is to combine them into a single cost/energy function and attempt global minimization, we use the DM as part of the approach known as Divide and Concur. In this approach, we expand the configuration space by introducing multiple replicas of each atom – one replica for each restraint it is involved in. Thus, by relaxing the requirement

(known as the *concur* constraint) that all replicas of a single atom coincide spatially, we can very easily satisfy all the restraints, since they are all independent. In fact, not only can we easily find a configuration (in the expanded space) that satisfies all restraints, but we can also find the closest such configuration to a given arbitrary configuration. We call such a configuration the *projection* of the given configuration onto the constraint set (the subset of configuration space containing all configurations satisfying all the restraints). Of course, to obtain a valid solution, we must find a configuration that satisfies not only this constraint (the *divide* constraint) but also the *concur* constraint. We achieve this using an iterated map that can be written as a composition of the projections to the two constraints and affine combinations. The dynamical system thus constructed, the DM, is designed to efficiently explore the important regions of the configuration space, and its fixed points correspond to solutions.

Formally, we can construct the configuration space, the constraints, and the map as follows. Let I be the set of atoms in the molecule and let A be the set of restraints. We consider a bipartite graph with edges E connecting restraints to the atoms they involve. Each restraint involves only a small fraction of the atoms in the molecule. Since the energy bound restraint (3) involves all the atom in the molecule, and it is the only one that does so, it turns out to be much more efficient to include it as part of the *concur* constraint than as part of the *divide* constraint. Therefore, A includes only the data restraints and the rigid unit restraints.

Our configuration space is the space of maps from the set of edges E to three dimensional Euclidean space $\mathbb{R}^3$. That is, a configuration $\mathbf{x} = (\mathbf{r}_e)$, where $e = \langle i, \alpha \rangle \in E$, assigns a position in space to each atom $i \in I$ for each restraint $\alpha \in A$ it is involved in. The configuration space is therefore an $M \times 3$-dimensional Euclidean space, where $M = |E| = \sum_{\alpha \in A} |E_\alpha| = \sum_{i \in I} |E_i|$, E_α is the set of edges incident on restraint α, and E_i is

the set of edges incident on atom i. We call $\mathbf{r}_{\langle i,\alpha\rangle}$ a replica of atom i involved in restraint α.

The *divide* constraint is the subset of our configuration space where a restraint is satisfied by the atomic positions assigned to its incident edges:

$$D = \{\mathbf{x} \text{ such that } V_\alpha\left(\mathbf{x}|_{E_\alpha}\right) = 0 \text{ for all } \alpha \in A\}, \tag{5.2}$$

where $\mathbf{x}|_{E_\alpha}$ is the restriction of the assignment $\mathbf{x}$ to the edges E_α incident on restraint α. The *concur* constraint is the subset where a unique atomic position is assigned to all edges incident on the same atom, and where this assignment of positions to atoms satisfies the energy bound restraint:

$$C = \{\mathbf{x} = (\mathbf{r}_e) \text{ such that } \mathbf{r}_e = \mathbf{r}_i \text{ for all } i, e \in E_i \text{ and } V_{\text{non-local}}(\mathbf{r}_1, \mathbf{r}_2, \ldots) \leq E_{\text{bound}}\}. \tag{5.3}$$

In the next section we discuss how to construct projections p_C and p_D to these two constraints. Provided these projections, we set up a dynamical system based on an iterated map. Given a configuration $\mathbf{x}_j$ at the jth stage of the iteration, the configuration at the next iteration is given by

$$\mathbf{x}'_j = \lambda \mathbf{x}_j + (1-\lambda) p_D(\mathbf{x}_j) \tag{5.4}$$

$$\mathbf{x}_{j+1} = DM(\mathbf{x}'_j) = \mathbf{x}'_j + p_D\left(2p_C(\mathbf{x}'_j) - \mathbf{x}'_j\right) - p_C(\mathbf{x}'_j). \tag{5.5}$$

For $\lambda = 1$ (i.e $\mathbf{x}'_j = \mathbf{x}_j$), these are purely iterations of the difference map DM. Note that every fixed point $\mathbf{x}_{\text{fp}}$ of DM has $p_D\left(2p_C(\mathbf{x}_{\text{fp}}) - \mathbf{x}_{\text{fp}}\right) = p_C(\mathbf{x}_{\text{fp}}) = \mathbf{x}_{\text{sol}}$ which lies in the intersection of D and C and is therefore a solution. However, it is sometimes the case that the two constraints are inconsistent, due to slight inaccuracies, and that only an approximate solution is possible. The modified iteration with $0 < \lambda < 1$ makes sure that these approximate solutions are also stable despite not being fixed points of DM [51]. We use the value $\lambda = 0.9$ in all our runs.

5.4 Implementation

In the previous section we have defined the projections p_C and p_D to the *concur* and *divide* constraints and used them to set up our difference map iteration scheme. In this section we focus on how to efficiently calculate these projections in a computational implementation. The calculations involved in projecting to the *divide* constraint will depend on the form of the underlying data restraints. We will discuss the case of two common types of restraints, distance bounds and torsion angle bounds, but many more cases are feasible in this type of approach, including restraints on bond orientation and distance bounds with uncertain assignment.

5.4.1 The *divide* constraint

Given an arbitrary configuration $\mathbf{x}$, in order to compute $p_D(\mathbf{x})$ we wish to find a configuration $\mathbf{x}' \in D$ (where D is given in (5.2)) that minimizes $\|\mathbf{x} - \mathbf{x}'\|$. It is easy to see that this optimization problem decomposes into independent optimization problems – one for each restraint. Namely, for each restraint (α), we must find a configuration $\mathbf{x}'|_{E_\alpha}$, restricted to edges incident on α, which minimizes $\|\mathbf{x}|_{E_\alpha} - \mathbf{x}'|_{E_\alpha}\|$, while satisfying $V_\alpha(\mathbf{x}'|_{E_\alpha}) = 0$. Each of these optimizations also take the form of a projection, and so we refer to them as subprojections or projections to the restraints. The calculation involved in each of these subprojections will depend on the form of the restraint V_α.

5.4.2 Distance bound restraints

The simplest restraint is the restraint bounding an interatomic distance $d_{\min} < \|\mathbf{r}_{\langle i,\alpha\rangle} - \mathbf{r}_{\langle i',\alpha\rangle}\| < d_{\max}$. This kind of restraint is commonly derived from cross-peaks in NOE spectroscopy [73], but can also arise from many other experimental measurements, or as a way of enforcing hydrogen bonding geometry for a known hydrogen bond [58].

The projection to this restraint is given simply by

$$\mathbf{r}'_{\langle i,\alpha\rangle} = \mathbf{r}_{\langle i,\alpha\rangle} + \frac{\Delta d}{2d}(\mathbf{r}_{\langle i,\alpha\rangle} - \mathbf{r}_{\langle i',\alpha\rangle}) \tag{5.6}$$

$$\mathbf{r}'_{\langle i',\alpha\rangle} = \mathbf{r}_{\langle i,\alpha\rangle} - \frac{\Delta d}{2d}(\mathbf{r}_{\langle i,\alpha\rangle} - \mathbf{r}_{\langle i',\alpha\rangle}), \tag{5.7}$$

where $d = \|\mathbf{r}_{\langle i,\alpha\rangle} - \mathbf{r}_{\langle i',\alpha\rangle}\|$ and $\Delta d = -(d_{\min} - d)$ if $d < d_{\min}$, $\Delta d = d - d_{\max}$ if $d > d_{\max}$, and $\Delta d = 0$ otherwise.

5.4.3 Rigid unit restraints

We impose the covalent geometry by use of rigid unit restraints of the form

$$\min_T \sum_{k=1}^{|E_\alpha|} \|\mathbf{r}_{e_k} - T(\mathbf{y}_k)\|^2 = 0, \tag{5.8}$$

where T may vary over all rigid transformations (compositions of rotations and translations), $e_k \in E_\alpha$ are the edges between the restraint α and the atoms included in the rigid unit, and $\mathbf{y}_1, \mathbf{y}_2, \ldots$ is the equilibrium configuration of the rigid unit. The projection of a configuration $\mathbf{x}|_{E_\alpha}$ to this restraint is then given by $\mathbf{r}'_{e_k} = T(\mathbf{y}_k)$, where T minimizes $\delta(T) = \sum_{k=1}^{|E_\alpha|} \|\mathbf{r}_{e_k} - T(\mathbf{y}_k)\|$. This minimization problem, known sometimes as absolute orientation, is well studied, and various closed-form solutions exist [39, 40]. It is identical to the problem of superposing two molecular structures so as to minimize root-mean-square distance (RMSD) between then.

We construct the reference structures $\mathbf{y}_1, \mathbf{y}_2, \ldots$ based on the all-atom CHARMM22 force field [52]. We identify the 38 rigid units that can occur in polypeptides that include the 20 standard amino acids. For each such rigid unit we build a small molecule that includes it and extract the reference structure for the rigid unit from the equilibrium structure of the molecule subject to the CHARMM22 force field. A more reliable set of reference structures might be derived from a database of high resolution X-ray structures of small compounds, as in Ref. [25].

5.4.4 Torsion angle restraints

The backbone torsion angles ϕ and ψ can often be estimated based on the chemical shifts of surrounding nuclei by comparison to a database of structures with known chemical shifts [64].

Suppose the angle ϕ is known to be in the range $\phi_{\min} \leq \phi \leq \phi_{\max}$. We can put this restraint in a similar form to the previous restraint:

$$\min_{T, \phi_{\min} \leq \phi \leq \phi_{\max}} \sum_{k=1}^{|E_\alpha|} \|\mathbf{r}_{e_k} - T(\mathbf{y}_k(\phi))\|^2 = 0, \tag{5.9}$$

where the restraint involves all atoms which form a maximal rigid unit if ϕ is held constant, and $(\mathbf{y}_1(\phi), \mathbf{y}_2(\phi), \ldots)$ is the equilibrium configuration of that rigid unit. As calculating $\delta(\phi) = \min_T \delta(T, \phi)$ is straight forward, as described above, we must simply numerically minimize $\delta(\phi)$ over $\phi_{\min} \leq \phi \leq \phi_{\max}$. Note that even though the set of atoms involved in this restraint is not a rigid unit, but includes two rigid units, this restraint implicitly includes the two rigid unit restraints and replaces them.

5.4.5 The *concur* constraint

Like the projection to the *divide* constraint, the projection to the *concur* constraint will be computed using a subprojection – a projection operation in a lower-dimensional space. Given an arbitrary configuration $\mathbf{x}$, in order to compute $p_C(\mathbf{x})$ we wish to find atomic positions $\mathbf{r}'_1, \mathbf{r}'_2, \ldots$, concurring across all restraints, which minimize the distance function

$$\delta\left(\mathbf{r}'_1, \mathbf{r}'_2, \ldots\right) = \sum_{\langle i,\alpha\rangle \in E} \|\mathbf{r}_{\langle i,\alpha\rangle} - \mathbf{r}'_i\|^2, \tag{5.10}$$

while satisfying a bound on the non-local energy

$$V_{\text{non-local}}(\mathbf{r}'_1, \mathbf{r}'_2, \ldots) \leq U_{\text{bound}}. \tag{5.11}$$

The projection would then be given by $\mathbf{r}'_{\langle i,\alpha\rangle} = \mathbf{r}'_i$. It is easy to show that $\delta(\mathbf{r}'_1, \mathbf{r}'_2, \ldots)$ depends only on the distances between $\mathbf{r}'_i$ and $\overline{\mathbf{r}}_i = (1/|E_i|)\sum_{e\in E_i} \mathbf{r}_e$, the averaged position of atom i across all its replicas. In fact, the distance function can be rewritten, up to a constant which does not depend on its arguments, as

$$\delta(\mathbf{r}'_1, \mathbf{r}'_2, \ldots) = \sum_i |E_i| \|\overline{\mathbf{r}}_i - \mathbf{r}'_i\|^2. \tag{5.12}$$

Therefore, the subprojection calculation involves projecting the replica-averaged configuration $\overline{\mathbf{r}}_1, \overline{\mathbf{r}}_2, \ldots$ to the energy bound restraint subject to the weighted metric (5.12).

5.4.6 Non-local energy bound

If the replica-averaged configuration already satisfies the energy bound, the subprojection leaves it unchanged, and the projection is given simply by the averaging operation. Otherwise, the subprojection must yield a configuration where the energy bound is marginally satisfied, $V_{\text{non-local}}(\mathbf{r}'_1, \mathbf{r}'_2, \ldots) = U_{\text{bound}}$. To find this configuration we use the

Lagrange multiplier method for constrained minimization. Consider a combined energy function $V'_k(\mathbf{r}'_1, \mathbf{r}'_2, \ldots) = V_{\text{non-local}}(\mathbf{r}'_1, \mathbf{r}'_2, \ldots) + k\delta(\mathbf{r}'_1, \mathbf{r}'_2, \ldots)$. For each value of the Lagrange multiplier k, a global minimization of V'_k yields a configuration $\mathbf{r}'_1(k), \mathbf{r}'_2(k), \ldots$ with an energy $U(k) = V_{\text{non-local}}\left(\mathbf{r}'_1(k), \mathbf{r}'_2(k), \ldots\right)$. The configuration we seek is the one for which $U(k) = U_{\text{bound}}$. A numerical root-finding algorithm can find the solution to this equation with a modest number of evaluations of $U(k)$. Each evaluation of $U(k)$ involves minimizing V'_k, the sum of the non-local potential and a harmonic potential, restraining each atom independently to its replica-averaged position in the input configuration. Such a potential is easy to implement in force-field software packages such as XPLOR-NIH, which we use to perform this minimization [63]. Although, formally, the Lagrange multiplier method above only holds if the global minimum is found in calculating $U(k)$, we are forced by considerations of efficiency to apply local minimization. However, due to the harmonic restraint, the global minimum cannot be very far from our initial point which is the replica-averaged input configuration.

The projection holds for enforcing a bound on any potential energy function. In this work we use a simple form of the van der Waals exclusion potential:

$$V_{\text{excl}}(\mathbf{r}_1, \mathbf{r}_2, \ldots) = \sum_{\langle i,i' \rangle} V_{ij}(\|\mathbf{r}_i - \mathbf{r}'_i\|), \tag{5.13}$$

where

$$V_{ij}(r) = \begin{cases} (\eta R_i + \eta R'_i - r)^2 & r < \eta R_i + \eta R'_i \\ 0 & \text{otherwise,} \end{cases} \tag{5.14}$$

R_i is the van der Waals radius of the ith atom as given by the CHARMM22 force field [52], $\eta = 0.81$ determines to what degree we allow van der Waals spheres to overlap without penalty, and the sum skips pairs that are connected by a path of three covalent bonds or fewer.

5.5 Results

As a demonstration of our new approach to NMR structure determination, we study a structure that has already been reconstructed with a traditional approach, so that we have a point of reference for our results. The structure is a three-fold symmetric amyloid fibril formed by a 40-residue peptide associated with Alzheimer's disease [58]. The experimental restraints we use are the same restraint as used in Ref. [58] (see supporting information there), which include distance bounds – both intramolecular in intermolecular – and backbone torsion angle bounds. As in Ref. [58], we ignore the eight residues of the peptide which form a disordered region.

We perform the reconstruction, based on the difference map iteration described above, in two steps. In the first step, we reconstruct the structure of one cross-beta unit, modeled by six polypeptide chains. We include only the restraints that apply within a single cross-beta unit. As an initial condition, we use six well-separated, parallel, extended chains with randomized backbone torsion angles, and with all replicas of each atom initially in agreement. In most runs, the difference map iterations quickly yield a structure that reasonably satisfies both constraints. In those runs, we then take three, well-separated copies of the model, arranged in a three-fold symmetric way about an axis, and perform more iterations of the difference map with all restraints being included. We evaluate the final models by how well the structure that satisfies the *concur* constraint, given by $\mathbf{x}_C = p_C(\mathbf{x}_{\text{final}})$ does at satisfying the various restraints included in the *divide* restraint. We can do this easily, by looking at the distances between the positions of the atomic replicas in $\mathbf{x}_D = p_D(\mathbf{x}_C)$ to the ones in $\mathbf{x}_C$. These distances, which we will call errors, indicate by what degree the restraint which involves the replica is unsatisfied.

Of fifty runs, taking approximately a total of 800 CPU hours, we pick the four which yielded models with the smallest root-mean-square error, and we compare them to the four models presented in Ref. [58]. We perform short relaxation runs on the four models of Ref. [58] using our difference map iterations. This relaxation run is necessary for a comparison on an equal footing because of our formulation of the restraints, which is presumably slightly different than the formulation used to derive these models. Indeed, the relaxed models have a lower root-mean-square error than the unrelaxed model. A quantitative comparison between the two sets of models is presented in Tables 5.1 and 5.2, Figure 5.2 compares the distribution of the errors in two models from the two sets, and Figure 5.3 compares the two models visually.

Though the models produced in this work have virtually the same distribution of error magnitudes as the relaxed version of the models in Ref. [58], they are quite different from each other. Though each run starts from a different random initial condition, our four lowest-error models, like in the other set of models, fall only ~ 2 angstroms from one another in terms of RMSD, but the two sets are ~ 7 angstroms apart. Visually, we observe that the models produced in this work have a greater twist along the fibril axis. As both models reasonably satisfy all the restraints, there is not enough information in the restraints alone to exclude either possibility. There is no obvious reason why our method, over many runs, would repeatedly converge to one cluster of models, but never to the cluster of models represented by the models in Ref. [58], which satisfy the constraints equally well. It is possible that without the bias introduced by the energy/cost minimization, the latter cluster is destabilized entropically with respect to the former cluster. However, it is also possible that this result simply speaks to the unavoidable inherent bias in any search dynamics used for structure determination.

	root-mean-square error (10^{-2} Å)			
model set 1	2.33	2.40	2.41	2.42
model set 2	9.37	9.44	9.56	9.66
model set 3	2.32	2.50	2.29	2.29

Table 5.1: Root-mean-square errors in four models of the amyloid fibril produced by the constraint based method (set 1) and four models produced by a traditional method (set 2) [58]. For proper comparison, we perform short relaxation runs on the four models of set 2 using our difference map iterations (set 3). The root-mean-square error is an average over the atomic replicas of the distance each needs to move from the position agreed upon by all replicas of the same atom to the position where it must be for the restraint it is involved in to be satisfied.

	model set 1			
RMSD1 (Å)	2.84	1.59	1.70	1.89
RMSD2 (Å)	9.54	7.37	7.43	6.96
RMSD3 (Å)	9.27	7.05	7.12	6.67
	model set 2			
RMSD1 (Å)	7.48	8.30	7.97	7.75
RMSD2 (Å)	2.08	2.49	1.60	1.93
RMSD3 (Å)	2.35	2.71	1.99	2.17
	model set 3			
RMSD1 (Å)	7.16	7.97	7.63	7.43
RMSD2 (Å)	2.25	2.57	1.72	2.11
RMSD3 (Å)	1.93	2.33	1.43	1.79

Table 5.2: Root-mean-square deviations between different models of the amyloid fibril. In calculating the RMSD, we consider only the alpha-carbons. We compute an average structure for each of the three sets of models (see Table 5.1) by aligning all models against a single model and taking the centroid position for each atom. The table gives the RMSD between each model and the average structure of each of the three sets (RMSD1 is the distance of a model to the average of set 1 and so on).

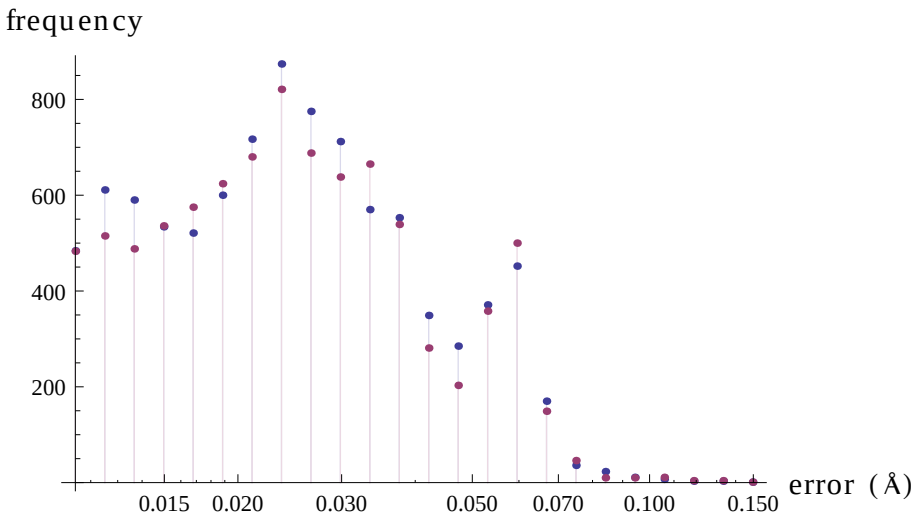

Figure 5.2: The distribution of errors in the lowest error model of the amyloid fibril constructed in this work (blue) and a representative model constructed by a traditional method [58] after a relaxation run (purple). The errors corresponding to each restraint are the distances by which the atoms involved in the restraint need to moved for the restraint to be satisfied. The left-most point represents all errors smaller than 0.01 angstroms.

5.6 Discussion

In this work we developed a constraint-based formulation of the problem of structure determination from NMR restraints, and proceeded to implement a numerical method based on the difference map and the Divide and Concur approach for solving this constraint satisfaction problem. We divided the information used for reconstruction into data restraints, local physical restraints, and non-local physical restraints. The data restraints and local physical restraints were formulated as hard restraints, which should be individually satisfied in a solution. These restraints became part of the *divide* constraint, which required all of them to be simultaneously satisfied, but allowed different replicas of a single atom to be in different positions. The *concur* constraint required all replicas of a single atom to agree on its position. Also, it included the non-local physical

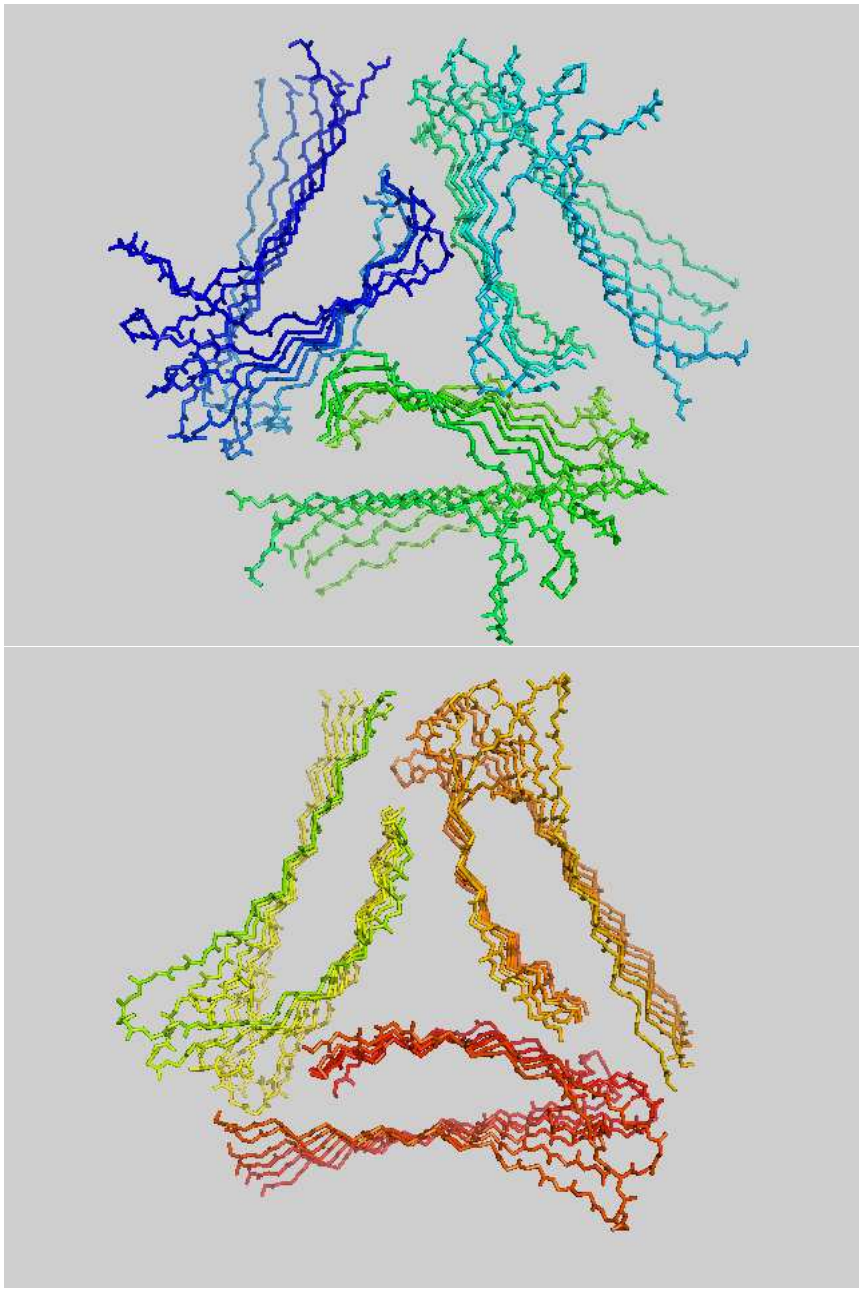

Figure 5.3: Backbone traces of a model of an amyloid fibril constructed in this work (top) and a representative model constructed by a traditional method [58] after a relaxation run (bottom). The colors serve to visually distinguish different chains and the two models.

restraints, which were formulated as an energy bound.

With the restraints thus divided, we can observe the essentially geometric nature of the structure determination problem. The restraints included in the *divide* constraint – distance bounds, and rigid units (with or without internal degrees of freedom) – all refer to how the different atoms of the molecules are held together, either locally along the chain by covalent bonds, or across the chain by prescribed distances, as measured in experiment. The atoms then form a network of hinges, joints, and pistons with either free or constrained ranges of motion. The exclusion restraint on the other hand, or by its more geometric name, the packing constraint, prevents atoms in contact from overlapping when they are pushed against each other, as if their centers were held apart by a bar. This formulation brings to mind Buckminster Fuller's tensegrity structures, whose structure is stabilized by a balance of tensile elements (cables) holding points of the structure together and compressive elements (bars) holding points apart, and which form an interesting topic in the geometrical study of rigidity [15].

In constructing the difference map scheme, there are many choices to make as to how to divide the many restraints into two sets, forming the *divide* and *concur* constraints. The difference map appears to find solutions most efficiently when the two projections it employs are in direct competition with each other [24]. This is the case here, where the competition is between the tensile restraints, holding the atoms together, and the compressive restraints, holding them apart.

The purpose of this work is not to compare the efficiency of the difference map method presented here to that of traditional methods, but to demonstrate its feasibility and discuss its possible advantages or disadvantages. We leave off the former task to future work. The results presented in the previous section clearly demonstrate that the method we developed here is capable of constructing a model satisfying the restraints

with as much accuracy as models produced by traditional methods. Also, the model is not much different, so that we may surmise that our method does not disrupt any of the important physics needed for structure determination by abandoning traditional physical dynamics in favor of the artificial difference map dynamics or by introducing unphysical replicas. To the extent that the differences in the resulting models are due to the lack of particular interactions, they can be easily added. In this work, the only non-local physical interaction included was the van der Waals exclusion potential, but the approach we present can accommodate any desired force field. To include electrostatic interactions, for example, all that is necessary is to change a flag in the force-field package used in Section 5.4.6.

While the approach developed here for constructing models based on structural restraints appears to be as powerful as traditional methods, it cannot now replace them. For one, further work will be needed to develop an interface for the computational environment that is more intuitive to spectroscopists. More work could be done to study and optimize the performance of the method and the quality of models produced, as measured by standard metrics. Though we address only two types of data restraints in this work, many more can be easily implemented.

The main advantage of employing an approach such as the one developed here is that it deals with restraints as restraints and not as potentials. Instead of combining disparate pieces of information into a single cost/energy function, our constraint-based approach handles each restraint individually as a hard restraint, and attempts to find a configuration that satisfies all of them. Since any model satisfying all of the restraints should a priori be considered an equivalently valid structure prediction, we avoid in this way biasing the predicted structure because of an incomplete or simplistic model of the physical forces.

CHAPTER 6

CONFORMATIONS OF A GRAPHENE-LIKE SHEET WITH HETEROGENEITY IN BOND LENGTHS

6.1 Abstract

We study a simple model of rippling in a two-dimensional netwrok of bonds due to bond length heterogeneity. We describe a form of dislocations which is not present in a homogeneous crystal and use a relationship between the dislocation density and the Gaussian curvature to characterize the relaxed conformation of the sheet. We find a relationship between this conformation and a surface in an abstract space associated with the combinatorial aspect of the bond length heterogeneity.

6.2 Bond length heterogeneity in an atomic sheet

One possibility that has been suggested as an explanation of intrinsic rippling of graphene sheets is the diversity of types of chemical bonds that two carbon atoms may form [26]. This suggestion raises the geometrical question of how might a two-dimensional network of bonds conform in three-dimensional space if its bonds vary in some non-regular way, and particularly, how might a flat sheet be perturbed away from flatness at the introduction of such heterogeneity. We attempt to answer this question for a simple, albeit historically important, model of bond heterogeneity: Kekulé structures [36]. Kekulé structures are ones in which each bond of the honeycomb lattice is designated either a single bond or a double bond, and each carbon atom participates in exactly two single bonds and one double bond. While this model is very unlikely as an explanation of mechanical instabilities in graphene, the problem from which it is inspired, the

geometrical problem it poses is of scientific interest. Particularly, it is potentially interesting as a mechanism for pattern formation in self-assembled and designer materials.

The model we wish to study is one wherein the conformation of the network minimizes a simple classical potential

$$U = \sum_{\langle ij \rangle} k_b (d_{ij} - l_{\sigma(i,j)})^2 - \sum_{\langle ijk \rangle} k_a \cos(\theta_{ijk} - 2\pi/3), \tag{6.1}$$

where $\sigma(i, j) \in \{s, d\}$ represents the type of bond between atoms i and j, d_{ij} is its length, and l_s and l_d are the relaxed lengths for single and double bonds respectively. In the limit where $l_s = l_d$, the equilibrium conformation of the network is the familiar two-dimensional honeycomb lattice. This is the reference structure to which we will relate the equilibrium structure when $l_d < l_s$ as a perturbation. Similarly, if $l_d < l_s$, but the double bonds are identified with one of the three sublattices of like-oriented bonds, then the equilibrium conformation is again the familiar structure, except it is compressed along the direction of double bonding. We would like to know what happens if $l_d < l_s$ for an arbitrary Kekulé structure. We restrict ourselves to the case where $l_s - l_d \ll l_s$

6.3 Fractional dislocations in a six-fold two-dimensional crystal

On a coarse-grained scale, we can think of the atomic network as tracing out a two-dimensional manifold in space. Much work has been done by Bowick and co-workers to describe how the structure of a six-fold two-dimensional crystals is disrupted when forced to lie on a curved manifold [7, 8, 6]. We can use the same results to investigate instead how a disruption to the structure of the crystal can affect the curvature of the manifold it traces out. The bond orientation of the crystal at each point on the manifold gives a local coordinate frame. By enforcing the topological requirement that as we follow a closed loop, the accumulated change to the coordinate frame vanishes (up to

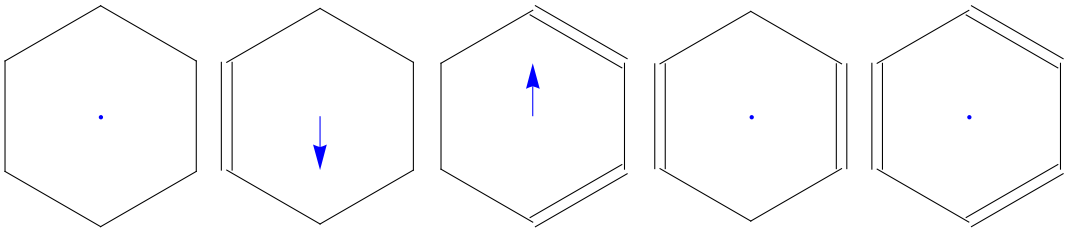

Figure 6.1: The five patterns of single and double bonds in a 6-cycle of the honeycomb lattice that are allowed in a Kekulé structure. The Burgers vector of each hexagon can be determined by travelling counterclockwise around the cycle, taking shorter steps when travelling on double bonds. The vector connecting the termini of the path is the Burgers vector (in blue, not to scale). Three of the cycles above have vanishing Burgers vectors.

$\pi/3$-rotations), we can associate the Gaussian curvature (density of total curvature) of the manifold with the sum of two contributing densities: the circulation density (curl) of Burgers vectors associated with dislocations and the density of disclination charges [8].

Our model 6.1 assumes a perfect honeycomb lattice with no dislocations or disclinations. However, we may view the heterogeneity in bond lengths as introducing a type of fractional dislocation that does not exist in homogeneous crystals. Namely, imagine following a cycle in the network and tracing out a related path using a fixed coordinated frame: each bond traversed in the cycle corresponds to a step in the path along one of the six bond directions given by the reference frame, and the length of the step is given by l_s or l_d depending on the type of bond traversed. Because of the heterogeneity in bond lengths, this path will not be a closed path, and we may think of the vector connecting its termini as a Burgers vector. We can thus associate a Burgers vector with any of the five possible 6-cycles in a Kekulé structure (see Figure 6.1).

Since the dislocations in our model are ubiquitous and the magnitude of each is small, we are in limit where we may consider a continuous density of Burgers vectors

b(**x**) forming a vector field over our manifold. Bowick and co-workers show that the Gaussian curvature is given by the differential 2-form $K(\mathbf{x}) = d\mathbf{b}(\mathbf{x})$ [8]. Note that mean curvature, since it lacks the topological nature of the Gaussian curvature, is not determined by the pattern of dislocations, and will probably depend on the particular parameters of the model 6.1.

6.4 Random tilings, projection, and the phason dimension

It is useful now to leave the geometrical problem for a while, and focus on the combinatorial problem of enumerating and characterizing Kekulé structures. In the field of combinatorics and statistical physics this problem has a long history and is known as the problem of dimer covers or perfect matching, as applied to the honeycomb lattice [48]. Associating each double bond with a rhombic tile decorated with two carbon atoms, a double bond, and four halves of single bonds (see Figure 6.2), we can now ask to enumerate the ways of tiling the plane with such tiles. Thus, a uniform (that is, drawn from a uniform distribution) Kekulé structure is equivalent to a uniform random tiling with $\pi/3$-rhombi.

In the field of random tiling, it is often useful to view a planar or spatial tiling, as the projection of a higher dimensional surface onto two or three dimensions [35]. The extra dimensions, which are projected out, are called the phason dimensions. In the case of $\pi/3$-rhombi, this projection construction is very easy to visualize, as illustrated in Figure 6.3. The three-dimensional surface whose projection is the tiling is formed by square plaquettes oriented normal to the x, y, or z directions, and the phason dimension is along the (**111**) direction. Note that if instead of fully applying the projection, we simply contract the phason dimension by a large factor, we are left with rhombi that are

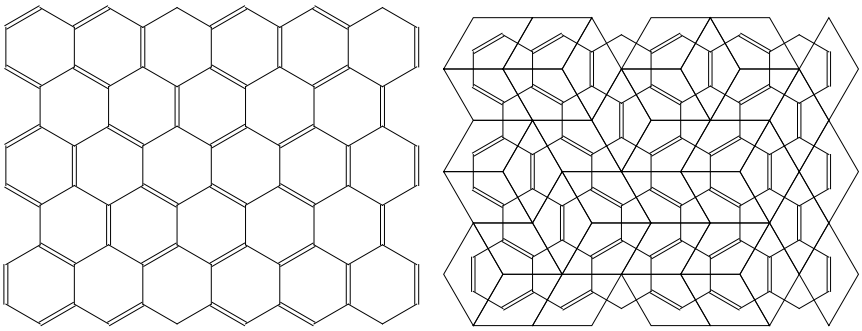

Figure 6.2: Correspondence of a Kekulé structure to a tiling by decorated rhombi: a portion of a uniform Kekulé structure composed of single and double bonds on a honeycomb lattice (left); and the corresponding tiling by rhombic tiles each decorated by a centered double bond and four halves of single bonds.

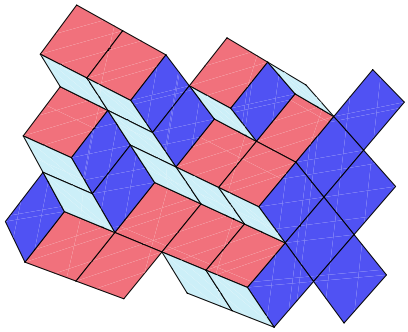

Figure 6.3: Correspondence of a Kekulé structure to the projection of a three dimensional surface: the tiling of Figure 6.2 can be obtained as a projection of a surface composed of square plaquettes, viewed here from slightly off the projection axis for ease of visualization.

related to the decorated $\pi/3$-rhombi by a small contraction along the double bonding direction. This observation raises the possibility that this surface, obtained by incomplete projection, is the same (at least viewed on a large scale) as the manifold traced out by the bond network in equilibrium.

Such a relationship, between the strain of a structure in physical space and strain

in phason space has been identified before in quasicrystalline random tilings. In Ref. [57], Nori, Ronchetti, and Elser conduct the following numerical experiment: As their reference structure, they start with some tiling, where each tile is decorated with atoms and bonds so that all bonds lengths are at their relaxed value. In Ref. [57] this results in two relaxed bond lengths, identified with bonds of two different types. Then, they perturb the structure by changing the relaxed length of one type of bond by a small amount, and they let the network relax to its equilibrium. The authors find that when the reference structure is given by the projection of a hypersurface whose phason coordinates remain in a bounded region, then the deviation of the relaxed structure from the reference structure also remains bounded everywhere and no strain accumulates. On the other hand, when the deviation of the phason coordinate accumulates linearly as a distance from some reference point, so does the physical strain accumulate linearly. The numerical experiment of Ref. [57] demonstrates an indirect relationship between phason strain and physical strain, in the sense that the pattern of deviation in physical space is not shown to be related to the pattern of deviation in phason space. Here, we seek a direct and analytical version of this relationship, by relating the Gaussian curvatures of the surface which is projected to give the tiling related to the Kekulé structure and the manifold traced out by the bond network in its equilibrium conformation.

6.5 A relationship between two apparently disparate surfaces

The Gaussian curvature of the surface which is composed of square plaquettes is, of course, vanishing everywhere, except at its vertices, where it diverges. At these vertices the contribution to the total curvature is proportional to the number of plaquettes meeting at the vertex, being equal to $\pi/2$ if three plaquettes meet and decreasing by $\pi/2$ for each additional plaquette (see Figure 6.4). Recall that the density of total curvature (i.e.

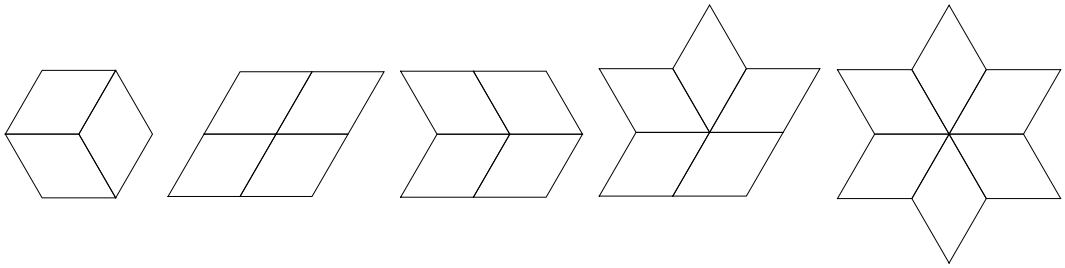

Figure 6.4: The five possible arrangements of rhombi around a vertex of the tiling. Equivalently, these are the five possible types of vertices present in the surface corresponding to the tiling. The Gaussian curvature of the lifted surface vanishes on its faces and edges, but it is singular at its vertices, contributing a total curvature of $\pi/2$, 0, 0,$-\pi/2$, and $-\pi$ respectively from left to right at the five vertices shown.

Gaussian curvature) in the manifold traced out by the bond network is given by the density of circulation (i.e. curl) of the Burgers vector density. In fact, it is easy to show by complete enumeration of possible local Kekulé structures, that the total curvature associated with the circulation of Burgers vectors in the three 6-cycles around an atom is proportional to the average of the total curvatures associated with the three tiling vertices surrounding it (see Figure 6.5).

Note that both surfaces can only appear continuous and smooth when viewed at a coarse-grained scale: one because it is traced out by point-like atoms, the other because it is composed of discrete plaquettes. However, we have shown that on scales larger than the lattice spacing, the total curvature in corresponding subregions of the two surfaces is proportional. The constant of proportionality can be gotten rid of by appropriately scaling the phason dimension so that the curvatures of the two surfaces are equal, as suggested by the incomplete projection construction above.

For a disordered, uniform Kekulé structures, this relation between the two surfaces is particularly hard to corroborate in a simulation. This is because the height variations in

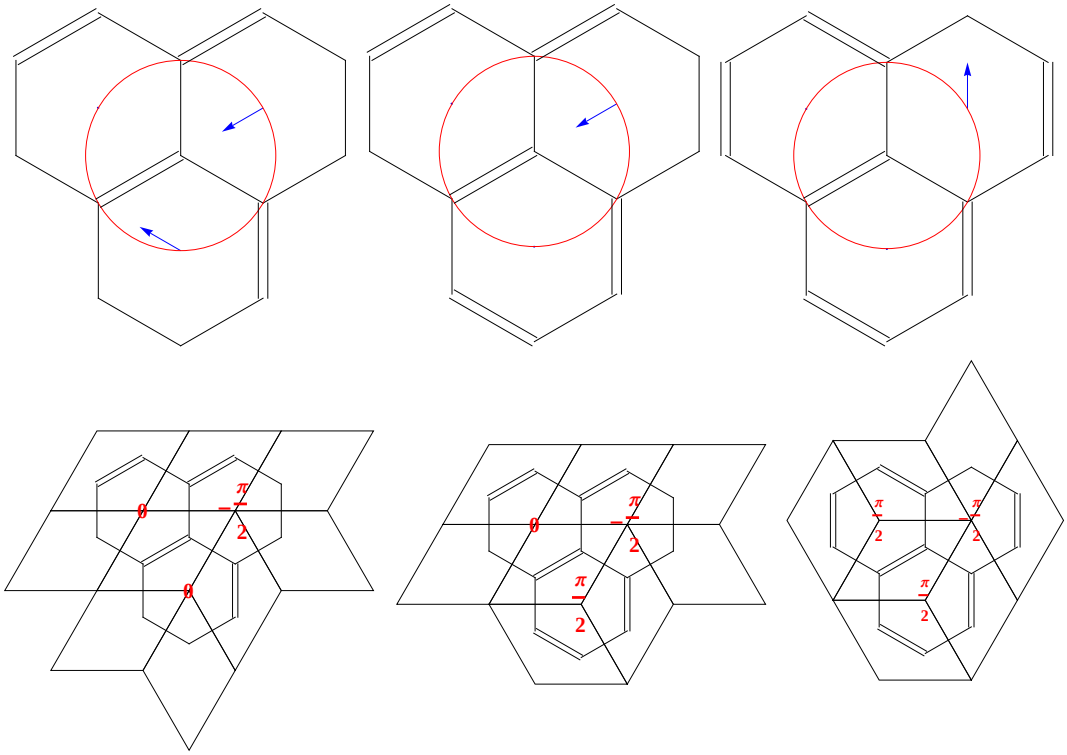

Figure 6.5: The Gaussian curvature in the manifold traced out by the bond network in equilibrium can be shown, by direct enumeration of local arrangements, to be proportional to the Gaussian curvature of the surface whose projection gives the rhombus tiling corresponding to the Kekulé structure. Three sample cases of the complete enumeration are presented. In each case, we traverse the loop (red) in a counterclockwise direction, adding up the components of the Burgers vectors encountered (blue) tangent to the loop. The results are $-\xi$, 0, and $+\xi$, where ξ is a positive total curvature value that depends on the relative lengths of double and single bonds. We compare this value to the average total curvature at the three surrounding vertices of the projected surface. The common ratio is $6\xi/\pi$.

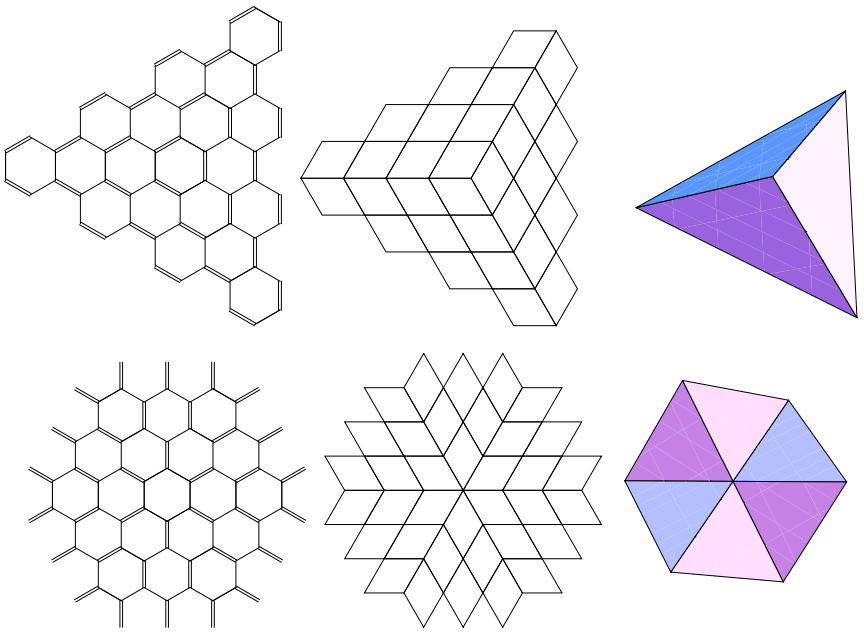

Figure 6.6: Two ordered Kekulé structures (left) which demonstrate the relationship between positive (top) or negative (bottom) Gaussian curvature in the surface whose projection is the corresponding tiling (center) and in the manifold traced out by the bond network in equilibrium (right).

surfaces associated with random tilings of $\pi/3$-rhombi grow only logarithmically with the size of the system [48]. Therefore, as the relationship holds only on scales larger than the lattice spacing, we require a huge system before the systematic height variations associated with the phason strain become noticeable over the fluctuations on the scale of the lattice spacing. However, for ordered Kekulé structures, where the height variations may grow linearly with the size of the system, we can corroborate the relationship by inspection, without even the need for simulation.

We considered above the Kekulé structure where the double bonds are identified with one of the three sublattices of bonds, for which the equilibrium conformation is a flat sheet, compressed along the direction of double bonding. Consider then the two Kekulé structures in Figure 6.6, where the sheet is divided into three or six sectors with

uniform direction of double bonding in each sector. The manifold that will be traced out by the network can be constructed by cutting a flat sheet into sectors, stretching or compressing the sectors along the bisector line, and stitching them back together. These manifolds, with vanishing Gaussian curvature except for a point of positive or negative total curvature at the origin, are clearly the same as the surfaces we get by performing the incomplete projection on the plaquette surfaces.

The slow growth of height fluctuations in the case of uniform Kekulé structure is a consequence of the slowly decaying correlations caused by the strong Kekulé constraint. If we depart from the simple Kekulé-constrained binary model of bond heterogeneity we chose at the beginning of the chapter, we might imagine that the situation would change. For example, if we allowed a certain density of defects in the Kekulé structure, such as atoms with no double bonds or with multiple ones, or made some allowance for conjugated bonds, then these defects will presumably screen the correlations, permitting the height fluctuations to grow faster. The analysis of the simple Kekulé case might be a good starting point for analyzing those more complicated cases. In any case, the interpretation of a bond heterogeneity as introducing fractional dislocations should hold no matter the distribution of these bonds.

Based on the similar previous results of Ref. [57] in a quasicrystalline tiling model, it stands to reason that the ultimate result of this paper, directly relating accumulation of strain in the phason space to accumulation of strain in the physical space, can be generalized to the vast family of dimer covering and random tiling models.

BIBLIOGRAPHY

[1] E. Agrell et al. Closest point search in lattices. *IEEE Trans. Inform. Theory*, 48:2201, 2002.

[2] J. Baker and A. Kudrollli. Maximum and minimum stable random packings of platonic solids. *Phys. Rev. E*, 82:061304, 2010.

[3] J. W. Berenschot et al. Chemically anisotropic single-crystalline silicon nanotetrahedra. *Nanotechnology*, 20:475302, 2009.

[4] A. Bezdek and W. Kuperberg. Dense packing of space with various convex solids. 2010. arXiv:1008.2398.

[5] P. Biswas et al. Semidefinite programming approaches for sensor network localization with noisy distance measurements. *IEEE Transactions on Automation Science and Engineering*, 3:360, 2006.

[6] M. J. Bowick et al. Crystalline order on a sphere and the generalized thomson problem. *Physical Review Letters*, 89:185502, 2002.

[7] M. J. Bowick, D. R. Nelson, and A. Travesset. Interacting topological defects on frozen topographies. *Phys Rev B*, 62:8738, 2000.

[8] M. J. Bowick and A. Travesset. The geometrical structure of 2d bond-orientational order. *J Phys A*, 34:1535, 2001.

[9] J. D. Bryngelson and P. G. Wolynes. Spin glasses and the statistical mechanics of protein folding. *Proc. Natl. Acad. Sci. USA*, 84:7524, 1987.

[10] S. Cameron. Enhancing gjk: computing minimum and penetration distance between convex polyhedra. In *Proceedings of International Conference on Robotics and Automation*, page 3112, 1997.

[11] T. M. Charlton. Maxwell, jenkin and cotterill and the theory of statically-indeterminate structures. *Notes and Records of the Royal Society*, 21:233, 1971.

[12] E. R. Chen. A dense packing of regular tetrahedra. *Discrete Comput. Geom.*, 5:214, 2008.

[13] E. R. Chen, M. Engel, and S. C. Glotzer. Dense crystalline dimer packings of regular tetrahedra. *Discrete Compu. Geom.*, 44:253, 2010.

[14] H. Cohn, A. Kumar, and A. Schürmann. Ground states and formal duality relations in the gaussian core model. *Phys. Rev. E*, 80:061116, 2009.

[15] R. Connelly. Tensegrity structures: Why are they stable? In M. F. Thorpe and P. M. Duxbury, editors, *Rigidity Theory and Applications*, Fundamental Materials Research, pages 47–54. Springer US, 2002.

[16] J. H. Conway and N. J. A. Sloane. *Sphere Packings, Lattices and Groups*. Springer-Verlag, New York, 3 edition, 1998.

[17] J. H. Conway and S. Torquato. Packing, tiling and covering with tetrahedra. *Proc. Natl. Acad. Sci. USA*, 103:10612, 2006.

[18] L. A. Danzer. A family of 3d-spacefillers not permitting any periodic or quasiperiodic tiling. In G. Chapuis and W. Paciorek, editors, *Aperiodic '94*, page 11. World Scientific, Singapore, 1994.

[19] A. Donev et al. Unusually dense crystal packing of ellipsoids. *Phys. Rev. Lett.*, 92:255506, 2004.

[20] V. Elser. Phase retrieval by iterated projections. *J. Optical Soc. Amer. A*, 20:40, 2003.

[21] V. Elser and S. Gravel. Laminating lattices with symmetrical glue. *Discrete Comput. Geom.*, 43:363, 2010.

[22] V. Elser and I. Rankenburg. Deconstructing the energy landscape: constraint-based algorithms for folding heteropolymers. *Phys. Rev. E*, 73:026702, 2006.

[23] V. Elser, I. Rankenburg, and P. Thibault. Searching with iterated maps. *Proc. Natl. Acad. Sci. USA*, 104:418, 2007.

[24] Veit Elser and Ivan Rankenburg. Deconstructing the energy landscape: Constraint-based algorithms for folding heteropolymers. *Phys. Rev. E*, 73(2):026702, Feb 2006.

[25] R. A. Engh and R. Huber. Accurate bond and angle parameters for x-ray protein structure refinement. *Acta Cryst.*, A47:392, 1991.

[26] A. Fasolino, J. H. Los, and M. I. Katsnelson. Intrinsic ripples in graphene. *Nature Materials*, 6:858, 2007.

[27] M. Gardner. *The Colossal Book of Mathematics*. Norton, New York, 2001.

[28] S. C. Glotzer and M. J. Solomon. Anisotropy of building blocks and their assembly into complex structures. *Nat. Mater.*, 6:557, 2007.

[29] S. Gravel. *Using Symmetries to Solve Asymmetric Problems*. PhD thesis, Cornell University, Ithaca, New York, January 2009.

[30] S. Gravel and V. Elser. Divide and concur: a general approach to constraint satisfaction. *Phys. Rev. E*, 78:036706, 2008.

[31] E. C. Greyson, J. E. Barton, and T. W. Odom. Tetrahedral zinc blende tin sulfide nano- and microcrystals. *Small*, 2:368, 2006.

[32] M. R. Gryk, J. Vyas, and M. W. Maciejewski. Biomolecular nmr data analysis. *Prog Nucl Magn Reson Spectrosc*.

[33] A. Haji-Akbari, M. Engel, et al. Disordered, quasicrystalline and crystalline phases of densely packed tetrahedra. *Nature*, 462:773, 2009.

[34] T. C. Hales. A proof of the kepler conjecture. *Ann. Math.*, 162:1065, 2005.

[35] C. L. Henley. Random tiling models. In *Quasicrystal: the state of the art*. World Scientific, Singapore, 1991.

[36] W. C. Herndon. Resonance theory and the enumeration of kekule structures. *J. Chem. Educ.*, 51:10, 1974.

[37] N. J. Higham. Matrix nearness problems and applications. In M. J. C. Gover and S. Barnett, editors, *Applications of Matrix Theory*. Oxford University Press, 1989.

[38] D.C. Hilbert. Matematical problems. *Bull. Am. Math. Soc.*, 8:437, 1902.

[39] B. K. P. Horn. Closed-form solution of absolute orientation using unit quaternions. *J. Opt. Soc. Am. A*, 4:629, 1987.

[40] B. K. P. Horn, H. M. Hilden, and S. Negahdaripour. Closed-form solution of absolute orientation using orthonormal matrices. *J. Opt. Soc. Am. A*, 5:1127, 1988.

[41] D. J. Hoylman. The densest lattice packing of tetrahedra. *Bull. Amer. Math. Soc.*, 76:135, 1970.

[42] D. J. Jacobs and M. F. Thorpe. Generic rigidity percolation: The pebble game. *Phys. Rev. Lett.*, 75:4051, 1995.

[43] A. Jaoshvili et al. Experiments on the random packing of tetrahedral dice. *Phys. Rev. Lett.*, 104:185501, 2010.

[44] Y. Jiao, F. H. Stillinger, and S. Torquato. Optimal packing of superballs. *Phys. Rev. E*, 79:041309, 2009.

[45] Y. Kallus and V. Elser. Dense-packing crystal structures of physical tetrahedra. *Phys. Rev. E*, 83:036703, 2011.

[46] Y. Kallus, V. Elser, and S. Gravel. Dense periodic packings of tetrahedra with small repeating units. *Discrete Compu. Geom.*, 44:245, 2010.

[47] Y. Kallus, V. Elser, and S. Gravel. A method for dense packing discovery. *Phys. Rev. E*, 82:056707, 2010.

[48] R. Kenyon. Height fluctuations in the honeycomb dimer model. *Communications in Mathematical Physics*, 281:675, 2008.

[49] G. Kuperberg and W. Kuperberg. Double-lattice packings of convex bodies in the plane. *Discrete Compu. Geom.*, 5:389, 1990.

[50] A. K. Lenstra, H. W. Lenstra, and L. Lovász. Factoring polynomials with rational coefficients. *Math. Ann.*, 261:515, 1982.

[51] Ne-Te Duane Loh, Stefan Eisebitt, Samuel Flewett, and Veit Elser. Recovering magnetization distributions from their noisy diffraction data. *Phys. Rev. E*, 82(6):061128, Dec 2010.

[52] A. D. MacKerell, D. Bashford, Bellott, R. L. Dunbrack, J. D. Evanseck, M. J. Field, S. Fischer, J. Gao, H. Guo, S. Ha, D. Joseph-McCarthy, L. Kuchnir, K. Kuczera, F. T. K. Lau, C. Mattos, S. Michnick, T. Ngo, D. T. Nguyen, B. Prodhom, W. E. Reiher, B. Roux, M. Schlenkrich, J. C. Smith, R. Stote, J. Straub, M. Watanabe, J. Wirkiewicz-Kuczera, D. Yin, and M. Karplus. All-atom empirical potential for molecular modeling and dynamics studies of proteins. *J. Phys. Chem. B*, 102:3586–3616, 1998.

[53] E. Meiner and F. Schilling. Drei gipsmodelle von flchen konstanter breite. *Z. Math. Phys.*, 60:92, 1912.

[54] N. D. Mermin. The space groups of icosahedral quasicrystals and cubic, orthorhombic, monoclinic, and triclinic crystals. *Rev. Modern Phys.*, 64:3, 1992.

[55] David Mitchell, Bart Selman, and Hector Levesque. Hard and easy distributions of sat problems. In *Proceedings of the Tenth National Conference on Artificial Intelligence*, page 459, 1992.

[56] Rmi Monasson, Riccardo Zecchina, Scott Kirkpatrick, Bart Selman, and Lidror Troyansky. Determining computational complexity from characteristic 'phase transitions'. *Nature*.

[57] F. Nori, M. Ronchetti, and V. Elser. Strain accumulation in quasicrystalline solids. *Phys Rev Lett*, 61:2774, 1988.

[58] Anant K. Paravastu, Richard D. Leapman, Wai-Ming Yau, and Robert Tycko. Molecular structural basis for polymorphism in alzheimer's -amyloid fibrils. *Proc. Natl. Acad. Sci. USA*, 105:18349, 2008.

[59] Z. Quan and J. Fang. Superlattices with non-spherical building blocks. *Nano Today*, 5:390, 2010.

[60] D. Rowe and J. Jeremy. *The Hilbert Challenge*. Oxford University Press, 2001.

[61] R. Schneider. *Convex Bodies: The Brunn-Minkowski Theory*. Cambridge University Press, 1993.

[62] A. Schürmann and F. Vallentin. Computational approaches to lattice packing and covering problems. *Discrete Comput. Geom.*, 35:73, 2006.

[63] C.D. Schwieters, J.J. Kuszewski, N. Tjandra, and G.M. Clore. The xplor-nih nmr molecular structure determination package. *J. Magn. Res.*, 160:66, 2003.

[64] Yang Shen, Frank Delaglio, Gabriel Cornilescu, and Ad Bax. Talos+: a hybrid method for predicting protein backbone torsion angles from nmr chemical shifts. *Journal of Biomolecular NMR*, 44:213, 2009.

[65] P. G. Szabo et al. *New approaches to circle packing in a square*. Springer-Verlag, New York, 2007.

[66] Z. Tang et al. Self-assembly of cdte nanocrystals into free-floating sheets. *Science*, 314:274, 2006.

[67] S. Torquato. Reformulation of the covering and quantizer problems as ground states of interacting particles. *Physical Review E*, 82:056109, 2010.

[68] S. Torquato and Y. Jiao. Dense packings of polyhedra: Platonic and archimedean solids. *Phys. Rev. E*, 80:041104, 2009.

[69] S. Torquato and Y. Jiao. Dense packings of the platonic and archimedean solids. *Nature*, 460:876, 2009.

[70] S. Torquato and Y. Jiao. Analytical construction of a family of dense tetrahedron packings and the role of symmetry. *Phys. Rev. E*, 81:041310, 2010.

[71] S. Torquato and F. H. Stillinger. Jammed hard-particle packings: From kepler to bernal and beyond. *Rev. Mod. Phys.*, 82:2633, 2010.

[72] G. van den Bergen. Proximity queries and penetration depth computation on 3d game objects, 2001. Game Developers Conference.

[73] M. K. Williamson. Applications of the noe in molecular biology. *Annu. Rep. NMR Spect.*, 65:77, 2009.

[74] M. P. Williamson, T. F. Havel, and K. Wüthrich. Solution conformation of proteinase inhibitor iia from bull seminal plasma by ^1H nuclear magnetic resonance and distance geometry. *J. Mol. Bio.*, 182:195, 1985.

[75] P. Yunker, Z. Zhang, K. B. Aptowicz, and A. G. Yodh. Irreversible rearrangements, correlated domains, and local structure in aging glasses. *Phys. Rev. Lett.*, 103:115701, 2009.

[76] Weixiong Zhang. Phase transitions and backbones of 3-sat and maximum 3-sat. In Toby Walsh, editor, *Principles and Practice of Constraint Programming*. Springer-Verlag, 2001.